Determining the Role of Sonic Hedgehog in Establishing Midbrain Dopaminergic Neuron Subclasses

Thesis

Submitted for a Doctoral Degree in Natural Sciences
(Dr. rer. nat.)

Faculty of Mathematics and Natural Sciences
Rheinische Friedrich-Wilhelms University of Bonn

Submitted by

Anna Kabanova

from Potsdam

Bonn 2013

Prepared with the consent of the Faculty of Mathematics and Natural Sciences
Rheinische Friedrich-Wilhelms University of Bonn

Publication Year: 2014

1. Reviewer: PD Dr. Sandra Blaess
2. Reviewer: Prof. Dr. Michael Hoch

Date of submission: 19. September 2013
Date of examination: 04. February 2014

To my Family

Table of content

1. Introduction

Midbrain dopaminergic neurons (MbDNs) are involved in regulating many important brain functions including motor control, reward behavior and cognitive tasks. Degeneration or dysfunction of MbDNs is implicated in several common human disorders. In Parkinson‘s disease (PD), degeneration of MbDNs in the substantia nigra pars compacta (SNpc) results in severe motor deficits (Hirsch et al., 1988; German et al., 1989; Marsden, 1994). Dysregulation of dopamine transmission in the forebrain has been linked to the emergence of substance disorders (Kelley et al., 2002; Wightman et al., 2002), depression (Dailly et al., 2004) and the psychotic and cognitive symptoms in schizophrenia (Sesack et al., 2002; Winterer et al., 2004). There is increasing evidence that functional and molecular diversity of MbDNs correlates with their relative vulnerability to disorders, for example to cell death in PD.

1.1 Dopaminergic neurons in the mammalian central nervous system

Dopamine (DA) belongs to the family of catecholamines (CA) and as a modulatory neurotransmitter it is involved in regulating diverse brain function. DA neurons are widely distributed in the mammalian central nervous system (CNS) with the largest population located in the ventral midbrain (vMb). The first study to identify the CA neurons in the brain was carried out in the early sixties (Dahlstrom and Fuxe, 1964). Immunohistochemical detection of the CA-synthesizing enzyme, tyrosine hydroxylase (TH), made it possible to detect and map the DA neurons in the mammalian brain. Thus, nine distinctive cell groups (A8-A16), distributed from the midbrain to the olfactory bulb (OB), were identified in the adult brain (Dahlstrom and Fuxe, 1964). The A11-A15 groups of DA neurons are located within the posterior aspect of the hypothalamus (A11), the arcuate nucleus (A12) and the periventricular nucleus (A13-A15). DA neurons of A16 are located in the OB. They play crucial regulatory roles in many neural functions, including sensorimotor integration and pain control at the spinal level (A11), neuroendocrine hormone release (A12–A14), as well as male sexual behavior (A13–A15) (Barraud et al., 2010). The MbDNs constitute about 75% of the total number of DA neurons and are categorized as A8, A9 and A10. MbDNs form an extensive network of connections throughout the forebrain, including the neocortex and striatum, as well as limbic system. MbDNs in group A9 contribute to the neurons of the SNpc (Figure 1A). The A10 DA neurons represent the ventral tegmental area (VTA), while the A8 group of MbDNs forms the retrorubral field (RRF). SNpc MbDNs project predominantly to the dorsal striatum and are involved in control of movement. The VTA neurons project to the

prefrontal cortex (PFC) and the limbic system, and regulate cognitive function and reward behavior, respectively (Figure 1B).

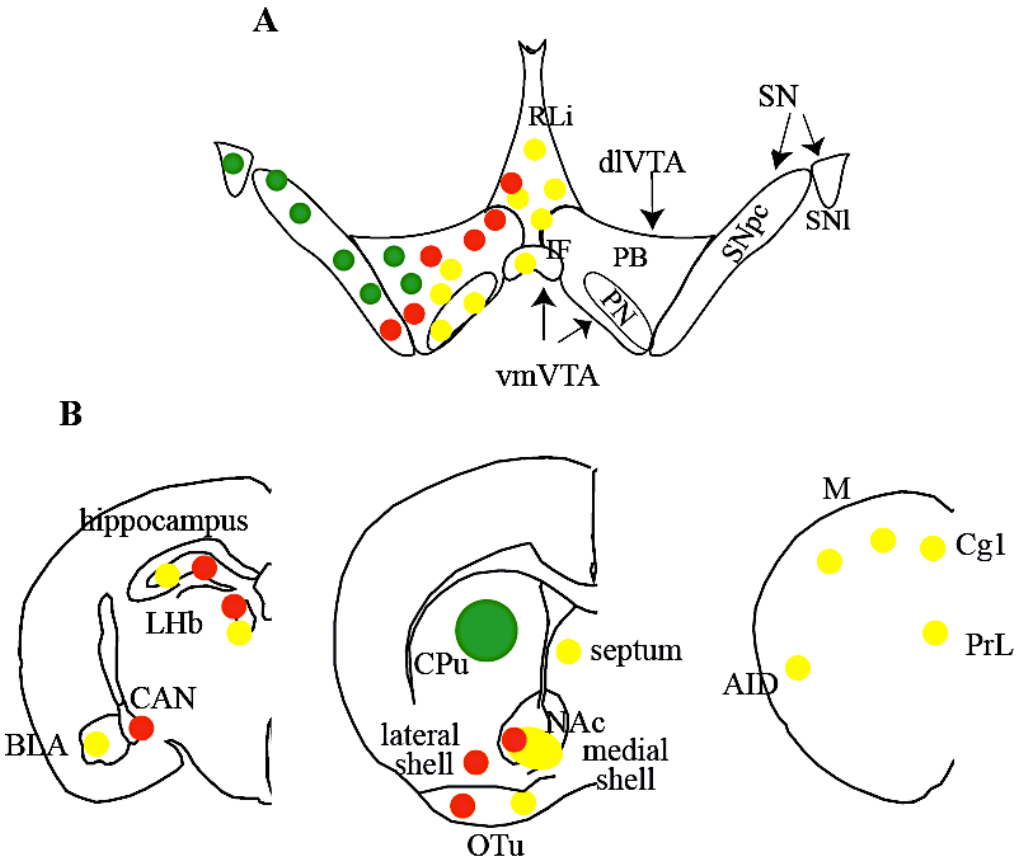

Figure 1 MbDN subpopulations and their projections. (A) Plane of section represents distinct subpopulations of MbDNs in the vMb. IF: nucleus intrafasciculus; PB: nucleus parabrachialis; PN: paranigral nucleus; RLi: rostral linear nucleus; SN: substantia nigra; SNpc: SN pars compacta; SNl: SN lateralis; dlVTA: dorsolateral ventral tegmental area; vmVTA: ventromedial VTA. **(B)** MbDN projections of SN and VTA. BLA: basolateral amygdala; CAN: central amygdaloid nucleus; LHb: lateral habenular nucleus; CPu: caudate-putamen complex; NAc: nucleus accumbens; OTu: olfactory tubercle; PrL: prelimbic cortex; Cg1: cingular cortex; M: motor cortex; AID: agranular insular cortex.

MbDN subpopulations are diverse on different levels, including somatic localization, axonal projections, electrophysiological activity and the susceptibility to death in PD. The different levels of diversity are described in the following sections and are summarized in Table 1.

1.2 Neuroanatomy of MbDNs

MbDN subpopulations are diverse in their anatomical position. Thus, MbDNs of the SNpc are located in the lateral vMb, whereas DA neurons of the VTA can be found in the medial vMb. Based on their localization, MbDNs of the VTA can be further divided into five subpopulations (Figure 1A, Table 1). The medially located nuclei form the ventromedial VTA

(vmVTA): these are the intrafascicular nucleus (IF), the rostral (RLi) and caudal (CLi) linear nucleus and the paranigral nucleus (PN). The parabrachial pigmented nucleus (PBP) is located laterally and forms the dorsolateral VTA (dlVTA). Both PN and IF, as well as CLi, are cell-body-rich zones, whereas PBP and RLi are cell-body-poor zones (Ikemoto, 2010). In addition, the MbDNs of the SN can be further divided into the SNpc and the SN lateralis (SNl); the SNl forms the most lateral aspect of the SNpc.

1.3 Morphology of MbDNs

Cells of different MbDN subpopulations can be defined morphologically. While the cell bodies in the SNpc are large, angular and elongated, with an average mean diameter of ~19 µm, the VTA MbDNs are small, rounded cells, with an average diameter of ~13 µm (Tork, et al., 1984; Thompson et al., 2005). In addition, MbDNs in the SNpc and VTA can be further distinguished by their dendritic morphology. Whereas the dendrites in the SNpc are organized in horizontal and vertical planes, there are no vertical dendrites in the VTA (Phillipson, 1979). Interestingly, different cell and dendrite morphology was demonstrated within the SNpc. Thus, MbDNs located in the dorsal regions of the SNpc are typically fusiform with 2-5 dendrites emanating from the pole of the neuron, branching sparsely within the area. In contrast, MbDNs located more ventrally are multipolar in shape with dendrites emanating from the soma and extending laterally. The neurons in the VTA have also 3-5 dendrites emanating radially from the soma (Phillipson, 1979). A recent study showed however no differences in dendritic size, complexity and relative extension into SN reticulata (SNr) between MbDNs of the SNpc and the VTA (Henny et al., 2012). The morphology of the RRF MbDNs has not been described.

1.4 Molecular marker profile expression of MbDNs

In addition to their anatomical position and morphology, MbDNs can be further distinguished by their expression of distinct molecular markers. It has been shown that MbDNs of the SNpc and the VTA differ in their expression of DA receptors. There are two families of G-protein-coupled DA receptors: the D1 and D2 family. The D1 family, which includes D1 and D5 receptors, stimulates adenylyl cyclase and activates cyclic AMP-dependent protein kinase, whereas receptors of D2 family (D2, D3 and D4) inhibit adenylyl cyclase (Missale et al., 1998). Both types of DA receptors are found in the MbDNs of the SNpc. However, MbDNs of the vmVTA do not have any functional somatodendritic D2 autoreceptors and express very low mRNA levels of D2 receptors (Lammel et al., 2008).

Furthermore, G-protein-regulated inward-rectifier potassium channel 2 (Girk2) is only expressed in MbDNs of the SNpc and in some MbDNs in the lateral VTA. MbDNs in the vmVTA, some dlVTA, the RRF as well as RLi and CLi nuclei express the calcium-binding proteins calbindin and calretinin (McRitchie et al., 1996). In addition, the DA transporter (DAT) is also differently expressed in MbDN subpopulations. DAT is a plasma membrane transporter protein controlling extracellular DA concentrations through the recapture of DA into nerve terminals of MbDN. MbDNs, located in the PN, IF and RLi have lower DAT expression than neurons of PBP and SNpc (Lammel et al., 2008; Di Salvio et al., 2010; Simeone et al., 2011). A similar expression pattern was observed for vesicular monoamine transporter of the type 2 (VMAT2), which controls synthesis and packaging of DA.

Finally, orthodentical homeobox 2 (Otx2), which plays an important role in the proper development of MbDN (Secsion 1.13) (Prakash et al., 2006) is exclusively expressed in a subset of dlVTA (PBP) MbDNs (Di Salvio et al., 2010). Interestingly, it is prevalently excluded from those neurons, which express Girk2 and high levels of glycosylated active form of DAT (Di Salvio et al., 2010; Simeone et al., 2011).

1.5 Subpopulation of MbDNs co-release other neurotransmitters

Accumulating evidence over the last ten years indicates that MbDNs may also release other neurotransmitter. It has been shown that a subset of MbDNs is able for co-express the vesicular glutamate transporter, vGlut2 (Joyece and Rayport, 2000; Dal Bo et al., 2004; Mendez et al., 2008; Berube-Carriere et al., 2009). vGlut2 transports glutamate into synaptic vesicles for release at presynaptic terminals in DA neurons. MbDNs co-expressing vGlut2 (MbDN-vGlut2) are primarily found in the VTA (Kawano et al., 2006; Yamaguchi et al., 2007). Detailed analysis of the vGlut2 mRNA content showed that only some cell groups in the VTA co-express vGlut2. MbDN-vGlut2 neurons were found in the rostral VTA, PBP, IF and the RLi (Yamaguchi et al., 2011; Gorelova et al., 2012), while vGlut2 neurons (vGlut2-only) are located in the PBP and PN (Yamaguchi et al., 2011).

In addition, recent study has demonstrated that MbDNs in the SNpc projecting to the striatum are capable of co-releasing gamma-aminobutyric acid (GABA). Interestingly, these neurons use VMAT2 for GABA release instead of the vesicular GABA transporter (VGAT) (Trisch et al., 2012).

1.6 Projections of MbDNs

MbDN subpopulations are diverse in their projections to different target areas. Classically, the following projections have been allocated to different MbDN subtypes: MbDNs of the SNpc primarily project to the dorsal striatum and form the nigrostriatal pathway (Veening et al. 1980; Gerfen et al., 1987), VTA neurons send their axons to the limbic structures, mainly to the ventromedial striatum (the Nucleus accumbens (NAc), the olfactory tubercle (OTu)), the amygdala and the PFC, giving rise to mesolimbic and mesocortical pathways, respectively (Berridge and Robinson, 1998; Salamone and Correa, 2002; Schultz, 2002; Wise, 2002; Ungless, 2004) (Figure 1B). MbDNs in the RRF primarily project to the SNpc and the VTA, but also to the hippocampal formation and the medullary and pontomedullary brainstem (Krosigk and Smith, 1991; Gasbarri et al., 1996). Accumulating evidence revealed that this type of distinction is oversimplified. Recent studies showed that there is a significant intermixing of MbDN subpopulations with different projection targets (Bjorklund and Dunnet, 2007; Ikemoto, 2007; Ferreira et al., 2008; Wise, 2009), which results in more complicated innervation of striatal and cortical areas.

A more detailed analysis of the VTA projections based on anatomical and functional criterion (Ikemoto, 2010) shows a mediolateral gradient in their innervation. Thus, vmVTA (IF and PN) MbDNs primarily project to the ventromedial striatum, consisting of the medial accumbens shell, as well as to the medial OTu, whereas the dlVTA (PBP) innervates the ventrolateral striatum, consisting of the lateral shell and core of NAc, and the lateral tubercle (Ikemoto, 2005 and 2010). Retrograde tracing studies revealed that the RLi provides inputs to the lateral shell of the NAc as well (Swanson, 1982; Hasue and Shammah-Lagnado, 2002). In addition, MbDNs of the RLi project into the diagonal band, as part of the septal nuclei, as well as into the pallidal zone of the OTu (Del-Fava et al., 2007; Ikemoto, 2010). Del-Fava et al. showed that most of the mesocortical projections originate from the RLi MbDNs. Thus, the RLi innervates the infralimbic, prelimbic and anterior cingulate cortices, as well as the agranular insular and orbital areas (Table 1) (Del-Fava et al., 2007).

In addition, MbDN subpopulations differ in their afferent connectivity, which subserves different behavioral functions. Areas projecting to MbDNs of the SNpc and the VTA are strongly segregated. Thus, MbDNs of the SNpc receive their inputs preferentially from dorsal regions, such as dorsal striatum, globus pallidus and entopeduncular nucleus, whereas projections to the VTA MbDNs originate from ventral areas, such as ventral striatum, OTu and ventral pallidum (Lammel et al., 2012; Watabe-Uchida et al., 2012).

1.7 Physiology of MbDN subpopulations

Electrophysiological studies using *ex vivo* brain slice preparation and *in vivo* recording show that MbDNs are spontaneous pacemakers that generate regularly spaced action potentials (AP) in frequencies between 1 and 10 Hz (Grace et al., 2007). However, MbDNs operate within two distinct frequency bands: tonic and phasic. Tonically firing MbDNs discharge at low frequencies individual AP without bursts (Grace and Bunney, 1984), whereas phasic MbDNs fire bursts of near 20 Hz and greater (Robinson et al., 2004). Patch-clamp recording from *in vitro* brain slices revealed that MbDNs of the SNpc and the dlVTA fire in tonic mode with typically broad single AP (1–3 Hz), while spontaneous discharge frequencies of the vmVTA neurons are much faster with the range upper limit of 10 Hz (Lammel et al., 2008). Interestingly, the vmVTA MbDNs with low DAT and VMAT2 mRNA expression are the fast-firing neurons (Lammel et al., 2008).

Furthermore, several studies have highlighted the important role of voltage-gated L-type calcium channels for creating the basic subthreshold membrane potential oscillations that underlie pacemaker activity (Puopolo et al., 2007). However, the calcium dependence of the spontaneous pacemaker is not a homogenous property of all MbDNs (Chan et al., 2007; Puopolo et al., 2007). When Ca^{2+} is replaced by equimolar concentration of cobalt, or when calcium channels are blocked, MbDNs of the SNpc completely stop firing (Puopolo et al., 2007; Khallq and Bean, 2010). In contrast, the inhibition of calcium channels does not prevent firing in MbDNs of the VTA (Chan et al., 2007). Moreover, it has been suggested that this difference in calcium currents between SNpc and VTA MbDNs is a possible mechanism for the selective vulnerability of SNpc MbDNs in PD (Section 1.9) (Chan et al., 2007).

The presence of hyperpolarization-activated cyclic nucleotide-gated (HCN) channels in the neurons of SNpc has been used in many studies as a functional criterion to identify and define MbDNs (Grace et al., 2007). The activation of HCN channels can be caused in response to injections of hyperpolarizing currents and leads to a so-called „sag-component“ (Seutin et al., 2001; Neuhoff et al., 2002; Zolles et al., 2006). In contrast, MbDNs in the medioposterior VTA possess only few functional HNC channels, indicating that their electrophysiological properties might be very different from that of the MbDNs in the SNpc (Neuhoff et al., 2002). It has been also confirmed in *in vitro* study, that mesocortical MbDNs in vmVTA demonstrate no obvious „sag components“, which correspond to a lack of functional HCN currents (Table 1) (Lammel et al., 2008, 2011). Moreover, mesocortical neurons also lack apamin-sensitive small-conductance calcium-activated potassium (SK) channel-mediated AP afterhyperpolarization compared to mesostriatal MbDNs (Wolfart et al., 2001).

Interestingly, it has been demonstrated, that VTA MbDNs display two different electrical activities. Thus, MbDNs in the vmVTA exhibit a smaller hyperpolarization-activated current than MbDNs in the dlVTA (Hnasko et al., 2012). dlVTA MbDNs also show larger and more prolongated afterhypopolarization than vmVTA MbDNs.

1.8 Functions of MbDNs

Because of their position and the target structure the MbDN subpopulations innervate, they can be further separated into functionally distinct subgroups. Since neurons of the SNpc almost exclusively innervate the dorsolateral striatum, the SNpc serves mainly as an input to the basal ganglia circuit and supplies the striatum with DA. The basal ganglia circuit is involved in enabling practiced motor acts and in gaiting the initiation of voluntary movements by modulating motor programs stored in the motor cortex. Inputs from the cortex enter this circuit via the striatum. There are two pathways, which have opposite effect on cortical neurons. The direct pathway excites the cortex via the globus pallidus external, whereas the indirect pathway inhibits the cortex through the nucleus subthalamicus and globus pallidus internal. The role of the nigrostriatal projections is to keep those two pathways in balance. Direct pathway striatal neurons have D1 receptors, which depolarize the cell in response to DA. In contrast, indirect pathway striatal neurons possess D2 receptors, which hyperpolarize the cell in response to DA. Thus, SNpc MbDN projections have the dual effect of exciting the direct pathway while simultaneously inhibiting the indirect pathway. Loss of SNpc MbDNs causes an imbalance by increasing the activity of indirect pathway and decreasing the activity of direct pathway. This imbalance results in motor symptoms of PD (Section 1.9).

VTA neurons, via projections onto forebrain structure such as the NAc, PFC, and amygdala, play a key role in operant conditioning (Pavlovian learning based on association of environmental stimuli with reward) and motivation. Electrophysiological and lesion studies have demonstrated that activation of MbDNs in the VTA have positive reinforcing properties, because pharmacological or electrical stimulation tends to facilitate reward seeking. In contrast, inhibition or lesion of the VTA MbDNs results in a reduced reward seeking (Cheer et al., 2007; Fields et al., 2007). Behavioral and pharmacological studies have identified different zones within the VTA, based on their projections to the striatal areas, which are differently responsible for rewarding effects or for drug abuse. For example, rats rapidly learn to self-administer psychomotor stimulants such as cocaine, amphetamine or DA receptor agonist into the medial OTu and medial accumbens shell, suggesting that axonal projections

from the vmVTA are involved in drug reward (Carlezon et al., 1995; Ikemoto et al., 1997; Rodd-Henricks et al., 2002; Ikemoto, 2003; Ikemoto et al., 2005).

A number of studies revealed a critical involvement of DA in the modulation of neuronal activity related to cognitive processing. Electrophysiological studies on rodent and non-human primates showed that VTA MbDNs innervation in the PFC potentiates the firing of delay-active neurons thought to be critical for working memory (Williams and Goldman-Rakic, 1995; Goldman-Rakic, 1998). Moreover, MbDN projections from the VTA to the amygdala are implicated in learning and memory processes, particularly those involving behavioral responses to rewarding or aversive stimuli (Maren and Fanselow, 1996; Everitt et al., 1999; Koob, 1999).

1.9 Neurodegeneration of MbDNs in Parkinson's disease

Because of their different functions and involvement in several common human neurological disorders, MbDNs have been the focus of clinical interest and a subject of intensive studies for a long time. Degeneration of the SNpc MbDNs is associated with PD, which is characterized by the cardinal motor features of rigidity, bradykinesia and tremor at rest along with non-motoric symptoms like autonomic, cognitive and psychiatric problems (Marsden, 1994). The classical neuropathological hallmark of PD is the pathogenetic fibrillization of the protein α-synuclein and the accumulation of abnormal cytoplasmatic inclusions, known as Lewy bodies that are present in the surviving MbDNs in SNpc (Spillamtini et al., 1997; Mezey et al., 1998). In the following decade numerous studies have established that the motor symptoms are attributed to the loss of MbDNs in the SNpc and the decline of DA in the striatum, which are responsible for most, if not all, motor symptoms (Fearnley and Lees, 1991; Marsden, 1994). Intensive research of PD revealed that the majority of cases are sporadic and thought to be caused by environmental factors, a genetic causation or a combination of the two, while less that 10% of PD has a strict familial etiology. Numerous studies indicate that oxidative stress, inflammation, aberrant protein degradation and, in particular, mitochondrial dysfunction may be involved in the PD-associated neuronal degeneration (Moore at al., 2005; Abou-Sleiman et al., 2006). In recent years, mutations or polymorphisms in numerous nuclear genes (α-synuclein, parkin, UCHL1, DJ-1, LRRK2, Pink1, tau, HTRA2, NR4A2 and ATP13A2) have been identified as associated with familial PD (Ramirez et al., 2006; Klein and Schlossmacher, 2006; Schapira, 2006).

Elevated intracellular Ca^{2+} concentrations and lack of intrinsic Ca^{2+} buffering capacity in the MbDNs SNpc create mitochondrial oxidant stress (Guzman et al., 2010). Furthermore, *in*

vitro studies demonstrated that DAT activity depends on its glycosylation status, with the glycosylated DAT form transporting DA more efficiently than the non-glycosylated form (Torres et al., 2003; Li et al., 2004). Interestingly, it has been shown that somata and terminals of the nigrostriatal compartment (ventrocaudal SNpc and dorsal striatum) have higher expression levels of glyco-DAT than those of the rostromedial SNpc (Afonso-Oramas et al., 2009). In PD MbDNs located in ventrolateral and caudal region of the SNpc are more vulnerable than those in the rostromedial and dorsal region (German et al., 1989; Damier et al., 1999), suggesting that differences in DAT post-transcriptional regulation may be involved in the differential vulnerability of MbDNs (Gonzales-Hernandez et al., 2004).

1.10 MbDNs in psychiatric and neurological disorders

The other important role of DA as a neuromodulator has been shown in abnormal neurotransmission of VTA MbDNs, which is thought to occur in a variety of psychiatric and neurological disorders, such as schizophrenia, attention-deficit/hyperactivity disorder (ADHD) and reinforcing effects of drug abuse.

Schizophrenia is one of the most common mental disorders characterized by a breakdown of thought processes and by poor emotional responsiveness. Common symptoms include visual and auditory hallucinations, disorganized speech and thinking, or paranoid delusions. It has been proposed that an imbalance in DA levels in the PFC and ventral striatum underlie the symptoms in schizophrenia ("DA hypothesis"). It is thought that a functional excess of DA or oversensitivity of certain DA receptors contributes to the psychotic symptoms such as delusions and hallucinations (Birtwistle and Baldwin, 1998; Sesack and Carr, 2002). In schizophrenic patients the number of D1 receptors is decreased in PFC (Kaplan and Sadock, 1995). This occurrence explains certain cognitive deficiencies and is thought to be responsible for the negative symptoms of schizophrenia such as restrictions in range intensity of emotion fluency and productivity of thought and speech, and goal-directed behavior. In contrast, DA receptors of the D2 family seemed to be abnormally increased in the basal ganglia and limbic system of schizophrenic patients (Sedvall and Farde, 1995; Kaplan and Sadock, 1995). Additional evidence for the DA hypothesis is that most antipsychotic drugs act by blocking the D2 receptor.

Dysregulation of the DA transmission in the limbic system has been linked to development of the drug addiction (Kelley and Berridge, 2002; Wightman and Robinson, 2002) and depression (Dailly et al., 2004). The involvement of DA in drug reinforcement is well established, however its role in drug addiction is much less clear. Interestingly, it has been

demonstrated that increase of DA in the striatum can be caused by drug conditioned cues in cocaine-addicted subjects. Moreover, the magnitude of the DA increase was correlated with the subjective experience of craving (Wong et al., 2006; Volkow et al., 2010). However, the molecular mechanism of addiction might involve impaired serotonin or noradrenalin neurotransmission. Mice in which DAT was disrupted, failed to alter baseline extracellular DA levels and to induce behavioral effects such as enhanced locomotor activity (Giros et al., 1996). However, these mice still can be trained to self-administer cocaine despite persistently high levels of DA in the striatum, suggesting a more complex basis for the reinforcement (Rocha et al., 1998).

Not only dysregulation of DA neurotransmitter, but also dysfunction of some proteins involved in DA synthesis, release or uptake, have been shown to be implicated in a number of DA-related disorders, including ADHD, bipolar disorder, clinical depression, and alcoholism. ADHD is a psychiatric and a neurobehavioral disorder, characterized by either significant difficulties of inattention or hyperactivity and impulsiveness. There is converging evidence that increased DAT plays a major role in the pathophysiology of ADHD (Krause et al., 2003; Spencer et al., 2005; Krause, 2008). Knockout studies with mice lacking D2 receptor have demonstrated the reduction of hyperactivity, suggesting that D2 receptor-selective agonist is good candidate for a specific therapeutic approach that could provide better mechanistic resolution that psychostimulants in the treatment of ADHD (Fan et al., 2010).

1.11 Diversity of MbDNs

The diversity of MbDNs can be described on many levels, ranging from classical anatomical and histological categories to molecular marker profiles, connectivity and functional electrophysiological properties (Liss et al., 2007; Lammel et al., 2008 and 2012). However, only little is known about whether and how these different levels of diversity are connected. There is evidence that the functional diversity is predominantly mediated by their specific inputs. For example, MbDNs in the dlVTA projecting to the lateral shell of NAc receive their afferents from the laterodorsal tegmentum and are involved in the reward behavior. Neurons of the lateral habenula form synapses with mesocorticolimbic neurons of the vmVTA, which project to the medial PFC and elicit aversion (Lammel et al., 2012). Furthermore, specific molecular profiles of MbDNs correlate with their projections and electrophysiological properties (Lammel et al., 2008). In addition, MbDNs show large differences in their susceptibility to cell death in PD, which is linked to their distinct molecular profiles.

Table 1 Distinct identities of MbDN

Subtype	Anatomy	Morphology	Molecular markers	Axonal projections	Physiology	Function	Diseases
SN	SNpc SNl	large, angular and elongated cell bodies (Tork et al., 1984; Thompson et al., 2005)	Girk2 (Chung et al., 2005), DAT, VMAT2 (Lammel et al., 2008)	CPu (Gerfen et al., 1987)	low frequency (Grace et al., 2007), tonic activity HCN-channel (Lammel et al., 2008)	Motor control (Wise et al., 2004), spatial learning (Da Cunha et al., 2006)	PD (Mardsen, 1994)
dlVTA	PBP	Medium size, rounded cell bodies (Tork et al., 1984; Thompson et al., 2005)	Girk2 (Reyes et al., 2012) Calbindin, DAT, VMAT2, low Otx2 (Di Salvio et al., 2008; Simeone et al., 2011)	lateral shell and core of NAc, lateral OTu, central nucleus of amygdala, lateral part of lateral habenular nucleus (Ikemoto, 2005, 2010)	low frequency, tonic activity, HCN-channel (Lammel et al., 2008)	Motivation, operant conditioning (Cheer et al., 2007; Fields et al., 2007)	Drug abuse, depression, ADHD (Kelley & Berridge, 2002; Wightman & Robinson, 2002; Dailly et al., 2004; Krause et al., 2005)
vmVTA	IF, PN, RLi, CLi	small, rounded cell bodies (Tork et al., 1984; Thompson et al., 2005)	Calbindin, calretinin (McRitchie et al., 1996), low DAT, low VMAT2 (Lammel et al., 2008), Otx2, vGlut2 (Kawano et al., 2006; Yamaguchi et al., 2011; Gorelova et al., 2012)	medial shell of NAc, medial OTu, BLA, anterior amygdaloid area, diagonal part of the septal nuclei, prelimbic and infralimbic cortices, anterior cingulate, sensory and motor cortices, agranular insular and orbital areas, hippocampus, medial part of lateral habenular nucleus (Del-Fava et al., 2007; Ikemoto, 2010)	High frequency, phasic activity, no HCN-channel (Neuhoff et al., 2002; Lammel et al., 2011)	Drug reward, cognition, working memory (Goldman-Rakic et al., 1998; Ikemoto, 2003, 2005)	Schizophrenia drug abuse, ADHD (Sesack & Carr, 2002)

However, it still unclear how and when this diversity is established. To better understand the MbDN diversity in the vMb, there is still the need to gain deeper insights into the developmental and phenotypic characteristics of distinct subpopulations of MbDNs, based on their axonal projections and circuitry, synaptic connectivity and functional properties.
Knowledge about how and when this diversity is established during development might help to connect the different levels of diversity.

1.12 Development of MbDNs

A number of recent studies have conclusively shown that MbDNs arise from neuronal progenitors in the ventral midline (floor plate: FP) of the embryonic midbrain (Andersson et al., 2006; Ono et al., 2007; Kittappa et al., 2007; Bonilla et al., 2008; Joksimovich et al, 2009; Blaess et al., 2011). The development of MbDNs from proliferating neural precursors can be broadly divided into three stages (Figure 2) (Abelovich et al., 2007).

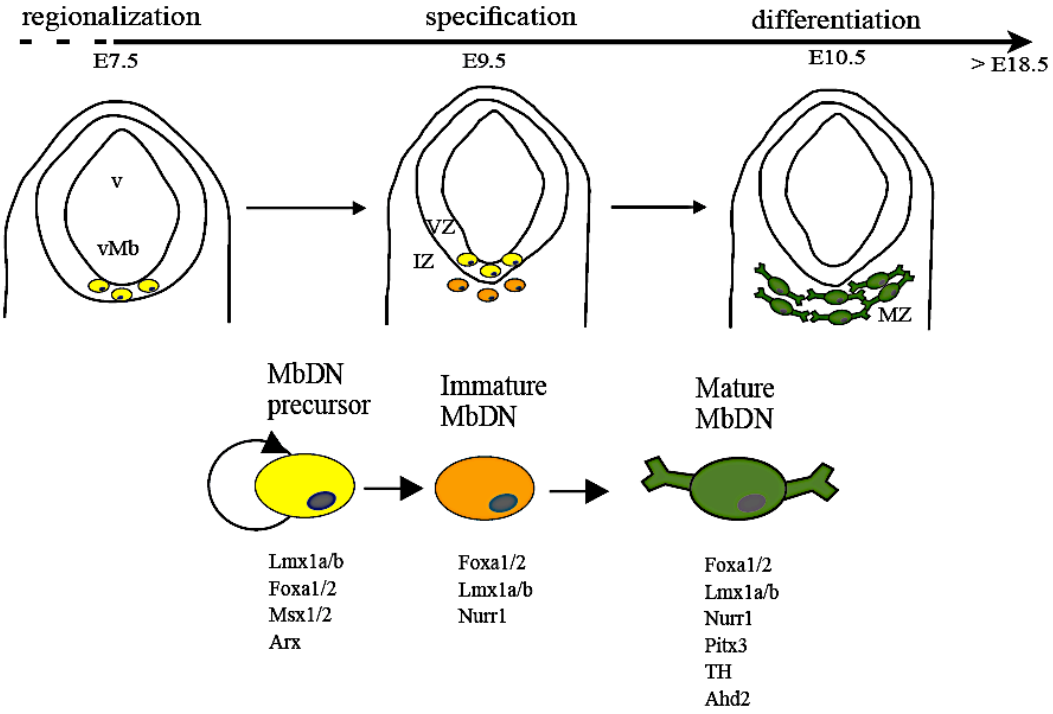

Figure 2 The timescale of MbDN development. During regionalization vMb tissue is determined and self-renewing precursors at the ventricular zone (VZ) give rise to MbDN precursors (MbDNp, yellow). In the specification stage MbDNp exit the cell cycle, enter the intermediate zone (IZ) and become immature MbDNs (orange). In the differentiation stage immature MbDNs migrate into the mantel zone (MZ) and establish appropriate connections. The curved arrow indicates proliferating cells. v: ventricle; vMb: ventral midbrain.

First, precursors at the ventral ventricular zone (VZ) of the anterior neural plate that have self-renewing properties and give rise to multiple cell types arise at embryonic day 7.5 (E7.5). In a second step, these are specified to a MbDN precursor (MbDNp) cell fate, and several molecular markers are associated with this population. In a third stage, the MbDNp exit the cell cycle, migrate into the mantel zone (MZ) and begin to display early MbDN markers (Figure 2). Finally, the early-differentiated MbDNs mature functionally, express mature MbDN markers, and establish appropriate connectivity. The development of MbDNs requires a complex combination of transcriptional regulators and diffusible signals to control both the acquisition and maintenance of the neurotransmitter-specific phenotype. However, little is known when and how different subgroups of MbDNs are specified during development.

1.13 Induction and regionalization of the ventral midbrain

Regionalization of the vMb begins early in neural plate development. During neurulation the lateral edges of the neural plate roll up along its anteroposterior axis to form the neural tube (Gale et al, 2008). Neuronal induction and pattering start around E7.5 and are mediated by a precise molecular coding along the anteroposterior and dorsoventral axis, which provides positional cues that are crucial in pattern formation. The anteroposterior axis is set up before the dorsoventral axis dividing the developing CNS into forebrain, midbrain, hindbrain and spinal cord. Dorsoventral patterning subdivides the neural tube from spinal cord to midbrain into the FP, basal plate, alar plate and roof plate (RP) (Liu and Joyner, 2001; Prakash and Wurst, 2006). Induction of the vMb is refined by local organizer, which provides vMb cells with positional information by expression of different diffusible signals (Figure 3).

The vMb (FP and alar plate) is induced by Sonic hedgehog (Shh) (Jessel, 2000; Lupo et al., 2006). *Shh* is secreted first from the notochord, which underlies the neural plate, and later on from the FP. Shh as a long-range morphogen is critical for the induction of ventral cell fates in many parts of the nervous system and directs the pattern of neurogenesis by conferring positional information to ventral progenitors (Jessell, 2000; Lupo et al., 2006). The crucial role of Shh in MbDNp induction is apparent in *Shh*-null mutant mice, in which MbDNs are completely missing (Agarwala et al., 2002; Fedtsova et al., 2001; Ishibashi et al., 2002; Blaess et al., 2006). Furthermore, conditional inactivation of Shh signaling by depletion of *Smoothened* (Smo), a Shh receptor, at E9.0 results in severe reduction of MbDNs (Blaess et al., 2006).

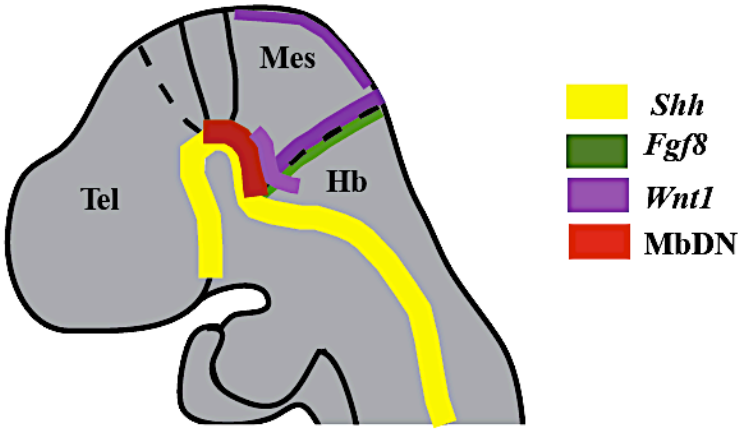

Figure 3 Expression of molecules involved in the regionalization and induction of MbDNp. Schematic of sagittal section through the mouse embryo. The region in the developing CNS where MbDNs develop is indicated in red. *Shh* (yellow line) is expressed in the FP along the neural tube, *Fgf8* (green line) is expressed at the mid-hindbrain border (MHB) and *Wnt1* (purple line) is expressed in the FP and RP of the midbrain, and at the MHB. Tel: telencephalon, Mes: mesencephalon, Hb: hindbrain.

Anteroposterior pattering is regulated by a neuroepithelial signaling center localized at the mid-hindbrain boundary (MHB) or isthmus. The isthmus is characterized by the expression of fibroblast growth factor (Fgf) 8 (Hynes et al., 1995a; Hynes et al., 1995b; Ye et al., 1998; Lee and Jessell, 1999; Andersson et al., 2006; Prakash et al., 2006). Conditional inactivation of Fgf8 in the midbrain and anterior hindbrain (aHb) results in cell death and failure in the midbrain development (Chi et al., 2003). Moreover, conditional inactivation of *Fgf* receptors, particularly *Fgf* receptor 1, results in midbrain and aHb defects (Trokovic et al., 2003 and 2005). Interestingly, explant culture experiments have demonstrated that both, Shh and Fgf8 are required for the induction of MbDNp before E9.5 (Ye et al., 1998), meaning that intersection of these secreted factors determines where the MbDNp domain will arise (Hynes et al., 1995; Jessel et al., 2000; Briscoe et al., 2001).

Along with Fgf8 and Shh, Otx2 and gastrulation brain homeobox 2 (Gbx2) are essential for the correct positioning of the MbDNp domain. Gbx2 and Otx2 are transcriptional repressors, which are expressed in the presumptive hindbrain and in the presumptive mid- and forebrain, respectively (Prakash et al., 2004; Ono et al., 2007; Liu et al., 2001). *Otx2* mutant mice show a complete depletion of the forebrain and midbrain (Ang et al., 1996). Furthermore, a subtle shifting of the Otx2 caudal expression boundary effects MbDN population in size (Acampora et al., 1997; Brocolli et al., 1999). Thus, expanded Otx2 expression in the caudal midbrain – aHb leads to a shift of MHB caudally and an increase of MbDNs (Brodski et al., 2003).

Furthermore, secreted molecule Wingless-type MMTV integration site family, member 1 (Wnt1) is expressed at the rostral border of the MHB and is known to regulate midbrain morphogenesis (Figure 3). *Wnt1* mutant mice show an abnormal posterior midbrain, isthmus and aHb, revealing its essential role in MHB formation (McMahon et al., 1990; Chilov et al., 2010). Moreover, a temporal requirement for Wnt1 in the induction of distinct MbDNp domains was demonstrated. Thus, inactivation of *Wnt1* at E9.0 results in almost complete loss of the medially positioned MbDNp domain (Yang et al., 2013). Furthermore, it has been shown that Wnt1 and Fgf8 cross-regulate each other (Matsunaga et al., 2002; Chi et al., 2003). Since Fgf8 failed to induce ectopic MbDN in *Wnt1* mutant embryos, it has been suggested that Wnt1, which can be induced by Fgf8, is a more direct regulator of initiation of the MbDNp field (Prakash et al., 2006).

1.14 Specification of MbDNs

While vMb precursor identity is established, the most ventrally located precursors start to be specified towards a MbDN fate. The neuroepithelium of the vMb first thickens by cell proliferation and then becomes layered. The cells in narrow band adjacent to the VZ maintain their proliferative precursor properties while other cells move out into the intermediate zone (IZ) (Figure 2). The induction of the MbDNp identity occurs within the VZ of the ventral midline. A network of transcriptional factors such as Foxa1/2 (forkhead/winged helix transcription factor 1 and 2), Lmx1a/b (LIM homeobox transcription factor 1, alpha and beta), Msx1/2 (homeobox msh-like 1) as well as Wnt1 signaling regulate the induction of MbDNp (Figure 4). Diffusible signaling molecules described above mediate the activation of these factors. Thus, *Shh* secreted from the notochord has been shown to directly induce the Foxa1/2 expression (Sasaki et al., 1997). Foxa2, in turn, directly induces vMb Shh expression through well-conserved Foxa2 binding sites in the *Shh* gene (Jeong and Epstein, 2003). Moreover, Foxa1/2 act downstream of Shh to alter a cell's competence to respond to Shh signaling by directly repressing *Gli2* expression (a main activator of Shh signaling, Section 1.17). In addition, Foxa1/2 regulate the pattering of vMb precursors by inhibiting the expression of Nkx2-2 (Figure 4) (Mavromatakis et al., 2011).

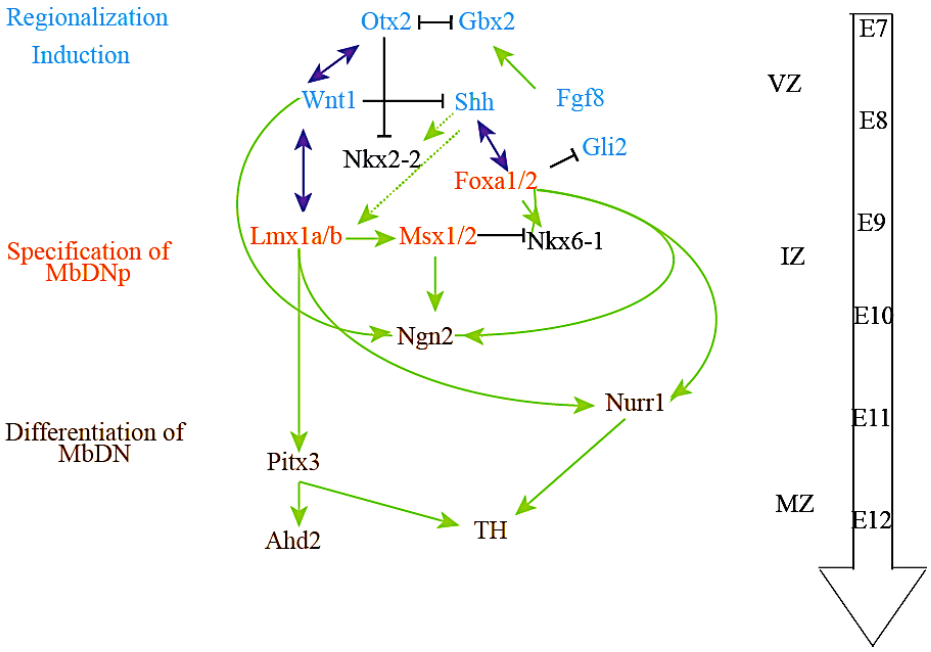

Figure 4 The genetic network regulating development of the MbDN. Arrows indicate the effect on expression: green = positive regulation, purple = autoregulatory loop, black = negative regulation. The factors are color-coded to indicate their role listed on the left side. VZ: ventricular zone; IZ: intermediate zone; MZ: mantel zone.

Several lines of evidence indicate that Wnt1 not only regulates the induction of MbDNp, but is also involved in MbDNp specification (Figure 3). ES cell culture studies identified that Wnt1 directly regulates the expression of the transcriptional factors Lmx1a/b and that removal of *Lmx1a* results in complete loss of *Wnt1* expression, revealing an autoregulatory loop between Wnt1 and Lmx1a (Chung et al., 2009; Yang et al., 2013). Lmx1a defines the MbDNp domain along with the aristaless related homeobox (Arx), transcriptional factor, which is expressed in the FP (Andersson et al., 2006; Joksimovic et al., 2009; Blaess et al., 2011; Hayes et al., 2011). *Lmx1b* null mice show a severe reduction in the number of MbDNs (Smidt et al., 2000), due to early loss of the midbrain (Guo et al., 2007). Furthermore, loss of *Lmx1a* results in pronounced loss of MbDNs (Andersson et al., 2006; Ono et al., 2007; Deng et al., 2011). Conditional inactivation of both transcriptional factors results in severe reduction in the MbDNp, suggesting that these two factors can compensate for each other's function (Deng et al., 2011). Furthermore, it has been shown that Lmx1a indirectly regulates neurogenesis by inducing expression of Msx1/2 transcriptional factors. Msx1/2 appear to induce neurogenesis by activating the proneural factor Ngn2 (neurogenin 2) (Andersson et al., 2006; Chung et al., 2009). *Msx1* null mice exhibit a 40% reduction in the normal number of MbDNs, likely as a result of the downregulation of Ngn2 expression (Andersson et al., 2006). Moreover, premature expression of Msx1 in the vMb in transgenic mice also leads to the

precocious expression of Ngn2, and to the downregulation of Shh in the FP (Chung et al., 2009) (Figure 4).

The transition of cells from the proliferation to differentiation is mediated by Ngn2. Ngn2 is severely reduced in double mutant mice for *Lmx1a/b* (Yan et al., 2011). Loss-of-function studies show that Ngn2 is the major proneural factor required for MbDN neurogenesis. Inactivation of *Ngn2* dramatically delays and reduces the number of MbDNs in the IZ (Kele et al., 2006; Andersson et al., 2006). Further findings suggest that Ngn2 controls differentiation of MbDNs through the regulation of Notch pathway genes, known to maintain precursor fate such as Hes5 (an effector of Notch signaling) and Dill1 (a Notch ligand) (Kele et al., 2006). Wnt1 regulates the development of MbDNs by controlling the cell cycle progression in the MbDNp. Thus, constitutive activation of Wnt/β-catenin (an intracellular signal transducer in the canonical Wnt pathway) results in an expansion of early MbDNp. However, it perturbs cell cycle progression in the progenitors and reduces the generation of MbDNs in vMb. Interestingly, further insights into the role of Wnt1/β-catenin pathway revealed that it is also required to maintain the integrity of radial glia, which actually give rise to MbDNs and provide scaffolds for newly generated MbDNs to migrate towards their final destination (Tang et al., 2009). Removal of β-catenin in MbDNp leads to a complete loss of cell polarity, which results in ectopic cell death and loss of MbDNs (Tang et al., 2009).

1.15 Differentiation of MbDNs

After MbDNp exit the cell cycle, they migrate ventrally along radial glia towards the MZ and begin to differentiate (Figure 2). These postmitotic MbDNp are not yet fully differentiated and continue to express a large set of genes from early MbDNp specification, but start to express the orphan nuclear receptor Nurr1 (nuclear receptor subfamily 4, group A, member 2) (Zetterstrom et al., 1997). In *Nurr1* knockout mice MbDNs fail to express genes, which are involved in DA synthesis, axonal transport, storage and release or reuptake of DA (Zetterstrom et al., 1997; Saucedo-Cardenas et al., 1998). Lmx1a/b directly regulate the expression of Nurr1 (Figure 4) (Chung et al., 2009).

The next step in the differentiation of MbDNs is characterized by the expression of pituitary homeobox 3 (Pitx3) transcriptional factor and TH, the rate limiting enzyme of DA synthesis. Lmx1b is involved in the initiating the expression of TH and Pitx3. Thus, in *Lmx1b* null mice, medially derived MbDNs are lost and the majority of remaining MbDNs fail to express TH and Pitx3 (Deng et al., 2011). Pitx3 is required for the proper differentiation of MbDNs by regulating TH expression (Maxwell et al., 2005). Interestingly, MbDN diversity is apparent

already during development. MbDNs located at the ventrolateral position of the MZ express Pitx3 prior to TH, whereas the dorsomedial MbDNs express TH ahead of Pitx3 at E12.5 (Maxwell et al., 2005). Later on, Pitx3 is expressed in all MbDN subpopulations. However, *Pitx3* deficient mice display severe reduction of the SNpc MbDNs, whereas the VTA neurons are relatively intact (Smidt et al., 1997 and 2004; Zhao et al., 2004).

A number of genes regulated by Pitx3 have been identified (Smits et al., 2006). One of these genes encodes the enzyme aldehyde dehydrogenase family 1 (Aldh 1a1: also known as Raldh1 or Ahd2). Ahd2 is under the transcriptional control of Pitx3, which binds to a highly conserved region of *Ahd2* gene (Jacobs et al., 2007). Ahd2 is involved in the production of retinoic acid (RA) from retinol, which is crucial for neuronal pattering and differentiation (McCaffery et al., 2003) and it is exclusively expressed in the lateral parts of the MbDN area. Prenatal RA treatment (E10.5-E13.5) of *Pitx3* deficient mice can rescue the phenotype and results in increased Ahd2 expression in the lateral parts of MbDNs at E14.5 (Jacobs et al., 2007).

Recent study suggested that Otx2 is also involved in the controlling of postmitotic aspects of MbDN differentiation and crucial for proper functioning of MbDNs in the adult brain (Di Salvio et al., 2010). Interestingly, Otx2 is expressed exclusively in a subset of MbDNs of the VTA and is completely excluded from the SNpc MbDNs in the adult brain.

1.16 Molecular heterogeneity of MbDNp domain

The diversity of MbDN system is created by a controlled ontogenetic process of their specification, migration and differentiation. The Lmx1a expression defines the MbDNp in the ventral midline. Medial progenitor cells express, besides Lmx1a, the transcription factors Msx1/2 and the cell surface molecule Corin, whereas laterally located progenitor populations express only Lmx1a (Andersson, 2006; Ono, 2007; Deng, 2011; Mavromatakis et al., 2011; Blaess et al., 2011). Analysis of *Lmx1a*- and *Lmx1b* deficient mice confirmed that there are at least two distinct MbDNp domains, which might contribute to discrete MbDN subtype populations. Thus, deletion of *Lmx1a* results in a specific loss of the medial MbDNp domain, whereas the lateral MbDNp domain is not established in *Lmx1b* null mutants, suggesting a selective requirement for Lmx1a/b in the specification of two distinct MbDNp. It has previously been demonstrated that Shh expression is dynamic in the vMb (Joksimovic et al., 2009; Blaess et al., 2011; Hayes et al., 2011 and 2013). First, *Shh* is released by cells in the notochord and induces *Shh* expression in the narrow medial domain overlying the notochord around E8.5. *Gli1* expression is a well-established readout for high levels of Shh signaling

and precedes *Shh* expression by about a day. Thus, *Gli* is initially expressed in the ventral midline of the neural tube at E7.5, while *Shh* is expressed by the cells of notochord (Hui et al., 1994). Once *Shh* expression is present in ventral midline cells around E8.5, *Gli1* expression is downregulated in the *Shh*-expressing cells and excluded from the midline, indicating that *Shh*-expressing cells cease responding to Shh signaling. The Shh domain expands more laterally until E10.5 and *Shh* expression begins to be downregulated medially (Ye et al., 1998; Prakash and Wurst, 2006; Blaess et al., 2011). The lateral expansion of *Shh*-expressing cells in the vMb over time results in gradually shifted lateral expression of Shh-responding cells (*Gli1*-expressing). At later developmental stages (E11.5 and E12.5) weak *Shh* expression is still detected in the medial domain (Blaess et al., 2011; Hayes et al., 2011). Genetic inducible fate mapping (GIFM) studies have demonstrated that the spatiotemporally dynamic *Shh* expression defines multiple progenitor pools and can potentially give rise to the distinct neuronal cell populations (Blaess et al., 2011; Hayes et al., 2011). In addition, conditional inactivation of Shh signaling pathway demonstrates that the crucial time period for Shh signaling in establishing MbDNs is between E8.0 and E10.0 (Blaess at al., 2006 and 2011). Making use of the changing *Shh*-expressing domains, GIFM sequentially defined two spatially distinct vMb progenitor domains that give rise to different subpopulations of MbDNs (Blaess et al., 2011; Hayes et al., 2011) (Figure 5).

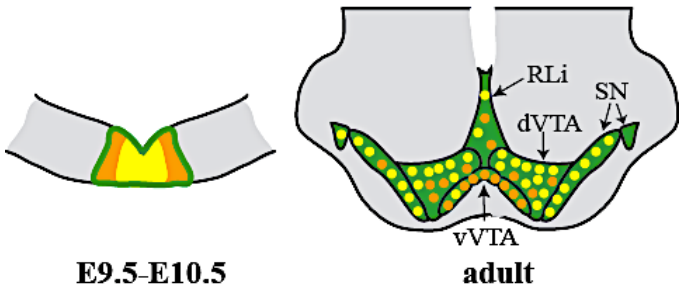

Figure 5 Distinct MbDN precursor domains give rise to different MbDN subpopulations. **(A)** Schematic of medial (yellow) and lateral (orange) MbDNp domains at E9.5-E10.5. **(B)** The medial domain contributes preferentially to the MbDNs of the SNpc (yellow dots) and dlVTA. The lateral MbDNp give rise to the MbDNs of the vmVTA and RLi.

After E9.5, precursor cells that continue to respond to Shh (express *Gli1*) are located in the lateroposterior aspects of the MbDNp domain and appear to adopt a certain fate of MbDN, since they preferentially give rise to MbDN in the vmVTA. Whereas MbDNp located at the ventral midline, which responds to Shh prior E9.5, show a bias to contribute to the SNpc (Blaess et al., 2011; Hayes et al., 2011). In addition, cells responding to Shh at E9.5 to E10.5 give rise to other vMb neurons, including the neurons in the oculomotor nucleus (OM) and

the non-MbDNs in the SNr (Figure 7). These data further support the idea that there are distinct subsets of MbDNp and suggest that the time or length of exposure to Shh signaling might be involved in pre-determining MbDN subset fate.

1.17 Shh pathway transduction

The transduction of Shh signaling occurs via the interaction of two cell surface receptors, the 12-transmembrane-domain protein patched (Ptch) and the seven-pass G-protein-coupled receptor smoothened (Smo) (Marigo et al., 1996; Stone et al., 1996; Goodrich et al., 1997; Ingham and McMahon, 2001) (Figure 6). Genetic and biochemical data indicate that in absence of Shh ligand, Ptch constitutively represses Smo activity (Chen et al., 1996). When bound by Shh, the inhibition of Smo by Ptch is relieved, allowing Smo to transduce Shh signaling intracellularly (Alcedo et al., 1996). Smo acts intracellularly by activating or repressing Gli family zinc-finger transcriptional factors. In mouse, there are three Gli proteins that transduce the Shh signal. Gli3 functions primarily as a transcriptional repressor whereas Gli1 and Gli2 function as activators (Matise et al., 1998; Bai et al., 2002, 2004; Pan et al., 2006). In the absence of Shh, Gli3 is proteolytically processed to generate a transcriptional repressor (Figure 6) and Gli2 is completely degraded (Pan et al., 2006).

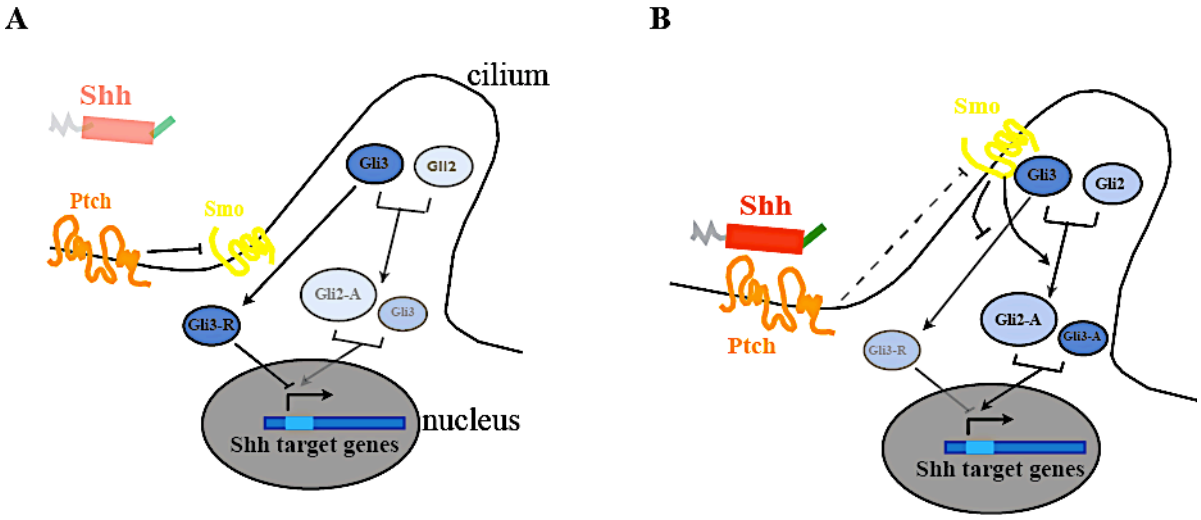

Figure 6 Schematic of canonical Shh signaling pathway. Shh signaling occurs in primary cilia. **(A)** In absence of Shh, the activity of Smoothened (Smo) is repressed by Patched (Ptch). Gli2 is degraded. Gli3 is processed into a Gli3 repressor (Gli3-R), which blocks the expression of Shh target genes. **(B)** Binding of Shh releases inhibition of Smo by Ptch and allows it to enter the cilium. Consequently, Gli2 and Gli3 are activated (Gli2A and Gli3A). Gli2A induces Shh target genes (e.g. Gli1 and Ptch).

Presence of Shh induces the formation of Gli2 and to a lesser extent Gli3 activators (Bai et al., 2002; Persson et al., 2002). Moreover, Shh inhibits the proteolytic processing of Gli3 into a repressor form and decreases its expression on a transcriptional level. Gli2 activator function is essential for the induction of the ventral most cell types, including the FP, whereas the proper regulation of Gli3 repressor levels controls the patterning of more dorsal region. *Gli1* expression is completely dependent on Gli2/Gli3 activator function and is readout for high levels of Shh signaling. A number of recent *in vivo* and *in vitro* studies have shown that Shh signaling occurs in primary cilia. In the absence of Shh, Ptch is localized to the primary cilium, whereas Smo is localized to the plasma membrane of the cell body (Figure 6). Upon Shh exposure, Ptch allows Smo to enter the cilium, where it promotes the activation of Gli2 and inhibits the formation of Gli3 repressor, resulting in the activation of target genes (Corbit et al., 2005). The formation of Gli3 in the absence of Shh signaling also requires primary cilia (Haycraft et al., 2005; Liu et al., 2005; May et al., 2005).

1.18 Other ventral midbrain cells regulated by Shh signaling

A number of developmental studies have shown that the VZ of the vMb can be divided into three molecularly distinct domains at E10.5 (Figure 7A). As described previously, cells at the ventral midline express Lmx1a and give rise to MbDNs. Oculomotor (OM) and red nucleus (RN) neurons are generated immediately lateral to the Lmx1a positive MbDNp domain from cells that express Foxa2, Sim1, Nkx6-1 and Nkx6-2. Progenitors located lateral to the Foxa2 domain express Nkx2.2 and differentiate into GABAergic neurons (Figure 7A) (Kala et al., 2009). The neurons of the RN and OM complex are involved in the control of movement. The OM nucleus gives rise to the third (nIII) cranial nerve and innervates the ipsilateral extraocular muscles and ciliary ganglion, thereby controlling most eye movements, eye accommodation and pupil contraction (Figure 7B). The neurons of OM complex are characterized by expression of the LIM homeodomain transcriptional factor islet1 (Isl1) and the homeobox gene Mnx1 (motor neuron and pancreas homeobox 1), generic motor neuron markers (Ericson et al., 1992; Agarwala and Ragsdale, 2002). The crucial role of Isl1 for survival of motor neurons in the spinal cord was demonstrated in the loss-of-function study (Pfaff et al., 1996), but its function in OM development remains unknown.

The RN consists of the anterior parvocellular and the posterior magnocellular part (Evinger, 1988). Both parts of the RN contain excitatory glutamate and inhibitory GABA-synthesizing neurons, which project to the cerebellum, brainstem and spinal cord (Keifer and Houk, 1994). Together with the corticospinal tract, the rubrospinal tract plays a fundamental role in the

control of limb movements (Kennedy, 1990). The neurons of the RN can be identified by expression of the POU homeobox transcription factor Pou4f1 (also known as Brn3a), which is required for survival of postmitotic RN neurons (Turner et al., 1994; Fedtsova and Turner, 1995; McEvilly et al., 1996; Xiang et al., 1996; Agarwala and Ragsdale, 2002).

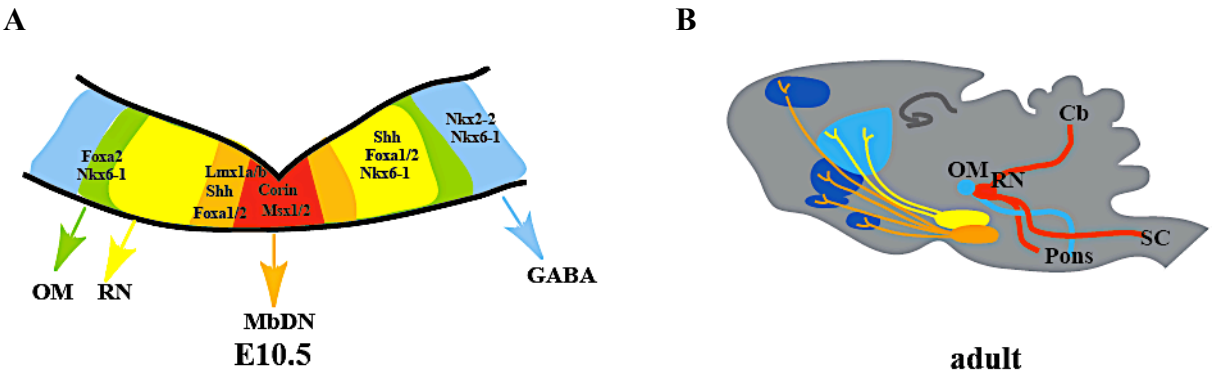

Figure 7 vMb precursor domains give rise to different neurons. (A) Schematic view of vMb precursor domains at E10.5. Lmx1a^{pos}/Shh^{pos}/Foxa2^{pos} domain (orange) gives rise to MbDNs. Medial Lmx1a^{pos}/Corin^{pos}/Msx1/2^{pos} domain (red) gives rise to the VTA MbDNs, whereas Lmx1a^{pos}/Corin^{neg}/Msx1/2^{neg} domain (orange) gives rise to the SNpc MbDNs. Shh^{pos}/Foxa2^{pos}/Nkx6-1^{pos} precursors (yellow) give rise to the neurons of the red nucleus (RN). The oculomotor nucleus (OM) is derived from the Foxa2^{pos}/Nkx6-1^{pos} domain (green), whereas GABAergic neurons arise from the Nkx2.2^{pos}/Nkx6-1^{pos} domain (blue). **(B)** RN (red) and OM (blue) projections into the cerebellum (Cb), pons and spinal cord (SC).

Birthdating experiments demonstrated that OM neurons develop between E9.2 and E9.7, whereas RN neurons are generated between E10.2 and 10.7 (Prakash et al., 2009). Shh plays a crucial role in the induction of these neurons (Watanabe and Nakamura, 2000; Fedtsova and Turner, 2001; Agarwala and Ragsdale, 2002; Blaess et al., 2006; Bayly et al., 2007; Fogel et al., 2008). *Nkx6-1* null mutant mice display a severe reduction in the number of RN and OM, demonstrating that Nkx6-1 is intrinsically required for the generation and identity of those neurons (Prakash et al., 2009). In addition, Otx2 plays an important role in the development of RN and OM nuclei. Conditional inactivation of *Otx2* in the midbrain results in a complete loss of the RN and hypoplasia of the OM (Puelles et al., 2004). In contrast, ectopic expression of Otx2 results in ectopic expression of Nkx6-1 and ectopic generation of RN, suggesting an important role of Otx in induction and maintenance of Nkx6-1 expression in the vMb (Prakash et al., 2009). Notably, only ectopic RN neurons were detected in the rostral hindbrain, but not OM neurons, meaning that Otx2 is sufficient for the generation of RN but not of OM complex.

Lmx1b and Foxa2 are also involved in the generation of OM and RN neurons (Deng et al., 2011), since *Lmx1b* null and *Foxa2* null mutants display an almost complete loss of OM neurons and a significant increase in the number of RN cells. The imbalance in *Lmx1a* and

Foxa2 expression determines the fate of these neurons. Thus, Lmx1b is necessary for the generation of OM and for the suppression of RN neurons at early developmental stages, whereas inactivation of Foxa2 results in a loss of OM and striking overproduction of RN neurons (Deng et al., 2011).

1.19 Shh signaling and its role in the development of the central nervous system

In the nervous system, Shh has been studied in detail in the induction of different ventral cell types in the spinal cord (Fuccillo et al., 2006; Dessaud, et al., 2007). Shh acts as a morphogen in a concentration-dependent manner and determines spatially distinct progenitor domains along the ventrodorsal axis (Jessel, 2000). Distinct concentration levels of Shh induce expression of specific sets of homeobox transcription factors. Each progenitor domain generates one or more distinct neuronal subtypes, the identity of which is determined by the combination of transcription factors expressed by the precursors (Lupo et al., 2006). The progenitor domain in the ventral midline of the developing spinal cord receives the highest concentration of Shh from the notochord and develops into the FP. Once FP cells are determined, they begin to express *Shh*. Overall, six different progenitor domains/neuronal cell types are generated in response to different levels of Shh (Briscoe, et al., 2000). In *Shh*-deficient mice neither the FP domain, nor six distinct cell types are generated (Wijgerde et al., 2002). A number of recent studies in the spinal cord have demonstrated that Shh does not only elicit a concentration-dependent response (as expected from a morphogen), but that the duration of Shh signaling can also influence the cell's fate decision (Dessaud, 2007 and 2008, Balaskas et al., 2012). A "temporal adaptation" model has been proposed, that relies on a progressive decrease in the sensitivity of receiving cells to ongoing Shh signaling (Dessaud et al., 2007). First, cells appear to be highly sensitive to Shh signaling and low concentration of Shh is sufficient to evoke high levels of Gli activity. With increasing time, cells become desensitized to ongoing Shh signaling and only high concentration of Shh can evoke the highest levels of Gli activity increases. Consistent with this model, gain-of-function experiments suggest that progressive changes in the level of Gli activity are sufficient to recapitulate the patterning activity of graded Shh signaling (Li et al., 2004). As a result, changes in the concentration or the duration of Shh have an effect on intracellular signaling in the spinal cord.

2. Aim of the thesis

MbDNs play pivotal roles in the regulation of many important brain functions including motor control, emotion and cognition. They form several subpopulations, which are divergent in their physiological and functional features as well as vulnerability to neurodegeneration in PD. The diversity of these subpopulations is partially correlated with their anatomical organization and incoming and outcoming connectives. However, little is known about how this diversity is established during development. Shh signaling is required for the generation of MbDNp between E8.0 to E10.5 (Andersson et al., 2006; Blaess et al., 2006). However, after E9.5 only precursors located in the lateroposterior aspects of the MbDNp domain continue to respond to Shh and preferentially give rise to MbDNs in the vmVTA (Blaess et al., 2011; Hayes et al., 2011). These data suggest that distinct subsets of MbDNp exist, and that their generation is governed by the temporospatial dynamics of Shh signaling.

To investigate whether Shh signaling plays an instructive role in determining different subsets of MbDNp, high level Shh signaling shall be inactivated between E8.5-E9.0, about a day after MbDNp start to respond to Shh signaling and day before lateral MbDNp cease to respond to Shh. This shall be achieved by conditional removal of *Gli2*, the main downstream activator of Shh signaling. Immunohistochemical and RNA *In Situ* hybridization analysis of MbDNp shall provide important insights into the mode (direct or indirect) and timing of Shh signaling in specification of MbDNs. Examination of MbDNp domain in the developing vMb and MbDNs in the adult brains shall identify whether and which subpopulation of MbDNs is affected by Shh inactivation. In addition, optogenetic and immunohistochemical approaches shall ascertain whether loss of specific MbDN subpopulations disturbs innervation of the target area in adult brain.

It is well known that MbDNs and their target structures are involved in the neural circuit modifications that underlie a variety of adaptive and pathological behaviors (Zhang et al., 2001; Wiese et al., 2004; Lammel et al., 2012; Stamatakis et al., 2012). To examine whether and how the preferential reduction of MbDN subpopulations impacts on the formation of dopaminergic circuitry, MbDN-derived projections shall be examined using viral tracing, optogenetics and physiological approaches.

Finally, to determine the temporal requirement of Shh signaling for the RN neuron specification, precursors in the ventral midline of the developing midbrain shall be analyzed using immunohistochemical and RNA *In Situ* hybridization approaches.

3. Materials and Methods

3.1 Technical equipment

Appliance	Name	Manufacturer	Registered office
Autoclave	DX-150	Systec	Wettenberg, Germany
Balance	Atilon	Sartorius	Göttingen, Germany
Block heater	Dry bath Typ15103	Thermo Scientific	Waltham, USA
Centrifuge	Labofuge 400R	Thermo Scientific	Waltham, USA
Centrifuge	Pico 17	Thermo Scientific	Waltham, USA
Confocal microscope	Fluoview 1000 Dualscan	Olympus	Tokyo, Japan
Cryostat	CM3050S	Leica	Wetzlar, Germany
Fluorescence lamp	Illuminator HXP120C	Zeiss	Jena, Germany
Galvanometer based scanning system	UGA-40, DL-473	Rapp Optoelectronics	Hamburg, Germany
Gel chamber	Model 41-1525	Peqlab	Erlangen, Germany
Horizontal puller	Model P-97	Sutter Instruments	Novato, USA
Hotplate	HI12220 Flattening Table	Leica	Wetzlar, Germany
Hotplate	Flattening Table OTS40	Medite	Burgdorf, Germany
Hybridization oven	InSlide Out 241000	Boekel Scientific	Feasterville, USA
Incubator	AL01-07	Advantage-Lab	Schilde, Belgium
Laser	473 nm	Omicron	Rodgau-Dudenhofen, Germany
Light fiber	BF-22	Thorlabs	New Jersey, USA
Magnetic stirrer	AGE 1200RPM	VELP Scientifica	Usmate, Italy
Microscope	Axio Observer. Z1	Zeiss	Jena, Germany
Microscope	DM1000LED	Leica	Wetzlar, Germany
Microscope camera	AxioCam MRm	Zeiss	Jena, Germany
Microscope camera	AxioCam MRc	Zeiss	Jena, Germany
Microwave	R-939-A	SHARP Electronic GmbH	Hamburg, Germany
Multiclamp amplifier	700 B	Molecular Devices	Sunnyvale, USA

PCR cycler	DNA engine PTC-200	Biorad	München, Germany
pH Meter	FE20 FiveEasy	Mettler Toledo	Gießen, Germany
Pipettes horizontal puller	P-97	Sutter Instruments	Hofheim, Germany
Power supply	Power supply 231	Zeiss	Jena, Germany
Refrigerator/Freezer 4°C and -20°C	G 2013 Comfort	Liebherr	Lindau, Germany
Reverse phase column	C18	Thermo Scientific	Waltham, USA
Shaker	Nutation mixer	VWR	Darmstadt, Germany
Slides boxes	Micro slide box (plastic)	VWR	Darmstadt, Germany
Spectrophotometer	Nanodrop 1000	Peqlab	Erlangen, Germany
Stereo microscope	Modular stereomicroscope MZ10F	Leica	Wetzlar, Germany
Thermal Shaker	Thriller	Peqlab	Erlangen, Germany
Ultrafast Ti:Sa laser	810 nm, Chameleon Ultra	Coherent	Santa Clara, USA
Water bath	WB Type 1012/1013	GFL	Burgwedel, Germany
Vacuum pump	Vacuubrand	Brand	Wertheim, Germany
Vibratome	VT 1200 S	Leica	Wetzlar, Germany
Vortex	Vortex genius	IKA	Staufen, Germany

3.2 Consumables

Appliance	**Name**	**Manufacturer**	**Registered office**
Butterfly needles	Butterfly-25	Venisystems, Hospira	Lake Forest, USA
Dissection tools		Fine Science Tools	Heidelberg, Germany
Embedding cassettes	Histosette embedding cassettes	VWR	Darmstadt, Germany
Embedding molds	Peel-A-Way	Polysciences Inc.	Warrington, USA

	embedding molds		
Glass capillaries	GB150F-8P	Science Products	Hofheim, Germany
Hybridization cover slips	HybriSlip HS 60	Sigma Aldrich	St. Louis, USA
Beveled needles	NanoFil	NanoFil, WPI	Sarasota, USA
Injection needles	27G x ¾´´-Nr.20 Microlance 3	BD Bioscience	Heidelberg, Germany
Microinjection syringe	0.001µL/hr-21mL/min	NanoFil, WPI	Sarasota, USA
Microscope Cover Glasses	40 mm/ 60 mm	Labomedic	Bonn, Germany
Microscope slides	Superfrost	Menzel-Gläser	Braunschweig, Germany
Microscope slides	Superfrost ultra plus	Menzel-Gläser	Braunschweig, Germany
Mini-pump	Micro4MicroSyringe Pump Controller	WPI	Sarasota, USA
Parafilm	Laboraty film `M	Pechiney Plastic Packaging	Chicago, USA
PCR tubes	PCR strip tubes 0,2 mL	VWR	Darmstadt, Germany
Perfusion tools		Fine Science Tools	Heidelberg, Germany
Petri dishes	Falcon petri dishes (15 mm)	BD Biosciences	Heidelberg, Germany
Pipettes	Pipetteman P10/20/200/1000	Gilson	Middleton, USA
Pipetteboy	Accu Jet Pro	Brand	Wertheim, Germany
Pipette tips	Gilson pipette Tipps (0,5-20 µL, 20-200 µL, 200-1000 µL)	Greiner Bio-One	Frickenhausen, Germany
Reagent tubes	Eppendorf tubes (0,5 mL; 1,5 mL; 2 mL)	Eppendorf	Hamburg, Germany
Serological pipettes	Costar plastic	Sigma Aldrich	St. Louis, USA

	serological pipettes		
Syringes	Plastipak 1 mL	BD Bioscience	San Jose, USA

3.3 Chemicals and reagents

Chemicals	**Manufacturer**	**Registered office**
2-Mercaptoethanol	Sigma Aldrich	St. Louis, USA
Acetic anhydride (Ac_2O)	VWR International	Darmstadt, Germany
Acetone	Roth	Karlsruhe, Germany
Acetonitrile	Sigma Aldrich	St. Louis, USA
Agarose (ultrapur)	Life Technologies	Carlsbad, USA
Albumin Boviene Serum (BSA)	Sigma Aldrich	St. Louis, USA
Ampicillin	VWR International	Darmstadt, Germany
Anti-DIG-AP Fab fragments	Roche Applied Science	Penzberg, Germany
Aqua-PolyMount	Polyscience Inc.	Eppelheim, Germany
Atipamezol	Provet AG	Lyssach b. Burgdorf, Switzerland
Biocytin	Sigma Aldrich	St. Louis, USA
Boric acid	VWR International	Darmstadt, Germany
BM Purple	Poche Applied Science	Penzberg, Germany
Bromodeoxyuridine (BrdU)	Sigma Aldrich	St. Louis, USA
Bromphenol blue	Sigma Aldrich	St. Louis, USA
Chloroform ($CHCl_3$)	VWR International	Darmstadt, Germany
Culture medium (LB)	AppliChem	Darmstadt, Germany
ddH_2O	Ampuwa, Fresenius	Bad Homburg, Germany
dH_2O	MilliQ, Merch-Millipore	Billerica, USA
Deoxycholate	AppliChem	Darmstadt, Germany
Dextran sulfate	AppliChem	Darmstadt, Germany
Digoxigenin-labeled NTPs	Roche Applied Science	Penzberg, Germany
Disodium phosphate (Na_2HPO_4)	VWR International	Darmstadt, Germany
DMSO	Sigma Aldrich	St. Louis, USA
DNA Ladder 1 kb plus	Life Technologies	Carlsbad, USA
DNA loading buffer	Life Technologies	Carlsbad, USA
dNTPs	Peqlab	Erlangen, Germany

DPBS	Life Technologies	Carlsbad, USA
Eosin Solution	Sigma Aldrich	St. Louis, USA
Ethidium bromide (EtBr)	Life Technologies	Carlsbad, USA
Ethanol (EtOH)	VWR International	Darmstadt, Germany
Ethylenediaminetetraacetic acid (EDTA)	VWR International	Darmstadt, Germany
Ethylenediaminetetraacetic acid (EDTA) (HPLC grade)	Sigma Aldrich	St. Louis, USA
Formamide	Life Technologies	Carlsbad, USA
Glycerol	Fisher Scientific	Schwerte, Germany
Hydrochloric acid (HCl)	VWR International	Darmstadt, Germany
Hoechst 33258	Life Technologies	Carlsbad, USA
Isoflorane	Abbott	Mumbai, India
Isopropanol	Sigma Aldrich	St. Louis, USA
Ketamine	Bela-Pharm	Vechta, Germany
Levamisole	Sigma Aldrich	St. Louis, USA
Lithium chloride (LiCl)	Sigma Aldrich	St. Louis, USA
Magnesium chloride ($MgCl_2$)	VWR International	Darmstadt, Germany
Medetomidine	Provet AG	Lyssach b. Burgdorf, Switzerland
Normal donkey serum (NDS)	Sigma Aldrich	St. Louis, USA
Normal goat serum (NGS)	Sigma Aldrich	St. Louis, USA
Octanesulfonic acid	Sigma Aldrich	St. Louis, USA
OGB-1-AM dye	Life Technologies	Carlsbad, USA
Orthophosphoric acid	Sigma Aldrich	St. Louis, USA
Paraffin	McCormick Scientific	Richmond, USA
Paraformaldehyde (PFA)	VWR International	Darmstadt, Germany
PCR run buffer (10x)	Life Technologies	Carlsbad, USA
Perchloric acid	Sigma Aldrich	St. Louis, USA
Phenol	AppliChem	Darmstadt, Germany
Phenol-Chloroform	AppliChem	Darmstadt, Germany
Pluronic	Life Technologies	Carlsbad, USA
Polymerase buffer (19x)	Life Technologies	Carlsbad, USA

Polysorbate 20 (Tween 20)	VWR International	Darmstadt, Germany
Potassium chloride (KCl)	VWR International	Darmstadt, Germany
Restriction enzyme	New England Biolabs	Ipswich, USA
Restriction enzyme	Roche Applied Science	Penzberg, Germany
RNase away	Life Technologies	Carlsbad, USA
RNase inhibitor	Roche Applied Science	Penzberg, Germany
Sodium acetate (NaOAc)	Merck	Darmstadt, Germany
Sodium azide (NaN_3)	Sigma Aldrich	St. Louis, USA
Sodium citrate	VWR International	Darmstadt, Germany
Sodium chloride (NaCl)	VWR International	Darmstadt, Germany
Sodium dihydrogen phosphate monohydrate	Sigma Aldrich	St. Louis, USA
Sodium diphosphate	VWR International	Darmstadt, Germany
Sodium hydroxide (NaOH)	VWR International	Darmstadt, Germany
Sodium tetraborate decahydrate	VWR International	Darmstadt, Germany
Sucrose	Sigma Aldrich	St. Louis, USA
Taq DNA polymerase	GE Healthcare	Buckinghamshire, UK
RNA (SP6, T3, T7) polymerase	Roche Applied Science	Penzberg, Germany
Tissue Tec O.C.T.	Sakura Finetek Inc.	Torrance, USA
Transcription buffer	Roche Applied Science	Penzberg, Germany
Triethanolamine (TEA)	VWR International	Darmstadt, Germany
Triethylamine	Sigma Aldrich	St. Louis, USA
Tris-aminomethane (TRIS)	Merck	Darmstadt, Germany
Triton X-100	Merck	Darmstadt, Germany
Xylol	Arcos Organics	Geel, Belgium

3.4 Buffer and solutions

Acetylation solution

125 µL acetic anhydride (Ac_2O)

650 µL HCL

130 µL Triethanolamine (TEA)

49 mL dH_2O

freshly prepared

Artificial cerebrospinal fluid (ACSF)

60 mM NaCl

100 mM sucrose

2.5 mM KCl

1.25 mM MaH_2PO_4

26 mM $NaHCO_3$

1 mM $CaCl_2$

5 mM $MgCl_2$

20 mM glucose

Blocking solution

3 mL/10 mL NDS/NGS

97 mL/90 mL PBS

For the immunohistochemistry 0.1-0.2% triton is added, for RNA *In Situ* hybridization 0.1% Tween is added. The blocking solution is prepared freshly before use.

Borate Buffer

3.1 g boric acid

4.8 g Sodium tetraborate decahydrate

1 L dH_2O

stored at room temperature

Ca^{2+}-free Ringer

150 mM NaCl

2.5 mM KCl

10 mM Hepes

Citrate Buffer

1.92 g Citric acid (anhydrous)

1 L dH_2O

pH adjust to 8.0

stored at room temperature

Hybridization Solution

50 mL Formamide (deionized) (50%)

20 mL 50% Dextran sulfate

1 mL 100x Denhardt's (1%)

2.5 mL yeast tRNA (10 mg/mL) (10%)

6 mL 5M NaCl (0.3 M)

2 mL 1M Tris-HCl, pH 8 (20 mM)

1 mL 0.5M EDTA (5 mM)

1 mL 1M $NaPO_4$ (pH 8) (10 mM)

5 mL 20% Sarcosyl (1%)

11.5 mL DEPC-H_2O (1%)

stored in 5 mL aliquots at -20°C

Intracellular solution

140 mM K-gluconate

5 mM HEPES-acid

0.16 mM EGTA

0.5 mM $MgCl_2$

5 mM phosphocreatine

0.3% biocytin

LB medium

10 g Tryptone/Peptone

5 g Yeast extract

10 g NaCl

800 mL dH2O

pH adjust to 7.5

Loading buffer (10x)

50% glycerol

1xTE Buffer

0.25% bromphenol blue

0.25% xylene cyanol

Lysis Buffer

2.5 mL 1M Tris pH 8.8

0.1 mL 0.5M EDTA

2.5 mL 10% Tween

44.9 mL dH_2O

stored at room temperature

NTMT

2 mL 5M NaCl (100 mM)

10 mL 1M Tris-HCl pH 9.5 (100 mM)

5 mL 1M $MgCl_2$ (50 mM)

0.1 mL Tween-20 (0.1%)

82.9 mL dH_2O

freshly prepared

PBS (5x)

40 g NaCl

1 g KCl

17,9 g Na_2HPO_4 * 12 H_2O

1.36 g KH_2PO_4

1 L dH_2O

pH adjust to 7.4

stored at room temperature

PBS (1x)

200 mL PBS (5x)

800 mL dH_2O

stored at room temperature

PBS-azide (0.1%)

1 g Sodium azide

1 L PBS (1x)

stored at room temperature

PBS-Triton (0.1%)

1 mL Triton X-100

1 L PBS (1x)

stored at room temperature

PBS-Tween (0.1%)

1 mL Tween-20

1 L PBS (1x)

stored at room temperature

PFA (20%)

500 g PFA

2.0 L ddH_2O

8.0 mL NaOH

stored in 5 mL aliquots at -20°C

To prepare 2 L of 20% PFA, 500 mL of ddH_2O was heated to 80°C under the hood. While stirring, 500 g PFA was added. 8 mL NaOH was added drop-wise until PFA crystals were dissolved. pH was adjusted to 7.4 with NaOH and the volume was filled up to 2 L with ddH_20. Subsequently, the 20% PFA solution was filtered and aliquoted in 50 mL Falcon tubes (10 mL per tube), and stored at -20°C. To prepare 4% PFA, 5 mL of 20% PFA was heated up in a water bath at 65°C. 1xPBS was added to a total volume of 50 mL.

RNase Buffer

100 mL 5M NaCl (0.5M)

10 mL 1M Tris-HCl, pH 7.5 (10 mM)

10 mL 0.5M EDTA, pH 8 (5 mM)

880 mL dH_2O

stored at room temperature

SSC (20x)

88.2 g Sodium citrate

174 g NaCl

1 L dH_2O

pH adjusted to 7.0

stored at room temperature

SSC (5x)

250 mL SSC (20x)

750 mL dH_2O

stored at room temperature

SSC (2x)

100 mL SSC (20x)

900 mL dH_2O

stored at room temperature

SSC (0.1x)

5 mL SSC (20x)

995 mL dH_2O

stored at room temperature

TAE (50x)

242 g Tris-base

57.1 mL Glacial acetic acid

100 mL 0.5M EDTA, pH 8.0

stored at room temperature

TE Buffer

1 mL 1M Tris-HCL pH 8.0

200 µL 0.5 M EDTA

98.8 mL dH_2O

3.5 Primary antibodies

ms = mouse, rb = rabbit, gt = goat, gp = guinea pig, rt = rat

Epitope and origin	Dilution	Order #	Manufacturer
α-activated-Caspase-3 (rb) IgG	1:200	9664	Cell Signaling, Danvers, USA
α-BrdU (ms) IgG	1:50	555627	BD Bioscience, San Jose, USA

α-Calbindin (rb) IgG	1:2500	CB38	Swant, Bellinzona, Switzerland
α-DAT (rt) IgG	1:1000	AB369	Merch-Millipore, Billerica, USA
α-Foxa2 (gt) IgG	1:100	SC-6554	Santa Cruz Antibodies, Santa Cruz, USA
α-GFP (gt) IgG	1:1000	AB5449	Abcam, Cambrige, UK
α-GFP (rb) IgG	1:500	A11122	Life Technologies, Carlsbad, USA
α-GFP (rt) IgG	1:2000	04404-26	Nacalai, San Diego, USA
α-Girk2 (rb) IgG	1:100	APC-006	Alomone Labs, Jerusalem, Israel
α-Lmx1a (rb) IgG	1:2500	AB10533	Merch-Millipore, Billerica, USA
α-Ngn2 (gt) IgG	1:50	SC-19233	Santa Cruz Antibodies, Santa Cruz, USA
α-Nkx6-1 (ms) IgG	1:50	F55A10	Developmental Studies Hybridoma Bank, Iowa-City, USA
α-Nurr1 (ms) IgG	1:200	SC-990	Santa Cruz Antibodies, Santa Cruz, USA
α-Pitx3 (rb) IgG	1:250	38-2850	Life Technologies, Carlsbad, USA
α-Pou4fl (ms) IgG	1:100	SC-8429	Santa Cruz Antibodies, Santa Cruz, USA
α-Tyrosine hydroxylase (TH) (ms) IgG	1:500	MAB318	Merch-Millipore, Billerica, USA
α-Tyrosine hydroxylase (TH) (rb) IgG	1:500	MAB152	Merch-Millipore, Billerica, USA

3.6 Secondary antibodies

Epitope and origin	**Dilution**	**Order #**	**Manufacturer**
anti-mouse, Alexa 488	1:500	A21202	Life Technologies, Carlsbad, USA
anti-rabbit, Alexa 488	1:500	A21206	Life Technologies, Carlsbad, USA
anti- guinea pig, Biotin	1:200	706-065-148	Jackson Immuno, West Grove, USA
anti- mouse, Biotin	1:200	715-065-150	Jackson Immuno, West Grove, USA
anti-goat, Cy3	1:200	715-165-147	Jackson Immuno, West Grove, USA

anti-mouse, Cy3	1:200	715-165-150	Jackson Immuno, West Grove, USA
anti-rabbit, Cy3	1:200	715-165-152	Jackson Immuno, West Grove, USA
anti-goat FITC	1:500	705-095-147	Dianova, Hamburg, Germany
streptavidin Alexa 555	1:500	S323555	Life Technologies, Carlsbad, USA

3.7 Oligonucleotides

Primer	**Sequence**	**Tm °C:**
CreF	5′-TAAAGATATCTCACGTACTGACGGTG-3′	58.4
CreR	5′-TCTCTGACCAGAGTCATCCTTAGC-3′	61.6
Gli2-floxC	5′-AGGTCCTCTTATTGTCAGGC-3′	57.8
Gli2-floxD	5′-GAGACTCCAAGGTACTTAGC-3′	55.4
Gli2-AS	5′-CACCCCAAAGCATGTGTTTT-3′	57.4
Gli2-S	5′-AAACAAAGCTCCTGTACACG-3′	55.6
Gli2neo-pA	5′-ATGCCTGCTCTTTACTGAAG-3′	54.7
SmoM2-wt1	5′-TCCTTGAAGAAGATGGTGCG-3′	58.8
SmoM2-wt2	5′-GGAGCGGGAGAAATGGATATG-3′	59.6
SmoM2-mt1	5′-AAGTTCATCTGCACCACCG-3′	58.8
SmoM2-mt2	5′-TCCTTGAAGAAGATGGTGCG-3′	58.8

3.8 Kits

Name	**Manufacturer**	**Registered office**
Hi Pure Plasmid Filter Maxiprep Kit	Life Technologies	Carlsbad, USA
Innuprep Plasmid Mini Kit	Analytik Jena	Jena, Germany
QIAquick PCR Purification Kit (50)	Qiagen	Hilden, Germany

3.9 Software

Name	**Manufacturer**	**Registered office**
Adobe Illustrator CS6	Adobe System Inc.	San Jose, USA

Adobe Photoshop CS6	Adobe System Inc.	San Jose, USA
Axio Vision Rel 4.7	Zeiss	Jena, Germany
Excel for Mac 2011; Version 14.2.3	Microsoft Corporation	Redmond, USA
Fiji	NIH	Bethesda, USA
IGOR	WaveMetrics	Portland, USA
ImageJ	NIH	Bethesda, USA
Keynote '09; Version 5.1.1	Apple Inc.	Cupertino, USA
pClamp Software	Molecular Devices	Sunnyvale, USA
Word for Mac 2011; Version 14.2.3	Microsoft Corporation	Redmond, USA

3.10 Mouse keeping and breeding

All mice were bred on a CD1 background. Experimental animals were housed in an animal facility with a 12 hrs dark/light cycle with lights on at 6 am and had access to food and water *ad libitum*. No more than 6 animals were kept in one cage. The room was temperature- and humidity-controlled. For maintenance of the lines as well as for experiments, two females (5-40 weeks old) were bred with one male (6-40 weeks old). Timed embryos were obtained from overnight matings and noon of the day that a vaginal plug was detected was designated as E0.5. Pups were genotyped at postnatal (P) stage P14 and were separated from the mother at P21. Animal studies were approved by the local University of Bonn Animal Care and Use Committee, as well as the Animal Care and Use board of the country of Nordrhein-Westfalen.

3.11 Mouse lines

3.11.1 *En1*$^{Cre/+}$

The *En1*$^{Cre/+}$ mice were generated by Kimmel et al. (2000). To generate the mutant allele, the first 111 amino acids of the target gene were replaced by the Cre cDNA (Kimmel et al., 2000). The insertion of the Cre cDNA interferes with the expression of the endogenous gene product. Therefore the *En1*$^{Cre/+}$ allele is a null allele. Heterozygous mice are viable and fertile. Breeding *En1*$^{Cre/+}$ mice with mice containing an allele with *loxP*-flanked sequence of interest results in the Cre-mediated recombination of the floxed sequences in *En1*-expressing tissues, particularly in the vMb and aHb around E9.0 (Li et al., 2002).

3.11.2 *Gli2*$^{zfd/+}$

Gli2$^{zfd/+}$ (*Gli2 zinc finger-deleted*) mouse line was generated in the laboratory of A. Joyner by replacing the exons encoding for zinc fingers 3 to 5 with 2.5 kb of the 5' and 5.0 kb of the 3' *Gli2* genomic sequences and a PGK neo cassette (Matise et al., 1998). The deletion results in an out-of-frame mutation, which causes disrupted transcription from the deletion site to the 3' end of the *Gli2* gene. The zinc fingers 4 and 5 are essential for DNA binding, therefore deletion of the sequence encoding for zinc fingers 3 to 5 results in translation of truncated protein, which is unable to bind to DNA (Pavletich and Pabo, 1993).

3.11.3 *Gli2*$^{flox/flox}$

The *Gli2*$^{flox/flox}$ mouse was generated in the laboratory of A. Joyner in 2006 (Corrales et al., 2006). Two loxP sites flank exon 7 and 8 upstream exon encoding for the zinc finger exons. *Gli2*$^{flox/flox}$ mice show a wild-type phenotype. *Gli2*$^{flox/flox}$ mice were used in this study to generate conditional knockout mice.

3.11.4 *R26*^{SmoM2}

The *R26*^{SmoM2} allele contains a constitutively active mouse Smo (W539L, SmoM2) fused to the enhanced yellow fluorescent protein (EYFP) under the control of the endogenous *Rosa26* ubiquitous promoter. However, expression of SmoM2 and EYFP is normally blocked by a *loxP*-flanked stop cassette, which can be removed upon Cre-mediated recombination, allowing tissue-specific expression of SmoM2. The constitutively active W539L point mutation has been found in human basal cell carcinoma (Xie et al., 1998) and is a tryptophan-to-leucine mutation, which results in translation of the correspondingly mutated protein capable of ligand-independent activation of the Hedgehog pathway (Taipale et al., 2000). Homozygous mice are viable, fertile and do not display any abnormalities (Jeong et al., 2003).

3.11.5 The *Gli2* conditional knockout mouse (*Gli2*$^{\Delta Mb>E9.0}$)

To create viable mutant mice in which *Gli2* was deleted from midbrain precursors, the *En1*$^{Cre/+}$ knock-in mouse line was crossed with *Gli2*$^{zfd/+}$ to generate *En1*$^{Cre/+}$:*Gli2*$^{zfd/+}$ mice. The *En1*$^{Cre/+}$:*Gli2*$^{zfd/+}$ were generated in the laboratory of A. Joyner. Those mice were crossed with *Gli2*$^{flox/flox}$ homozygotes to generate the conditional knockout mice *En1*$^{Cre/+}$:*Gli2*$^{flox/zfd}$, termed *Gli2*$^{\Delta Mb>E9.0}$ throughout this study (Figure 8B). *Gli2*$^{flox/+}$ littermate mice were used as a control.

3.11.6 The *SmoM2* conditional overactivation (*SmoM2*$^{\uparrow Mb>E9.0}$)

To constitutively activate the Shh pathway in the midbrain precursors, the *R26*^{SmoM2} mouse line was crossed with the *En1*$^{Cre/+}$ knock-in mouse line (Jeong et al., 2003). As a result, *En1*$^{Cre/+}$*:R26*^{SmoM2} mice were generated (termed *SmoM2*$^{\uparrow Mb>E9.0}$ throughout this study), in which Shh signaling was permanently activated upon Cre-mediated recombination in the midbrain precursor cells expressing *En1*. These mice have enlarged midbrain and die at birth. *En1*$^{Cre/+}$ littermates were used as control.

3.12 Genotyping of knockout mice

For deoxyribonucleic acid (DNA) analysis, small pieces of tissue from the mouse tail (about 5 mm) for E12.5-18.5, from the ear (ear punch) for postnatal mice and from yolk sac for E9.5-11.5 embryos were obtained. To digest the tissue, 100 µL lysis buffer with 1 µL proteinase K was added and briefly vortexed. The samples were incubated at 60°C for 8 hrs or longer and subsequently heated at 95°C for 15 min to inactivate the proteinase K. Afterwards, the digested solution was centrifuged for 1 min at 13000 rpm to bring down moisture on sides of tubes and to precipitate digested tissue fragments. 1 µL of the supernatant was used for polymerase chain reaction (PCR).

3.13 Molecular biological methods

3.13.1 Polymerase chain reaction

To determine the genotypes of the mice, polymerase chain reaction (PCR) approach was used. The first step (denaturation) requires high temperatures of 94°-96°C to denature double stranded DNA. It is a cyclic process based on the elongation of DNA strands in between two reverse oligonucleotide primers by a DNA polymerase. With repeated cycle of DNA melting and enzymatic replication of the DNA sequences in between the two primers, an amplification of the desired DNA sequence is achieved.

3.13.2 PCR Programs

3.13.2.1 Cre PCR

PCR Sample solution	**Program for Thermal Cycle**		
2.00 µL PCR Buffer (1x)			
0.16 µL dNTPs (25 nM)	**Step**	**Temp.**	**Time (min)**
1.00 µL P1: Cre-F (5 µM)	1. First Denaturing	95°C	2:00
1.00 µL P2: Cre-R (5 µM)	2. Denaturing	95°C	0:40
0.60 µL $MgCl_2$ (1.5 mM)	3. Annealing	59°C	1:00

14.04 µL dH_2O	4. Extension	72°C	0:50
0.20 µL Taq Polymerase (1U)	5. Incubation	8°C	∞
19.00 µL Solution (total)	35 x Cycles step 2-4		
Agarose gel: 1.5%			
Mutant band: 300 nt			

3.13.2.2 Gli2 flox PCR

PCR Sample solution	**Program for Thermal Cycle**		
2.00 µL PCR Buffer (1x)			
0.16 µL dNTPs (25 nM)	**Step**	**Temp.**	**Time (min)**
1.00 µL P1: Gli2-flox C (5 µM)	1. First Denaturing	94°C	5:00
1.00 µL P2: Gli2-flox D (5 µM)	2. Denaturing	94°C	1:00
0.60 µL $MgCl_2$ (1.5 mM)	3. Annealing	58°C	1:00
14.04 µL dH_2O	4. Extension	72°C	1:30
0.20 µL Taq Polymerase (1U)	5. Last Extension	72°C	10:00
19.00 µL Solution (total)	6. Incubation	8°C	∞
	35 x Cycles step 2-4		
Agarose gel: 1.5%			
Wildtype band: 231 nt, mutant band: 247 nt			

3.13.2.3 Gli2 zfd PCR

PCR Sample solution	**Program for Thermal Cycle**		
2.00 µL PCR Buffer (1x)			
0.16 µL dNTPs (25 nM)	**Step**	**Temp.**	**Time (min)**
1.00 µL P1: Gli2-S (5 µM)	1. First Denaturing	94°C	5:00
1.00 µL P2: Gli2-AS (5 µM)	2. Denaturing	94°C	1:00
1.00 µL P3: Gli2 neo-pA (5 µM)	3. Annealing	58°C	1:00
0.60 µL $MgCl_2$ (1.5 mM)	4. Extension	72°C	1:30
13.04 µL dH_2O	5. Last Extension	72°C	10:00
0.20 µL Taq Polymerase (1U)	6. Incubation	8°C	∞
19.00 µL Solution (total)	35 x Cycles step 2-4		
Agarose gel: 1.5%			
Wildtype band: 300 nt, mutant band: 550 nt			

3.13.2.4 SmoM2 PCR

PCR Sample solution	**Program for Thermal Cycle**		
2.00 µL PCR Buffer (1x)			
0.16 µL dNTPs (25 nM)	**Step**	**Temp.**	**Time (min)**
1.00 µL P1: SmoM2-mt1 (5 µM)	1. First Denaturing	94°C	3:00
1.00 µL P2: SmoM2-mt2 (5 µM)	2. Denaturing	94°C	0:30
1.00 µL P3: SmoM2-wt1 (5 µM)	3. Annealing	60°C	1:00
1.00 µL P3: SmoM2-wt2 (5 µM)	4. Extension	72°C	1:00
0.60 µL $MgCl_2$ (1.5 mM)	5. Last Extension	72°C	2:00
12.04 µL dH_2O	6. Incubation	10°C	∞
0.20 µL Taq Polymerase (1U)	35 x Cycles step 2-4		
19.00 µL Solution (total)			
Agarose gel: 2%			
Wildtype band: 410 nt, mutant band: 173 nt			

3.13.3 Agarose gel electrophoresis

Agarose gel electrophoresis is a method to determine the presence and size of PCR products by separating DNA/RNA based on the rate of movement while under the influence of an electric field. The DNA/RNA to be analyzed is forced through the pores of the gel by the electrical current. Under an electrical field, DNA/RNA moves away from the negative towards the positive electrode. The speed of DNA/RNA movement is influenced by the strength of the electrical field, the concentration of agarose gel and the size of the DNA/RNA molecules. Smaller DNA/RNA molecules move through the agarose faster than larger molecules. The DNA/RNA is visualized in the gel by addition of ethidium bromide (EtBr). EtBr is fluorescent meaning that it absorbs invisible UV light and transmits the energy as visible orange light. To prepare a 1.5% agarose gel, 2.25 g agarose powder was dissolved in 150 mL 1xTAE Buffer. For 2% or 0.5% agarose gel, 3 g or 0.75 g of agarose powder was dissolved in 150 mL 1xTAE buffer, respectively. The solution was boiled in the microwave until the agarose dissolved and became clear. The agarose solution was cooled at room temperature and 0.5 µg/mL of EtBr was added to it. The agarose solution was poured into a gel-casting tray fitted with a well-forming comb. Agarose gel was submersed in a chamber containing a buffer solution (1xTAE) and a positive and negative electrode. The DNA/RNA samples were mixed with the gel tracking dye (DNA loading buffer) and loaded into the

sample wells. The gel with the samples was run at 120 V for 30 min at room temperature. 0.5 and 1 kb marker was used to identify fragments between 0.1 kb and 0.6 kb.

3.13.4 Generation of RNA *In Situ* Probes

3.13.4.1 Transformation of E. coli

To amplify a specific vector, medium competent bacteria (DH5α) were transformed with a DNA plasmid containing a cassette with ampicillin resistance. 50 µL of competent cells of *E. coli* (DH5α) were thawed on ice or briefly warmed in hand and 1 µg of the DNA plasmid was added. Next, the bacteria were incubated on ice for 5 min and heat-shocked at 42°C for 30 sec allowing the DNA plasmid to enter the cells. Finally, the bacteria were chilled on ice for 2 min and 10 µL of the bacteria were plated on LB agar plates, containing 20 µL/mL ampicillin and incubated at 37°C overnight.

3.13.4.2 Maxi-preparation

To obtain a bigger amount of pure plasmid, a single colony was picked and first transferred into a 10 mL falcon tube containing LB-medium with ampicillin (20 µL/mL). The bacterial culture was incubated for 7-8 hrs at 37°C on a shaker (starter culture). After that, the 10 mL culture was transferred to a flask containing 100 mL of LB-medium (+ 20 µL/mL ampicillin). The culture was incubated at 37°C on a shaker overnight. The bacteria were centrifuged at 8000 rpm at 4°C for 60 min. The pellet was processed for the maxi-preparation carried out with a HiPure Plasmid Maxiprep Kit from Invitrogen according to the manufacturer's instruction. The concentration of the DNA was determined by Nanodrop measurement. The plasmid was stored at 4°C.

3.13.4.3 Digest of plasmid

Plasmid containing the DNA inserts for creating the anti-sense RNA probes for the RNA *In Situ* hybridization had to be linearized by restriction enzymes before *in vitro* transcription could be performed. In order to do this, solution mix to digest the plasmid was prepared:

A digestion mix:

20 µg Plasmid
10 µL 10xNEB1-4 Buffer
10 µL 10xBSA
5 µL restriction enzyme (100 U)
x µL dH_2O
100 µL Solution (final)

The digestion mix was incubated at 37°C for 3 hrs. To ensure that the plasmid was cut properly, 5 µL of the digestion mix was run on an agarose gel with 1 µg of undigested plasmid. To purify the DNA of interest from other nucleic acids, phenol-chloroform extraction was performed. 100 µL of phenol-chloroform was added to the digestion mix (100 µL) and centrifuged at 13000 rpm for 10 min. The upper (aqueous) phase (containing DNA) was transferred to a new 1.5 mL tube. Next, 0.3 M sodium acetate (pH 5.2) was added to the tube containing the DNA and vortexed. Then 220 µL of ice cold 100% EtOH was added and mixed. The DNA was then precipitated at -80°C for 30 min and centrifuged at 13000 rpm for 10-15 min at 4°C. Afterwards, the supernatant was discarded and the pellet was washed with 100 µL 70% EtOH and centrifuged at 13000 rpm for another 15 min at 4°C. After discarding the supernatant, the pellet was air-dried for 10-15 min. Subsequently, the pellet was resuspended in 50 µL RNase free H_2O with 0.5 µL RNAse inhibitor and stored at -20°C.

3.13.4.4 In vitro transcription

To generate the labeled anti-sense (AS) RNA probes (riboprobes), the digested and purified plasmid (containing the marker gene sequence) was transcribed to the AS RNA probe by *in vitro* transcription. To this end, DIG-labeled NTP mix was used, which includes UTP labeled with DIG (Digoxigenin-11-uridine-5'-triphosphate) and can be detected with anti-DIG-AP Fab fragments. The *in vitro* transcription solution mix (20 µL) contained:

1.5 µL Purified DNA (1-2 µg)
2 µL (10x) Transcription Buffer
2 µL (10x) DIG-NTP labeling mix
0.5 µL RNase inhibitor (10 U)
1.5 µL RNA polymerase (30 U)
12.5 µL dH_2O

The transcription solution mix was incubated at 37°C for 2 hrs. Next, 1 µL of DNase was added to remove the plasmid DNA and the solution was incubated at 37°C for another 15 min. The RNA was precipitated at -80°C by adding 2 µL of EDTA (4 mM), 2.5 µL LiCl (100 mM) and 75 mL of 100% EtOH. The suspension was centrifuged at 13000 rpm for 15 min at room temperature, washed with 70% EtOH and centrifuged again for another 10 min. The pellet was air-dried at room temperature for 3-5 min and resuspended in 50 µL ddH_2O + 1% RNase inhibitor. Subsequently, the RNA concentration was measured with Nanodrop and the RNA was stored at -20°C.

3.14 Histology

3.14.1 Dissection of embryos

Embryos at different embryonic stages (E9.5-E12.5, E14.5 and E18.5) were dissected. Pregnant mice were anesthetized with isoflurane and sacrificed by cervical dislocation. A midline skin incision was made from the thorax to the pelvis and the uterus was exposed. The embryos were removed from the uterus and transferred to a petri dish filled with chilled 1xPBS on ice. By using fine forceps, the muscular wall of the uterus and visceral yolk sac was removed. At stages E9.5-E11.5 whole embryos were collected, while at stages E12.5 and E14.5 the heads were dissected. At stage E18.5 the brains were dissected out by removing the skin from the head and the skull. Tissue was fixed in 4% PFA (E9.5-E10.5 for 30 min, E11.5-E12.5 for 60 min and E14.5 and E18.5 for 2 hrs) at 4°C.

3.14.2 Perfusion of postnatal mice

Three and six week old animals were used for intracardial perfusion. First at all, mice were anesthetized by lethal dose of intraperitoneal injection of Ketamine-Rompun mixture (50:10 mg/kg of body weight) or by exposure to a tissue soaked with isoflorane. To assure adequate depth of anesthesia, the withdrawal reflex was checked by pinching the toes or tip of tail until no response was observed. Then, the animal was placed on a corked surface on its back and each limb was taped down with a needle. A midline skin incision was made from the thoracic inlet to the pelvis, so that the abdomen was open and the liver was exposed. To expose the heart, further incision of the sternum was done. The butterfly needle was placed into the left ventricle toward the aorta. Using scissors a small cut in the right atrium was made to allow the perfusate to exit the circulation. At the same time, using syringe 1xPBS was injected with a flow no higher than 0.5 mL/min. When the fluid exiting the mouse was clear and when the liver became a light color, the syringe with 1xPBS was exchanged to a syringe with 4% PFA. Perfusion was complete when all muscle contractions stopped and the mouse became stiff. Afterwards, the mouse was decapitated at the level of the shoulders. The skin of the head was cut up to the eyes and the skull was carefully removed with scissors. After most of the skull was removed, the brain was dissected by cutting the olfactory and optical nerves as well as spinal cord at the level of the brain stem. Subsequently, the brain was postfixed in 4% PFA at 4°C overnight.

3.14.3 Cryo-embedding

After fixation in 4% PFA tissue was washed in 1xPBS three times for 10 min. To cryoprotect tissue, the brains were incubated in 15% sucrose at 4°C for at least 6-12 hrs, or until tissue was submerged. Afterwards the tissue was incubated in 30% sucrose at 4°C overnight or until the brains were submerged. All procedures were carried out on a rocking platform. The cryo-molds were filled with tissue-tek O.C.T. compound medium and placed on dry ice. Once the O.C.T. medium starts to solidify (turn white) at the bottom, the cryo-molds were removed from dry ice and the brain, heads or embryos were placed in the center of the mold. Embryonic tissue (E9.5-18.5) was immediately frozen on dry ice. The blocks with the embryos as well as the postnatal brains imbedded in the cryo-molds were stored at -80°C.

3.14.4 Cryo-sectioning

About 30 min prior the sectioning, blocks were removed from the -80°C freezer and placed in the cryostat to allow them to warm up to the sectioning temperature. The temperature of the cryostat was set to -25°C. Embedded tissue was removed from the plastic molds and attached to the cryostat object holder with a small amount of O.C.T. The blocks were sectioned coronally at a thickness of 12 µm (E10.5-E12.5), 16 µm (E18.5), 20 µm (P21) or 40 µm (P21 and P48). The 12 µm, 16 µm and 20 µm slices were collected on „superfrost ultra plus“ adhesion slides in series of ten slides, in such a way that the slide contained every tenth section from the anterior to posterior axis. After cutting, the sections were dried at room temperature for 60 min and processed for further immunohistochemistry/RNA *In Situ* hybridization or stored in slide boxes at -20°C.
40 µm thick slices (P21 and P48) were collected in 96 well plates filled with 1xPBS with 1% (final concentration) Sodium azide (free floating sections). The plates were stored at 4°C.

3.14.5 Paraffin embedding

For embedding tissue in paraffin the tissue (E9.5 and E10.5 embryos and E14.5 heads) was washed in 1xPBS three times for 5 min. All steps were carried out at room temperature. The tissue was dehydrated as follows: (2x) in 70% EtOH, (1x) in 80% EtOH, (2x) in 95% EtOH and (2x) in 100% EtOH. Each dehydration step was 10 min for E9.5, 15 min for E10.5 and 20 min for E14.5 embryos. Next, the tissue was cleared with 1:1 100% EtOH: 100% Xylol two times for 10-20 min. Afterwards, tissue was placed in embedding cassettes and transferred into 100% Xylol and incubated three times (E9.5: 5 min, E10.5: 10 min, E14.5: 15 min). Subsequently, the specimens were transferred into paraffin heated to 58°C in water bath and

processed in to fresh paraffin for two more times (E9.5: 10 min, E10.5: 15 min and E14.5: 20 min). The embedding molds were filled with heated paraffin and the tissue was transferred into the molds on a heating plate at 64°C. Using heated forceps, the tissue was properly oriented in the mold. Once the tissue was oriented as desired, the mold was covered with the labeled embedding cassette and removed from the heating plate. Paraffin blocks with embedded embryos or heads were stored at room temperature till they were sectioned at the microtome.

3.14.6 Paraffin sectioning

After paraffin was solidified hard, block was removed from the mold and attached to the microtome chuck. The specimens were sectioned coronally at 7 µm. To unroll the sections, they were picked up with a fine paintbrush and floated in water at 37°C. The sections were floated onto „superfrost ultra plus“ adhesion slides. The sections were arranged on slides in pairs of one (E9.5), two (E10.5) or three (E14.5), in series of ten, in this way adjacent slices on every slide had the same spacing on the anteroposterior axis. The slides were allowed to dry on a flattening plate at 38°C overnight to bind the tissue to the glass. The sections were stored in slide boxes at room temperature or processed further for RNA *In Situ* hybridization and/or immunohistochemistry.

3.14.7 Immunohistochemistry on frozen and free-floating sections

Frozen section were thawed at room temperature for 5 min and rinsed with PBS for 5 min to remove the O.C.T. Next, the tissue was re-fixed with 4% PFA for 5 min at room temperature. After washing two times with PBS and one time with PBT (0.1% TritonX-100 in PBS), sections were blocked in 10% normal donkey serum (NDS) in PBT for 1 hr at room temperature. After that, they were incubated with primary antibody in 3% NDS/PBT (300 µL per slide) for 2 hrs at room temperature or at 4°C overnight. Afterwards, the sections were washed again three times in PBT and incubated with secondary antibody 3% NDS/PBT for at least 1 hr at room temperature. To visualize the cell nuclei, a Hoechst fluorescent counterstaining (Hoechst 33258, 1:10000) was added to the solution with secondary antibody. Finally, the sections were washed three times with PBT for 5 min, mounted with AquaPolymount and covered with coverslips. The immunostained sections were stored at 4°C.

Free-floating sections were washed in 1xPBS for 5 min and blocked in 10% NDS in PBT for 1 hr at room temperature. All procedures were carried out in 12 or 24 well plates and on the

rocking platform. Next, they were incubated with primary antibodies in 3% NDS/PBT (500 µL per well) overnight at 4°C. Afterwards, the sections were washed three times in PBT for 10 min and incubated with secondary antibody in 3% NDS/PBT for at least 2 hrs at room temperature. To the secondary antibody mixture, Hoechst was added to visualize the cell nuclei. Subsequently, sections were washed again in PBT three times for 10 min. Sections were placed in a petri dish filled with 1xPBS and floated with a fine paintbrush onto „superfrost“ adhesion slides. Afterwards, slides were dried for 5 min. Finally, sections were mounted with AquaPolymount and covered with coverslips. The immunostained sections were stored at 4°C.

For detection of transcription factors, frozen section were thawed and washed in 1xPBS as described above. Next, they were fixed in 4% PFA for 10 min followed by three washing steps with 1xPBS for 5 min each, then incubated in 0.1 mM EDTA for 10 min at 65°C water bath prior to the immunostaining. The free-floating sections were washed in 1xPBS for 5 min and then incubated in 0.1 mM EDTA for 1hr at 65°C.

3.14.8 Immunohistochemistry on paraffin sections

Sections were de-waxed and rehydrated as follows: (3x) in 100% Xylol for 3 min, (2x) in 100% EtOH for 1 min, (2x) in 95% EtOH for 1 min, (1x) in 70% EtOH for 1 min and (2x) in 1xPBS for 1 min. To break the protein cross-links formed by PFA and paraffin fixation, an antigen retrieval method was used. The slides were placed in a coplin jar with citrate buffer and boiled in the microwave for 1-2 min. This step was repeated with fresh buffer for two more times. Afterwards the slides were cooled to room temperature in the same buffer for 20 min and then rinsed twice with dH_2O. Next, the sections were washed twice with 1xPBS and once with PBT for 5 min. Blocking solutions and antibodies were applied as described in Subsection 3.14.7.

For BrdU and Caspase-3 immunostainings, after the antigen-retrieval step, the DNA was denatured by treating the tissue with 4 M HCL for 10 min and neutralized afterwards with 0.1 M borate buffer (pH 8.5) for 5 min. Before applying primary antibodies, sections were washed two times with PBS and one time with PBT for 5 min as described above.

3.14.9 RNA *In Situ* hybridization

RNA *In Situ* hybridization was used to analyze gene expression in the developing mouse vMb. Paraffin sections were de-waxed with xylol and rehydrated with 100%, 95% and 70% EtOH, as described in Subsection 3.14.8. Frozen sections were thawed at room temperature

and washed in 1xPBS for 5 min. Afterwards both kind of sections were postfixed in 4% PFA for 10 min, followed by two washing steps with 1xPBS. The slides were incubated in 50 mL 1xPBS with 4 µL proteinase K (frozen section) for 5 min or with 8 µL proteinase K (paraffin sections) for 10 min. Then slides were again fixed in 4% PFA for 5 min and washed three times with 1xPBS. Afterwards, only paraffin sections were acetylated in 50 mL acetylation solution for 10 min, followed by three washing steps in 1xPBS for 5 min each. Subsequently, the sections (paraffin and frozen) were dehydrated in 70% EtOH for 5 min and afterwards in 95% EtOH for a few seconds. The sections were placed horizontally in a humid box filled with 50 mL Formamide/water (in ratio 1:1) and preheated in a hybridization oven at 55°C. Approximately 1 µg of the desired RNA probe was added to 1 mL of hybridization solution and heated at 80°C for 2 min to denature RNA. 300 µL of riboprobe/hybridization solution was applied on the sections and then they were covered with RNase-free hybridization coverslips. The humidified box with the slides was inserted into the preheated oven and hybridized overnight at 55°C. On the next day, coverslips were removed in pre-warmed 5x SSC and washed in pre-warmed 1xFormamide and 2xSSC (in ratio of 1:1) for 30 min in a 65°C water bath. Afterwards, they were washed three times with RNase Buffer at 37°C and incubated in the same Buffer with RNase A (in ratio of 1000:1) for 30 min. Then the slides were washed one more time with RNase Buffer for 15 min and washed twice in pre-warmed 1xFormamid:2xSSC solution for 20 min in 65°C water bath. Two additional washing steps in 2xSSC and 0.1xSSC for 15 min at 37°C were followed by a washing step with PBT (1xPBS with 0.1% Tween-20) for 15 min at room temperature. The slides were placed horizontally in a humidified box with H_2O soaked tissue (to avoid drying-out of the slides) and blocked with 10% normal goat serum (NGS) in PBT for 1hr at room temperature. After that, blocking solution was removed and the sections were incubated with anti-DIG-AP Fab fragments (1:3000) in 1% NGS/PBT for 3 hrs at room temperature. After removal of the antibody, slides were washed four times with PBT for 15 min at room temperature, following by two washing steps with freshly prepared alkaline phosphatase buffer (NTMT) containing 0.5 mg/mL levamisole for 10 min at room temperature. Finally, sections were incubated in BM purple solution containing 0.5 mg/mL levamisole at room temperature overnight or till a signal was visible. Then the sections were washed with PBS, briefly postfixed with 4% PFA, followed by additional PBS and dH_2O washing steps. The slides were mounted in AquaPolymount and covered with coverslips. Sections were stored in slide boxes at room temperature.

3.14.9 List of RNA *In Situ* probes

Probe	Description	Provided by
Ahd2	Aldehyde dehydrogenase family 1, subfamily A1	Martin P. Smidt (Rudolf Magnus Institute of Neuroscience, Utrecht, The Netherlands)
Arx	Aristaless related homeobox gene	ImaGenes/SourceBioscience, UK
Corin		ImaGenes/SourceBioscience, UK
Foxa2	Forkhead box A2 transcription factor	Alexandra L. Joyner (Memorial Sloan Kettering Cancer Center, New York, USA
Lmx1a	LIM homeobox transcriptional factor 1 alpha	Alexandra L. Joyner (Memorial Sloan Kettering Cancer Center, New York, USA
Msx1/2	Homeobox, msh-like 1 transcriptional factor	Alexandra L. Joyner (Memorial Sloan Kettering Cancer Center, New York, USA
Shh	Sonic hedgehog	Alexandra L. Joyner (Memorial Sloan Kettering Cancer Center, New York, USA
Sim1	Single-minded homolog 1	Jacques Michaud (University of Montreal, Canada)
vGlut2	Solute carrier family 17 (sodium-dependent inorganic phosphate cotransporter) member	Robert Edwards (University of California, San Francisco, USA)

3.14.10 Combined RNA *In Situ* hybridization and Immunohistochemistry

For combined RNA *In Situ* hybridization and immunohistochemistry the protocol was modified according to Eisenstat (Eisenstat et al., 1999). 20 µm thick frozen sections were used. The slides were thawed at room temperature and washed in 1xPBS for 5 min. After fixation in 4% PFA for 5 min, slides were washed three times in 1xPBS and then one more time in Ampuwater for 5 min each. The sections were incubated for 5 min stirring and for another 5 min still in acetylation solution. After washing the sections for 5 min with Ampuwater, sections were dehydrated in as follows: 1 min in 70% EtOH, 1 min in 80% EtOH, 2 min in 95% EtOH, 1 min in 100% EtOH, 5 min in chloroform, 1 min in 100% EtOH, 1 min in 95% EtOH. The slides were drained on paper towel and air dried. 2 µL of probes (approximately 1 µg) in 1 mL of hybridization solution was heated at 80°C for 5 min and then

cooled on ice for another 2 min. The slides were placed horizontally in humidified box filled with 50 mL Formamide/Ampuwater (in ratio of 1:1), 300 µL riboprobe/hybridization solution mix was applied on each slide and sections were covered with RNase free coverslips. The humidified box with the slides was placed in the hyboven at 55°C overnight. Next day washing, antibody staining and visualization were carried out as described above (Subsection 3.14.8). When the signal was visible, the reaction was stopped in TE Buffer. Then, the sections were postfixed in 4% PFA for 20 min and washed with 1xPBS three times for 5 min. Next, the slides were incubated with blocking solution 10% NDS in PBT (PBS-0.2% Triton x100) for 4 hrs and afterwards with primary antibody diluted in 3% NDS/PBT at 4°C overnight. Next day, sections were washed with 1xPBS three times for 5 min and incubated with secondary antibody in 3% NDS/PBS for at least 2 hrs at room temperature. Finally, slides were washed again with 1xPBS three times for 5 min and coversliped with AquaPolymount. The sections were stored in slide boxes at 4°C.

3.15 BrdU injection

Timed pregnant females were injected intraperitoneally (i.p.) with 100 µg bromodeoxyuridine (BrdU) in 1xPBS per g body weight. Pregnant females (E10.5) were injected one hour prior to the dissection.

3.16 High performance liquid chromatography analysis*

6 week old control and mutant mice were used for high performance liquid chromatography (HPLC) analysis. PFC and CPu were quickly dissected following cervical dislocation. To extract catecholamine, tissue was placed in 0.4 M perchloric acid. Afterwards it was homogenized by sonification and centrifuged at 15000 rpm (4°C). The concentrations of DA and 3,4-dihydroxyphenylacetic acid (DOPAC) were determined by reverse phase HPLC, coupled with electrochemical detection as described (Kilpatrick et al., 1986). The samples were injected into a guard column, connected to a reverse phase column of C18. DA and DOPAC were separated at a flow rate of 0.6 mL/min. The composition of mobile phase was as follows: 10% acetonitrile, 75 mM sodium dihydrogen phosphate monohydrate, 0.17 mM octanesulfonic acid, 2.5 mM triethylamine and 25 mM EDTA, adjusted to pH 3.0 with orthophosphoric acid. All reagents were HPLC grade. Catecholamine concentrations are

* Isolation of PFC and CPu tissue as well as HPLC analysis was performed by Dr. Ruth Musgrove, laboratory of Prof. Donato A. Di Monte, DZNE, Bonn

expressed per mg of protein.

3.17 Viral transduction and Optogenetics

Cell-type selective expression of Channelrhodopsin-2 (ChR2) and enhanced yellow fluorescent protein (EYFP) was achieved using a recombinant adeno-associated virus (rAAV) harboring a ChR2-EYFP fusion gene with an inverted open reading frame, flanked by two incompatible loxP sites and driven by an EF1α promoter. In the presence of Cre recombinase, the ChR2-EYFP fusion gene is inverted, with subsequent deletion of a loxP site leading to irreversible Cre-dependent expression of ChR2-EYFP (Cardin et al., 2009; Sohal et al., 2009).

3.18 Stereotaxic injections of rAAV into the VTA, brain slice preparation and histological analysis of the section*

Under sterile conditions, three to four week old control ($En1^{Cre/+}$) and mutant ($Gli2^{\Delta Mb>E9.0}$) mice were anesthetized (0.1 mL/10 mg body weight) with a cocktail of 0.1 mg/mL medetomidine and 10 mg/mL ketamine. After achieving deep anesthesia, animals were secured in a stereotaxic frame. Holes the size of the injection needle were drilled into the skull (Fine Science Tools) and the rAAV harboring a ChR2-YEFP fusion gene was injected into the medial VTA (anteroposterior (AP): -3.44 mm, mediolateral (ML): 0.48 mm and dorsoventral (DV): 4.4 mm) (Franklin and Paxinos, 2007) using a 34 g beveled needle. 1 µL of viral suspension containing 10^8 transducing units was injected unilaterally. The injection syringe delivered vector at a constant volume of 100 nL/min using a microprocessor controlled mini-pump. The needle was left in place for 3 to 5 min after each injection to minimize upward flow of viral solution after raising the needle and then slowly retracted over a course of 1 to 3 min. Finally, the incision was sutured and the animal was given atipamezole (0.05 mg/10 mg body weight). For immunohistochemical quantification of the VTA projections to the NAc and the PFC the virus was allowed 14 days to incubate before the analysis was carried out. For electrophysiological experiments mice were sacrificed 2 to 6 weeks post-injection.

For immunohistochemical analysis, mice were anesthetized and perfused (Subsection 3.14.2). Overnight post-fixed brains were processed for cryo-embedding (Subsection 3.14.3). 20 µm thick brain sections were collected on „superfrost ultra plus" adhesion slides in series of ten slides (Subsection 3.14.4) and processed for combined RNA *In Situ* hybridization and

* Stereotaxic injections of rAAV were performed by Milan Pabst, laboratory of Prof. Heinz Beck, Department of Epileptology, University of Bonn, Medical Center

immunostaining (Subsection 3.14.11). 40 µm thick free-floating sections were immunostained for TH and GFP (Subsection 3.14.7) to analyze the MbDN axonal projections.

3.19 Electrophysiological analysis*

For cell-type specific light-based stimulation of VTA neurons mice were sacrificed 2 weeks post virus injection. The brain was removed and transferred into cold artificial cerebrospinal fluid (ACSF). 300 µm coronal slices of the VTA or the PFC were made using a vibratome. Slices were incubated for 30 min at 37°C and subsequently transferred into ASCF. For electrophysiology, slices were transferred one at a time into a submerged chamber and superfused with ACSF at 35°C. EYFP-expressing neurons were identified using an upright fluorescence microscope (filter settings: excitation, 500/24; dichroic, 520; emission, 542/27). Whole-cell patch-clamp recordings were then achieved from identified cells using IR-DIC microscopy. Voltage- and current clamp experiments were carried out with a Multiclamp 700B amplifier. Data were sampled at 50 kHz or 100 kHz with a Digidata 1322A interface controlled by pClamp Software lowpass filtered at 10 Hz and stored on a hard disk for offline analysis. Pipettes were made using a horizontal puller and borosilicate glass capillaries and filled with an intracellular solution. Electrode resistance in the bath ranged from 3-5 MΩ and series resistance ranged from 17 -24 MΩ for VTA neurons and 12-22 MΩ for PFC neurons. Light stimulation of individual neurons in the VTA was carried out via the microscope objective using a galvanometer based scanning system coupled to a 473 nm diode-pumped solid state laser. EYFP-expressing neurons in the VTA were targeted with brief flashes of light (4-15 ms) that caused clear light-evoked responses. For light-based stimulation experiments in the medial PFC (mPFC), an identical laser was coupled into a customized light fiber that was positioned just above the mPFC slice surface.

3.20 Reconstruction of the morphology of medial PFC neurons and VTA neurons†

For reconstruction of mPFC and VTA neuron morphology, slices were incubated in 4% PFA overnight. Next day, slices were washed 3x in PBS (0.1 M) and incubated with α-gt GFP at 4°C overnight and accordingly incubated with α-gt FITC and streptavidin for 1-2 hrs at room

* Electrophysiological analysis and reconstruction of medial PFC and VTA neuron morphology were performed by Milan Pabst, laboratory of Prof. Heinz Beck, Department of Epileptology, University of Bonn, Medical Center

temperature. Imaging was carried out using a confocal microscope and Z-stacks were analyzed using ImageJ (1.37c).

3.21 Image acquisition and optogenetic stimulation*

To monitor neuronal activation following optogenetic stimulation time series were acquired using two-photon excitation fluorescence microscopy using an ultrafast Ti:Sa laser coupled to a microscope equipped with a galvanometer-based scanning system and a 20x Objective. Videos were acquired with an average frame rate of >3 Hz and duration of approximately 5 s. Optogenetic stimulation was achieved using a 473 nm laser coupled to a multimode light fiber, which was placed directly above the slice illuminating the entire mPFC. A flash of 20 ms duration and 50 mW was triggered 2 s following the beginning of image acquisition. Blockers were bath applied cumulatively in the following order with three to four videos acquired for each of the conditions: 10 µM SCH-23390 and 100 nM L-741.626; 10 µM CNQX.

3.22 Calcium imaging†

For Ca^{2+}-imaging experiment 300 µm slices were obtained (Section 3.19). Slices were perfused in a submerged chamber with carbogen-saturated ACSF (3 mL/min) at 32°C and loaded with the $Ca2^{+}$ indicator dye OGB-1-AM (Oregon green 488 BAPTA-1 AM) as described previously (Garaschuk et al., 2006). 50 µg OGB-1-AM was dissolved in 4.5 µL 20% Pluronic in DMSO. 45 µL simplified Ca^{2+}-free Ringer was added to obtain a final concentration of 1mM. The dye was filtered and pressure injected using a patch pipette with a resistance of 4 MΩ at four evenly spaced sites within the mPFC. Imaging was commenced at least 30 min after dye loading procedure. Standard ACSF was used for recording.

3.23 Quantification

3.23.1 Progenitor domains

To determine the progenitor domains in control and mutant animals, every tenth section of E9.5, E10.5 and E11.5 embryos was processed for fluorescent immunostaining (Lmx1a) or RNA *In Situ* hybridization (Arx, Corin, Msx1). The sections were imaged on a Zeiss Axio observer using a 20x objective. For immunostained sections the Apotome setup was used. The

* Calcium imaging was performed by Oliver Braganza, laboratory of Prof. Heinz Beck, Department of Epileptology, University of Bonn, Medical Center

† Image acquisition and optogenetic stimulation was performed by Milan Pabst, laboratory of Prof. Heinz Beck, Department of Epileptology, University of Bonn, Medical Center

domains were outlined in the acquired images and measured using Fiji software (ImageJA 1.45e). The medial domain was defined as the Corin^{pos}/Lmx1a^{pos} progenitor domain, whereas lateral domain was defined as the Lmx1a^{pos}/Corin^{neg} domain. Sections from three mutants and three control animals were analyzed.

To analyze the proliferation, neurogenesis and cell death in control and knockout mice, the total number of BrdU^{pos}/Lmx1a^{pos}, Ngn2^{pos}/Lmx1a^{pos} and cleaved Caspase3^{pos}/Lmx1a^{pos} cells was counted in every tenth section using Photoshop Software. The number of BrdU^{pos,} Ngn2^{pos}, Caspase3^{pos} cells was normalized for the size of the Lmx1a domain measured by Fiji Software (ImageJA 1.45e). Sections were counted from at least three mutant and three control animals. The sections were imaged on a Zeiss Axio observer using a 20x objective and an Apotome setup.

3.23.2 MbDN subsets in postnatal brains (P21)

To quantify the number of MbDNs, sections from four rostrocaudal levels (from Bregma -2.92, -3.28, -3.64 and -3.88 mm; Franklin and Paxinos, 2007) were immunostained with TH. To determine two subpopulations of MbDNs, adjacent sections were immunostained for Girk2 and Calbindin, which are expressed in MbDNs of the SNpc and the VTA, respectively. Sections from at least three control and three mutant animals were imaged on a Zeiss Axio observer using 20x objective and the Zeiss MosaiX Software as well as an Apotome setup to assess double labeling (Axiovision, Zeiss). Double-labeled cells for TH and Girk2, and TH and Calbindin were counted bilaterally for each level using Photoshop Software.

3.23.3 MbDN projections to the forebrain, the amygdala and the striatum

Projections were quantified in sections in three control and three mutant animals at P48. Animals were injected with rAAV harboring a ChR2-EYFP fusion gene. To visualize the projections, sections were immunostained for TH and GFP. To quantify projections to the PFC, TH or GFP positive area in the mPFC (infralimbic cortex) from three rostrocaudal levels was selected (H x W: 0.47 mm x 0.36 mm) in coronal sections (AP: 2.58-2.10 mm; ML: ± 0.5 mm from Bregma; DV: 2.2-2.5 mm from dura; Franklin and Paxinos, 2007). Z-stack images (TH and GFP) of the selected areas were acquired on a Zeiss Axio observer using a 40x objective and an ApoTome Setup. To quantify projections to the amygdala, TH positive areas (H x W: 0.47 mm x 0.36 mm) in the amygdala were selected from three rostrocaudal levels in coronal sections (AP: -1.82 to -2.54 mm; ML: ±2.6-3.3 mm from Bregma: DV: 4.6-5.1 mm from dura; Franklin and Paxinos, 2007). For each animal, Z-stack images of selected areas

were acquired on a Zeiss Axio observer using a 20x objective and an ApoTome Setup. The acquisition parameters were kept the same for all images. To identify axonal structures for both PFC and amygdala as foreground objects pixel-based segmentations were produced using a segmentation algorithm (Advanced Weka Segmentation Plugin, Fiji Software). Potential axonal structures (TH or GFP positive) were assigned as class 1 and background (TH or GFP negative area) as class 2. The parameters were kept constant across images of control and mutant samples. The number of pixels in class 1 was quantified per selected area for each image (Fiji Software). MbDN projections to the PFC and amygdala were quantified unilaterally for each level.

Projections to the striatum (CPu, NAc and OTu) were analyzed on four rostrocaudal levels (AP: +1.54 to -0.22 mm). Images were acquired using a 10x objective on a Zeiss Axio observer and an ApoTome setup. To analyze the projections, Fiji Software was used. The area of interest was outlined and average raw integrated intensities or pixels of TH or GFP positive MbDN projections were quantified for the three areas (Fiji Software). The average integrated intensity above background was normalized for the area. MbDN projections to the striatum were quantified bilaterally for each level.

3.23.4 Quantification of rAAV injections in the VTA

To analyze injection sites and EYFP expression in the vMb, rAAV harboring a ChR2-EYFP fusion gene injected mice were sacrificed two weeks after injections. To visualize EYFP expression in MbDNs, TH and GFP immunohistochemistry was performed on coronal sections. Four rostrocaudal levels (Bregma: -2.92, -3.28, -3.64, -3.88; Franklin and Paxinos, 2007) were analyzed. TH and GFP positive area in the anterior VTA, RLi, CLi, IF and PN nuclei were imaged on a Zeiss Axio observer using 40x oil objective and an Apotome setup. Cells positive for GFP, as well as double positive cells for TH and GFP were counted for all four levels and then normalized to the total number of GFP^{pos} cells.

3.23.5 Quantification of vGlut2/TH and vGlut2/TH/GFP positive cells in the ventral midbrain

To analyze co-expression of vGlut2 and TH, and vGlut2, TH and GFP, combined RNA *In Situ* hybridization/Immunohistochemistry was performed on coronal sections. The expression of vGlut2 was visualized by RNA *In Situ* hybridization, while expression of TH and/or GFP was detected by immunohistochemistry. The vGlut2/TH expression was analyzed on three mutants and three wildtypes ($Gli2^{flox/+}$) at P21. The number of MbDN (TH^{pos}/$vGlut2^{neg}$),

vGlut2-only ($TH^{neg}/Glut2^{pos}$) cells was counted on four rostrocaudal levels (from Bregma: -2.92 mm, -3.28 mm, -3.64 mm, and -3.88 mm; Franklin and Paxinos, 2007). Cells were counted in the entire TH positive areas (SNpc, VTA, RLi, CLi) for each level.

$EYFP^{pos}$ cells co-expressing TH (MbDN), vGlut2 (vGlut2-only) or vGlut2 and TH (MbDN-vGlut2) were counted on two rostrocaudal levels and normalized for the total number of cells counted (from Bregma: -3.28 mm, -3.64 mm; Franklin and Paxinos, 2007) for three control and three mutant animals at P48. The histological analysis was performed two weeks after mice were injected with rAAV harboring a ChR2-EYFP fusion gene. Sections were imaged on a Zeiss Axio observer, using a 20x objective and a Bright Field Setup for vGlut2 expression and the Zeiss MosaiX Setup to assess an immunohistochemical labeling for TH and GFP (Axiovision Zeiss). For each level, cells were counted in the VTA (RLi, IF, PN and PBP).

3.23.6 Quantification of Calcium imaging data*

Imaging data were preprocessed in ImageJ and analyzed using Igor. Videos were registered and translated to the reference image in order to remove movement artifacts and drift. Regions of interest were manually placed on OGB1 positive cell somata. Only cells visible over the course of the entire experiment were included. Raw fluorescence intensity traces over time of individual cells were extracted and further processed using Igor. Traces of individual cells were normalized to baseline.

3.24 Statistical analysis

To determine statistical significance between control and mutant animals, unpaired Student's t-test (Excel Software) was used. Statistical significance levels were set at: *$p<0.05$, **$p<0.01$, ***$p<0.001$. Error bars indicate Standard error of the mean (SEM). All results are expressed as mean ± SEM.

Statistical analysis of electrophysiological data† was performed as appropriate using paired and unpaired Student's t-test, as well as Mann-Whitney tests, Friedman test with Dunn's multiple comparison, Kruskal-Wallis test with Dunn's multiple comparison and repeated measures ANOVA with Newman-Keuls post test.

* Quantification of Ca^{2+} imaging data was performed by Oliver Braganza, laboratory of Prof. Heinz Beck, Department of Epileptology, University of Bonn, Medical Center

† Statistical analysis of electrophysiological data was performed by Milan Pabst, laboratory of Prof. Heinz Beck, Department of Epileptology, University of Bonn, Medical Center

4. Results

4.1 Inactivation of Gli2-mediated Shh signaling after E9.0 in the midbrain

GIFM and conditional inactivation studies have demonstrated that the crucial time period for Shh signaling in establishing MbDNs is between E8.0 and E10.0 (Blaess et al., 2006 and 2011; Hayes et al., 2011). As described previously, the timing and duration of Shh signaling plays a role in the specification of MbDNp into SNpc versus VTA progenitors (Figure 5) (Section 1.16). After E9.0, medially located precursors cease to respond to Shh signaling, whereas laterally located precursors continue to respond to Shh signaling up to E10.0. Importantly, GIFM studies have shown, that the lateral precursors contribute preferentially to MbDN in the vmVTA (Blaess et al., 2011; Hayes et al., 2011), whereas medial precursors give rise to all MbDNs. To assess whether Shh signaling plays an instructive role in subset specification of MbDNs, mice in which Shh signaling was inactivated during the Shh-responsive period of MbDNp were analyzed. To this end conditional knockout mice were generated in which the zinc finger transcription factor *Gli2* was inactivated using Engrailed1 $En1^{Cre/+}$:$Gli2^{flox/zfd}$ (further referred to as a $Gli2^{\Delta Mb>E9.0}$) (Figure 8) (Kimmel et al., 2000; Blaess et al., 2006).

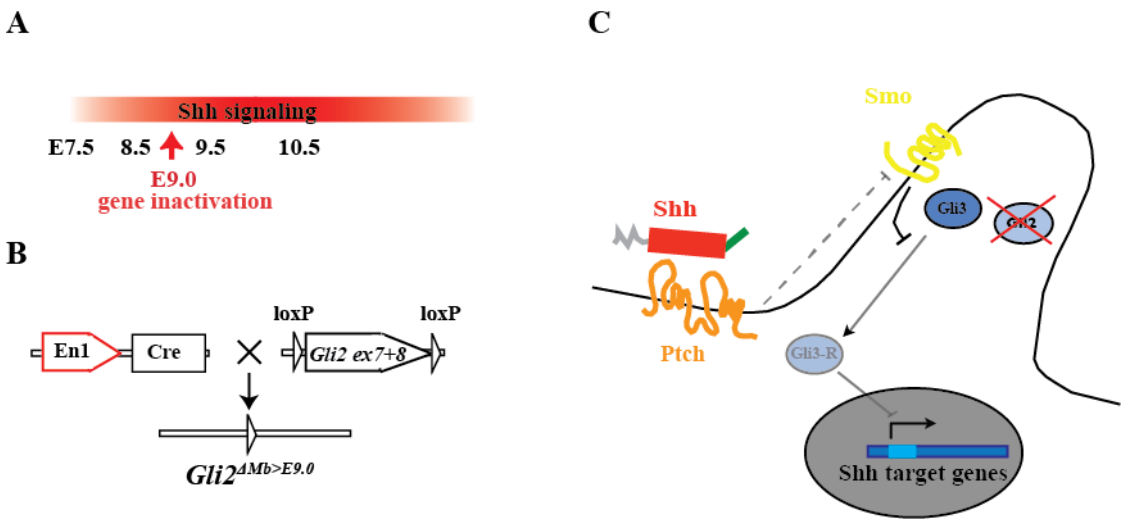

Figure 8 Conditional inactivation of Shh signaling. (A) Timeline of *Shh* expression in the vMb. Shh signaling is inactivated at E9.0 in $Gli2^{\Delta Mb>E9.0}$ mice. **(B)** Schematic of the conditional inactivation of *Gli2* in $Gli2^{\Delta Mb>E9.0}$ mice. Cre-recombinase is driven by the En1 promoter. Cre mediated recombination leads to the exclusion of exons 7 and 8 of *Gli2*, which are flanked by loxP sites. **(C)** Inactivation of *Gli2* results in no transcription of Shh target genes.

In these mice, Cre-mediated recombination occurs specifically in the midbrain and the aHb starting around E8.5 (Li et al., 2002). *Gli2* was inactivated instead of the Shh receptor Smo,

since *Gli2* is the primary activator downstream of Shh signaling and the main mediator of Shh-mediated MbDN induction (Matise et al., 1998; Bai et al., 2001 and 2002; Blaess et al., 2006). *Gli2*$^{\Delta Mb>E9.0}$ mice have a reduced number of MbDNs at E18.5 (Blaess et al., 2006). Despite these defects, *Gli2*$^{\Delta Mb>E9.0}$ mice are viable, allowing the analysis of MbDNs in the postnatal and adult brains. In contrast, conditional inactivation of Shh receptor Smo results in increased cell death in the vMb and aHb and early postnatal lethality (Blaess et al., 2006).

4.2 Medial but not lateral MbDNp are induced when Shh signaling is inactivated at E9.0

To investigate whether the inactivation of Gli2-mediated Shh signaling results in altered MbDNp generation, the expression domains of the genes known to be involved in MbDNp induction and specification of MbDNs were analyzed (Section 1.13 and 1.14). First, the expression of *Lmx1a* in the *Gli2*$^{\Delta Mb>E9.0}$ mice between E9.5 and E14.5 was assessed. In E9.5 *Gli2*$^{\Delta Mb>E9.0}$ embryos, the Lmx1a^{pos} area was not significantly smaller than in control embryos (Figure 9A). However, the Lmx1a^{pos} domain was significantly reduced in size in E10.5 *Gli2*$^{\Delta Mb>E9.0}$ embryos compared to wildtype littermates (56.5% ± 4% of wildtype) (Figure 9A, 10A-B). The expression domain of Arx, another transcription factor expressed in the MbDNp domain was only slightly reduced (95.9% ± 5.3% of wildtype) in E9.5 *Gli2*$^{\Delta Mb>E9.0}$ embryos, while in E10.5 *Gli2*$^{\Delta Mb>E9.0}$ embryos the Arx^{pos} area was significantly smaller than in the control littermates (56.9% ± 3.5% of wildtype) (Figure 9B, 10C-D). These data suggest that after E9.0, Shh signaling is required for the expansion of the MbDNp domain.

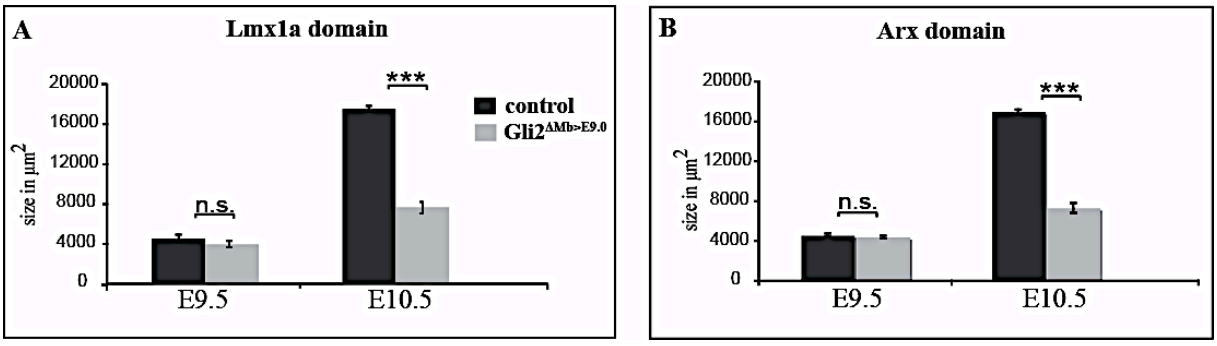

Figure 9 MbDNp domain is significantly decreased in *Gli2*$^{\Delta Mb>E9.0}$. (A) Quantitative analysis of the size of the Lmx1a^{pos} precursor domain in the vMb of E9.5 and E10.5 embryos. **(B)** Quantitative analysis of the size of the Arx^{pos} precursor domain in the vMb of E9.5 and E10.5 embryos. Error bars indicate SEM. Significance (p***<0.001) was determined by Student's t-test.

To investigate whether the remaining MbDNp domain is properly specified in *Gli2*$^{\Delta Mb>E9.0}$ mutants, the expression of further markers expressed within the MbDNp domain, Shh and

Foxa2, was analyzed (Figure 10E-H). In the wildtype vMb, Shh and Foxa2 expression is initially restricted to the Lmx1a^{pos} domain, but their expression then expands laterally to Lmx1a^{neg} precursors between E9.5 and E10.5 (Joksimovic et al., 2009; Blaess et al., 2011). At E11.5, Shh expression then starts to be downregulated in the medial MbDNp domain (Figure 11C) (Joksimovic et al., 2009; Blaess et al., 2011). In E9.5-E10.5 *Gli2*$^{\Delta Mb>E9.0}$ embryos, MbDNp in the Lmx1a^{pos} domain expressed Foxa2 and Shh (Figure 10E-H, Figure 11A-B; E9.5 data for Foxa2 expression not shown).

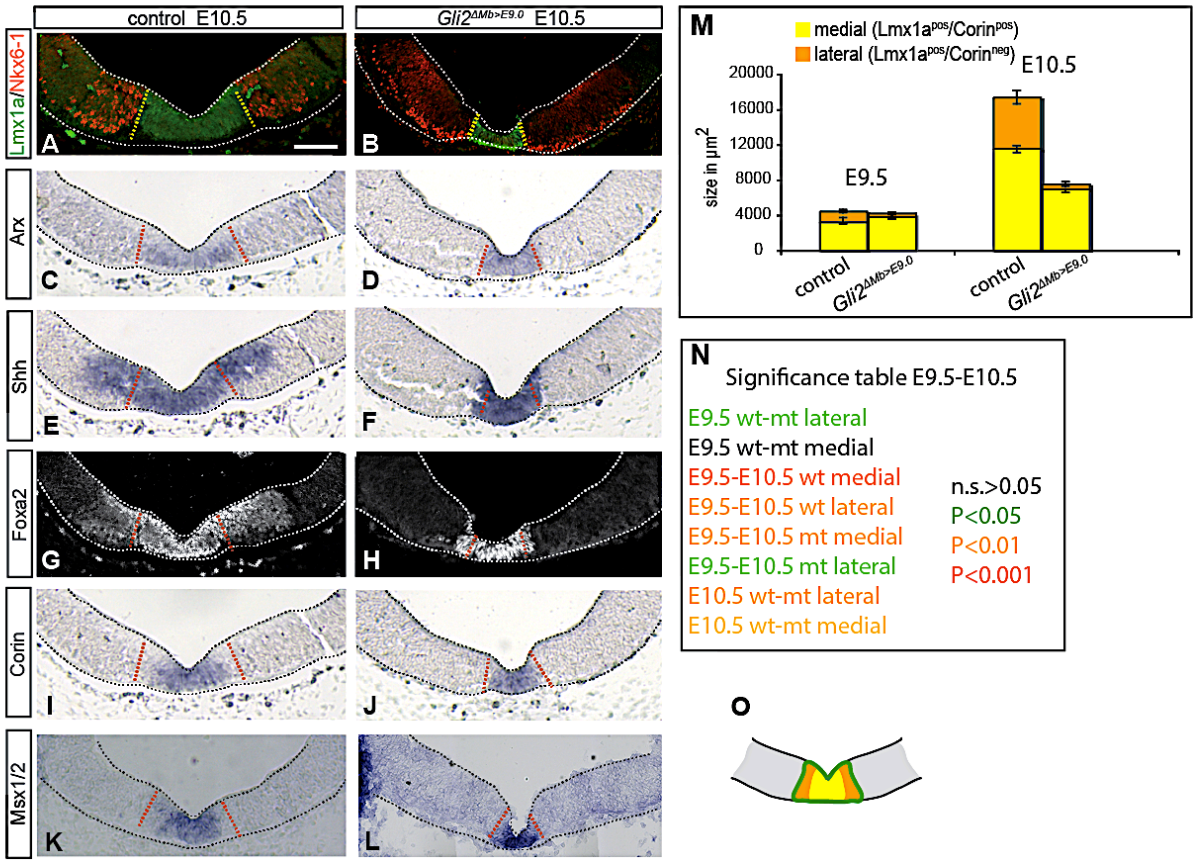

Figure 10 Shh is required for induction of lateral MbDNp domain after E9.0. (A-B, G-H) Immunofluorescent staining and RNA *In Situ* hybridization **(C-F, I-L)** on E10.5 coronal sections for markers of MbDNp domain (Lmx1a, Arx, Corin, Msx1/2, Shh, Foxa2) and Nkx6-1. The dashed line indicates Lmx1a^{pos} domain. Scale bar 100 µm. **(M)** Quantitative analysis of the size of the medial (Lmx1a^{pos}/Corin^{pos}, yellow) and lateral (Lmx1a^{pos}/Corin^{neg}, orange) precursor domain in the vMb of E9.5 and E10.5 embryos. Error bars indicate SEM. Significance was determined by Student's t-test. **(N)** Table indicating significant changes for the size of the medial and lateral domains for E9.5 and E10.5 control and mutant embryos. **(O)** Schematic of the medial (yellow) and lateral (orange) MbDNp (green) domains in E9.5-E10.5 wildtype embryo.

These data show that the remaining Lmx1a^{pos} progenitor domain appears to be properly specified in *Gli2*$^{\Delta Mb>E9.0}$ mutants. However, at E11.5, *Shh* expression was still detectable in

the medial MbDNp domain in *Gli2*$^{\Delta Mb>E9.0}$ embryos (Figure 11C-D). The lateral Lmx1a^{neg}/Foxa^{pos}/Shh^{pos} expression domain, which gives rise to non-MbDN (Section 1.18), was almost entirely missing in the mutants (Figure 10B, F, H, 11B, D). Furthermore, the data indicate that Shh signaling prior to E9.0 is sufficient to induce *Shh* and *Foxa2* in the ventral midline, and is not required for the maintenance of their expression. However, Shh signaling is required after E9.0 for the further expansion of the Foxa2 and Shh domain into the ventrolateral midbrain.

In the wildtype vMb, Nkx6-1 expression overlaps with Lmx1a up to E9.5, but it is excluded from the Lmx1a domain at later stages (Andersson et al., 2006). In E10.5 and E11.5 *Gli2*$^{\Delta Mb>E9.0}$ embryos, Nkx6-1 expression was shifted ventrally, but as in control animals it did not overlap with the Lmx1a^{pos} precursor domain (Figure 10 A-B). These results demonstrate that the regulation of gene expression in the remaining MbDNp domain of *Gli2*$^{\Delta Mb>E9.0}$ embryos occurred normally.

The Lmx1a^{pos} MbDNp domain can be further subdivided into a medial and a lateral domain based on gene expression and GIFM studies (Joksimovic et al., 2009; Blaess et al., 2011) (Section 1.16). The medial MbDNp domain expresses Msx1/2 and Corin, while laterally located MbDNp express only Lmx1a (Andersson et al., 2006; Ono et al., 2007; Blaess et al., 2011; Yan et al., 2011). To examine whether reduction of the Lmx1a^{pos} domain can be ascribed to a specific loss of either the medial or lateral MbDNp population, the expression of Corin and Msx1/2 in E9.5-10.5 control and *Gli2*$^{\Delta Mb>E9.0}$ embryos was analyzed (Figure 10I-L). Interestingly, in E9.5 and E10.5 *Gli2*$^{\Delta Mb>E9.0}$ embryos, Corin and Msx1/2 domain filled almost the entire Lmx1a^{pos} domain in the vMb, indicating that the lateral domain (Lmx1a^{pos}/Corin^{neg}/Msx1/2^{neg}) was lost in the mutant (Figure 10I-L). Indeed, quantification of the Corin^{pos} and Lmx1a^{pos} areas on adjacent sections of the posterior vMb showed that the Lmx1a^{pos}/Corin^{neg} domain was severely reduced, in both E9.5 (31.7% ± 12.4% of wildtype) and E10.5 (11.2% ± 6.5% of wildtype) *Gli2*$^{\Delta Mb>E9.0}$ embryos (Figure 10M). In contrast, the medial domain (Lmx1a^{pos}/Corin^{pos}/Msx1/2^{pos}) was not reduced at E9.5 in the mutants. However, by E10.5, the medial domain was altered in the mutants (60.3% ± 2% of wildtype), compared to control embryos, but was not as severely reduced as the lateral domain (Figure 10M). In summary, these data indicate that, prior to E9.0, Shh signaling is sufficient to induce the Lmx1a^{pos} MbDNp domain. After E9.0 Shh signaling is required for the further expansion of the MbDNp domain and in particular for the induction of the lateral (Lmx1a^{pos}/Corin^{neg}/Msx1/2^{neg}) MbDNp domain.

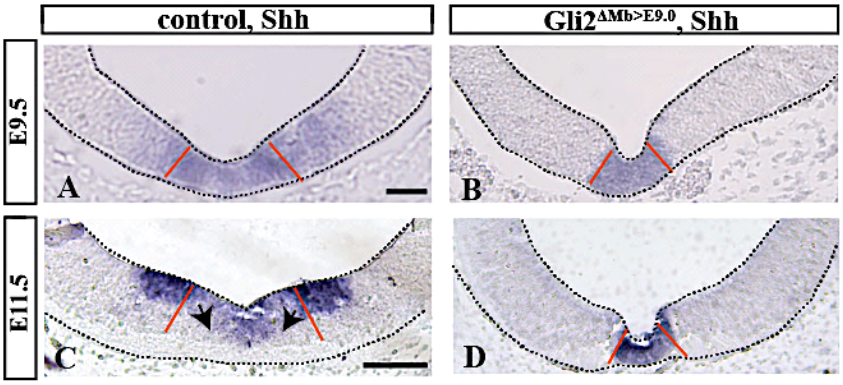

Figure 11 Shh signaling is required for Shh domain expansion after E9.0, but not for its maintenance. (A-B, C-D) RNA *In Situ* hybridization for *Shh* on E9.5 (A-B) and E11.5 (C-D) coronal sections. Lmx1a domain is indicated in red. Arrows: medial downregulation of *Shh* expression. Scale bars (A-B) 100 µm, (C-D) 50 µm

Wnt1 has been implicated in an autoregulatory induction loop with Lmx1a (Chung et al., 2009) (Figure 4, Section 1.14). Since Wnt1 plays an important role in MbDN development (Sections 1.13 and 1.14), Wnt1 expression might be affected in *Gli2*$^{\Delta Mb>E9.0}$ mutants.

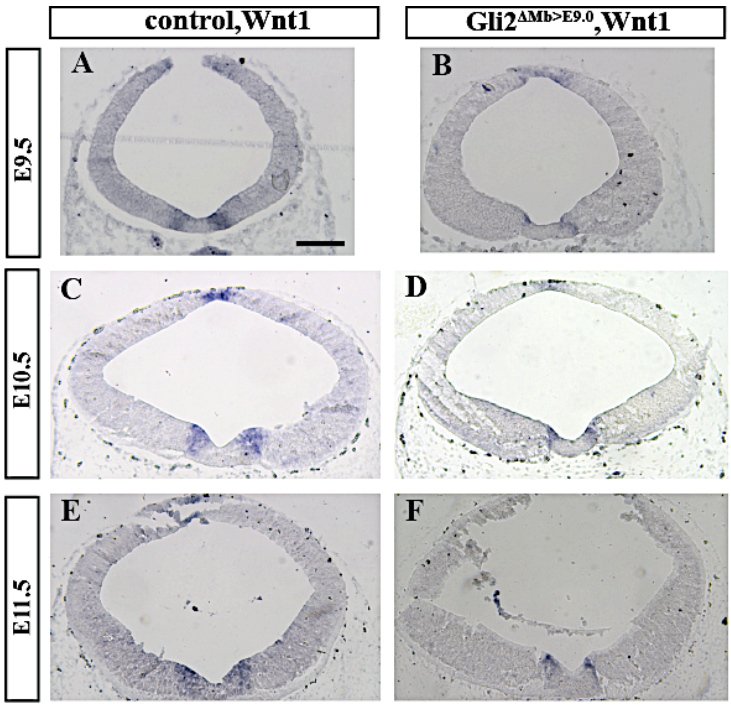

Figure 12 Reduction in Wnt1 expression in *Gli2*$^{\Delta Mb>E9.0}$. (A-F) RNA *In Situ* hybridization for Wnt1 on E9.5 (A-B), E10.5 (C-D) and E11.5 (E-F) coronal sections. Scale bar 100 µm.

Indeed, RNA *In Situ* hybridization for Wnt1 at E9.5-E12.5 showed that Wnt1 expression appeared to be reduced *Gli2*$^{\Delta Mb>E9.0}$ embryos (Figure 12 A-F, E12.5 data not shown).

4.3 Reduction of the lateral MbDN precursor domain in *Gli2*$^{\Delta Mb>E9.0}$ embryos is not caused by a decrease in proliferation

The severe reduction of the lateral MbDNp domain in *Gli2*$^{\Delta Mb>E9.0}$ embryos indicates that Shh signaling is required for the expansion of this domain after E9.0. Shh-induced expansion of the domain could either be mediated through the regulation of proliferation of pre-existing medial Lmx1a^{pos} precursors or through the induction of Lmx1a expression in lateral precursors previously negative for Lmx1a. To assess proliferation, proliferating cells were labeled with an one hour BrdU pulse in E9.5 and E10.5 control and *Gli2*$^{\Delta Mb>E9.0}$ embryos. BrdU is an analogue of thymidine and is incorporated into the DNA during the S-Phase of the cell cycle. Quantification of BrdU^{pos} cells within the Lmx1a^{pos} domain in E9.5 and E10.5 embryos showed that the proliferation in the MbDNp domain in *Gli2*$^{\Delta Mb>E9.0}$ mutants (E9.5: 42 ± 4 cells/10^4 μm^2 and E10.5: 55 ± 8 cells/10^4 μm^2) was not significantly different from control littermates (E9.5: 70 ± 10 cells/10^4 μm^2 and E10.5: 62 ± 5 cells/10^4 μm^2) (Figure 13A-B, G; E9.5 data not shown). To exclude that the decrease in MbDNp is caused by an increase in cell death, immunostainings for activated Caspase-3 were carried out on E9.5-E10.5 control and *Gli2*$^{\Delta Mb>E9.0}$ embryos. No changes in the number of apoptotic cells in the MbDNp domain in E10.5 *Gli2*$^{\Delta Mb>E9.0}$ mutants (0.95 ± 0.83 cells/10^4 μm^2) were observed compared to control littermates (0.97 ± 0.88 cells/10^4 μm^2). These data indicate that the reduction in the Lmx1a^{pos} domain in *Gli2*$^{\Delta Mb>E9.0}$ mice is likely due to an impaired induction of Lmx1a expression in lateral, initially Lmx1a^{neg} precursors, rather than an impaired capacity of *Lmx1a* expressing precursors to proliferate or to survive.

To assess whether the Lmx1a^{pos} cells maintained their proper progenitor fate in *Gli2*$^{\Delta Mb>E9.0}$ embryos, the expression of hairy and enhancer of split 5 (Hes5*)* was analyzed. Hes5 is downstream of Delta-like 1 in the Notch signaling pathway and suppresses the expression of proneural genes (Ohtsuka et al., 1999). Hes5 was expressed in the MbDNp domain in both *Gli2*$^{\Delta Mb>E9.0}$ and control embryos at E11.5 (Figure 13 C-D).

To investigate whether the progenitors in the remaining Lmx1a^{pos} domain can undergo normal neurogenesis, the expression of the proneural gene *Ngn2* was examined (Section 1.14). Quantification of the number of Ngn2^{pos} cells within the Lmx1a^{pos} domain in *Gli2*$^{\Delta Mb>E9.0}$ and control embryos at E11.5 demonstrated that the number of Ngn2^{pos} cells was similar in control and mutant embryos when normalized for the size of the MbDNp domain (Figure 13E-F, H).

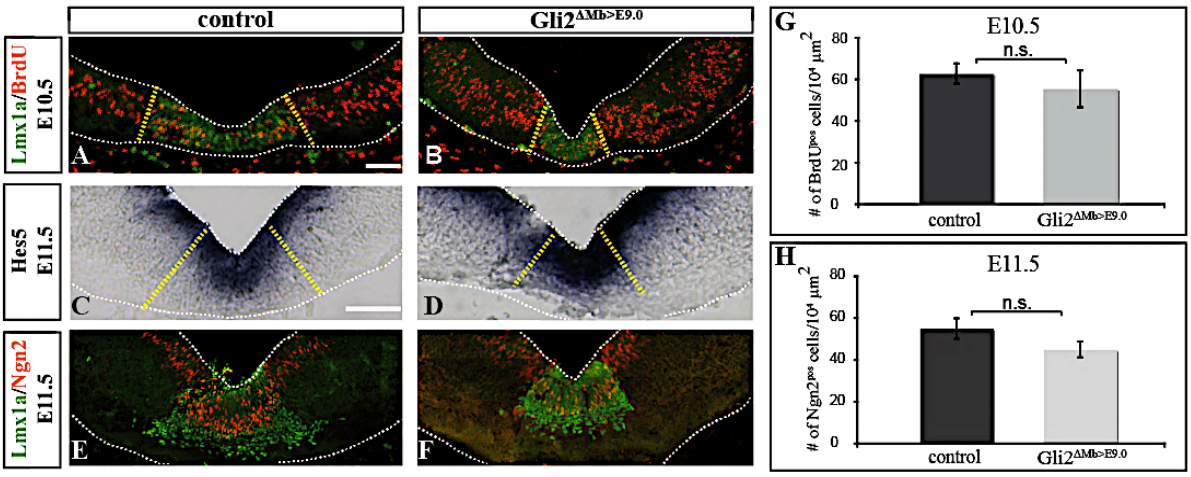

Figure 13 Proliferation and neurogenesis in the MbDNp domain is not affected in *Gli2*$^{\Delta Mb>E9.0}$ mice. (A-B) One hour BrdU pulse to label proliferating precursors in the vMb at E10.5. **(C-D)** RNA *In Situ* hybridization for Hes5 expressed in the MbDNp domain at E11.5. **(E-F)** Immunofluorescent staining for Ngn2 on E11.5 coronal section. Dashed yellow lines indicate the Lmx1a^{pos} domain. Scale bars (A-B) 100 µm; (C-F) 50 µm. **(G)** Quantitative analysis of the number of BrdU^{pos} cells normalized to the size of Lmx1a^{pos} domain for level of section shown in A-B. **(H)** Quantitative analysis of the number of Ngn2^{pos} cells normalized to the size of Lmx1a^{pos} domain for level of sections shown in E-F. Error bars indicate SEM. Significance was determined by Student's t-test.

However, analysis at E10.5 showed that the onset of neurogenesis was delayed in the vMb of *Gli2*$^{\Delta Mb>E9.0}$ embryos, since Ngn2^{pos} cells were present in the control but not the mutant Lmx1a^{pos} precursor domain at this stage (data not shown). These results show that the remaining MbDNp in *Gli2*$^{\Delta Mb>E9.0}$ embryos are capable of normal neurogenesis.

4.4 Shh signaling is required after E9.0 for the generation of MbDN

To investigate how the almost complete loss of the lateral MbDNp domain and the reduced size of the medial MbDNp domain affects the generation of differentiated MbDNs, immunohistochemistry for TH was performed on coronal sections through the rostrocaudal extent of the developing vMb in E10.5, E11.5, E12.5, E14.5 and E18.5 control and *Gli2*$^{\Delta Mb>E9.0}$ embryos (Figure 14A-F, 15A-B). The first differentiated MbDNs expressing TH appear already at E10.5 in control mice, whereas TH^{pos} MbDNs could not be detected in the *Gli2*$^{\Delta Mb>E9.0}$ vMb (data not shown). This could be explained by the delayed neurogenesis in the *Gli2*$^{\Delta Mb>E9.0}$ embryos (Section 4.3).

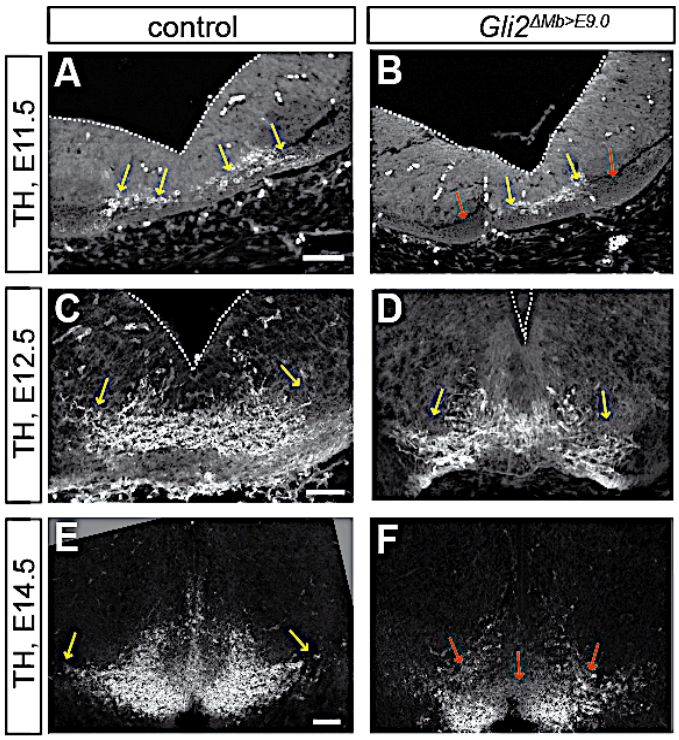

Figure 14 Shh signaling is required after E9.0 for the proper generation of MbDNs. (A-F) Immunostaining for differentiating MbDNs (TH) in E11.5 (A-B), E12.5 (C-D) and E14.5 (E-F) wildtype and *Gli2*$^{\Delta Mb>E9.0}$ embryos. Yellow arrows indicate TH^{pos} cells. Red arrows indicate loss of MbDNs in the *Gli2*$^{\Delta Mb>E9.0}$ mutants. Scale bar 100 µm.

At E11.5 MbDNs in the *Gli2*$^{\Delta Mb>E9.0}$ vMb were severely reduced (Figure 14A-B). In contrast to control embryos, where the newly generated TH^{pos} MbDNs are clustered off-midline, TH^{pos} cells in the mutant were all located medially. At E12.5 and E14.5 MbDNs were still reduced and excluded from the ventral midline (Figure 14C-F). In addition, TH^{pos} cells were scattered and disorganized in *Gli2*$^{\Delta Mb>E9.0}$ mutants.

At E18.5 vmVTA and dlVTA first can be identified anatomically. MbDNs were severely reduced in E18.5 *Gli2*$^{\Delta Mb>E9.0}$ embryos (Figure 15A-B). The decrease in MbDNs was particularly obvious in areas that would correspond to the vmVTA and the SNpc in the control brains (Figure 15A-F). To exclude that the apparent reduction in MbDNs is due to a downregulation of TH expression, rather than a reduction in the number of MbDNs, other typical MbDN markers such as Nurr1 and Foxa2 at E18.5 were analyzed (Figure 15C-F).

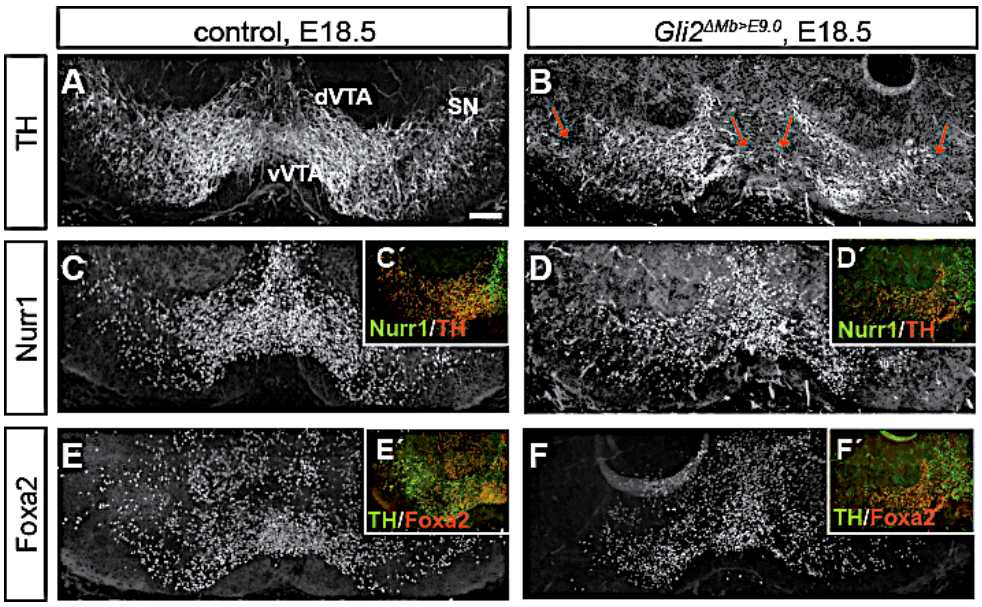

Figure 15 Reduced MbDNs in *Gli2*$^{\Delta Mb>E9.0}$ embryos express MbDN markers. (A-B) Immunostaining for differentiated MbDNs (TH) in E18.5 control and *Gli2*$^{\Delta Mb>E9.0}$ embryos. Red arrows indicate loss of MbDNs in *Gli2*$^{\Delta Mb>E9.0}$ mutants. **(C-F)** Immunostaining for Nurr1 and Foxa2 on E18.5 coronal sections. **(C'-F')** Enlarged boxes show co-expression of Nurr1 and TH, Foxa2 and TH. Scale bar 100 µm.

Nurr1 is expressed in differentiating and mature MbDNs (Section 1.15), whereas Foxa2 is not only expressed in MbDNp and MbDNs, but also in the other vMb cells (Kittappa et al., 2007) (Section 1.14). Both Foxa2 and Nurr1 are expressed in the MbDNs of *Gli2*$^{\Delta Mb>E9.0}$ mice, meaning that remaining MbDNs are properly specified. However, the decrease in TH^{pos}/Nurr1^{pos} and TH^{pos}/Foxa2^{pos} MbDNs was more obvious in areas that correspond to the vmVTA and the SNpc in the control animals. Nurr1^{pos}/TH^{neg} cells can be found in the vmVTA, particularly in RLi. There was no obvious difference between *Gli2*$^{\Delta Mb>E9.0}$ and control brains in the amount of TH^{neg}, Nurr1^{pos} or TH^{neg}, Foxa2^{pos} cells in the RLi (Figure 15C-F). In summary, these results demonstrate that inactivation of Gli2-mediated Shh signaling at E9.0 in the vMb results in severe reduction of MbDNs in *Gli2*$^{\Delta Mb>E9.0}$ mice, however the remaining MbDNs are properly specified.

4.5 Inactivation of Shh signaling at E9.0 results in a preferential loss of Calbindin positive VTA neurons

A detailed anatomical analysis of different subgroups of MbDNs is only possible in the mature brain. To quantitatively assess the number and distribution of MbDNs, P21 *Gli2*$^{\Delta Mb>E9.0}$ and control brains were analyzed. This stage was chosen, since mice heterozygous for *En1* show degeneration of MbDNs after 8 weeks of age (Sonnier et al., 2007). In *Gli2*$^{\Delta Mb>E9.0}$ mice (*En1*$^{Cre/+}$:*Gli2*$^{zfd/flox}$) part of the *En1* coding sequence is replaced

by the Cre cDNA, making these mice heterozygous for *En1* (Kimmel et al., 2000). Therefore, TH^{pos} MbDNs were counted bilaterally in sections from four rostrocaudal levels (approximately from Bregma in mm: -2.92, -3.28, -3.64 and -3.88; Franklin and Paxinos, 2007) of at least three $Gli2^{\Delta Mb>E9.0}$ and three control mice. The total number of TH^{pos} MbDNs in $Gli2^{\Delta Mb>E9.0}$ brains was reduced to 53.5% ± 3.21% of the MbDN number in control brains (Figure 16 A-D, E).

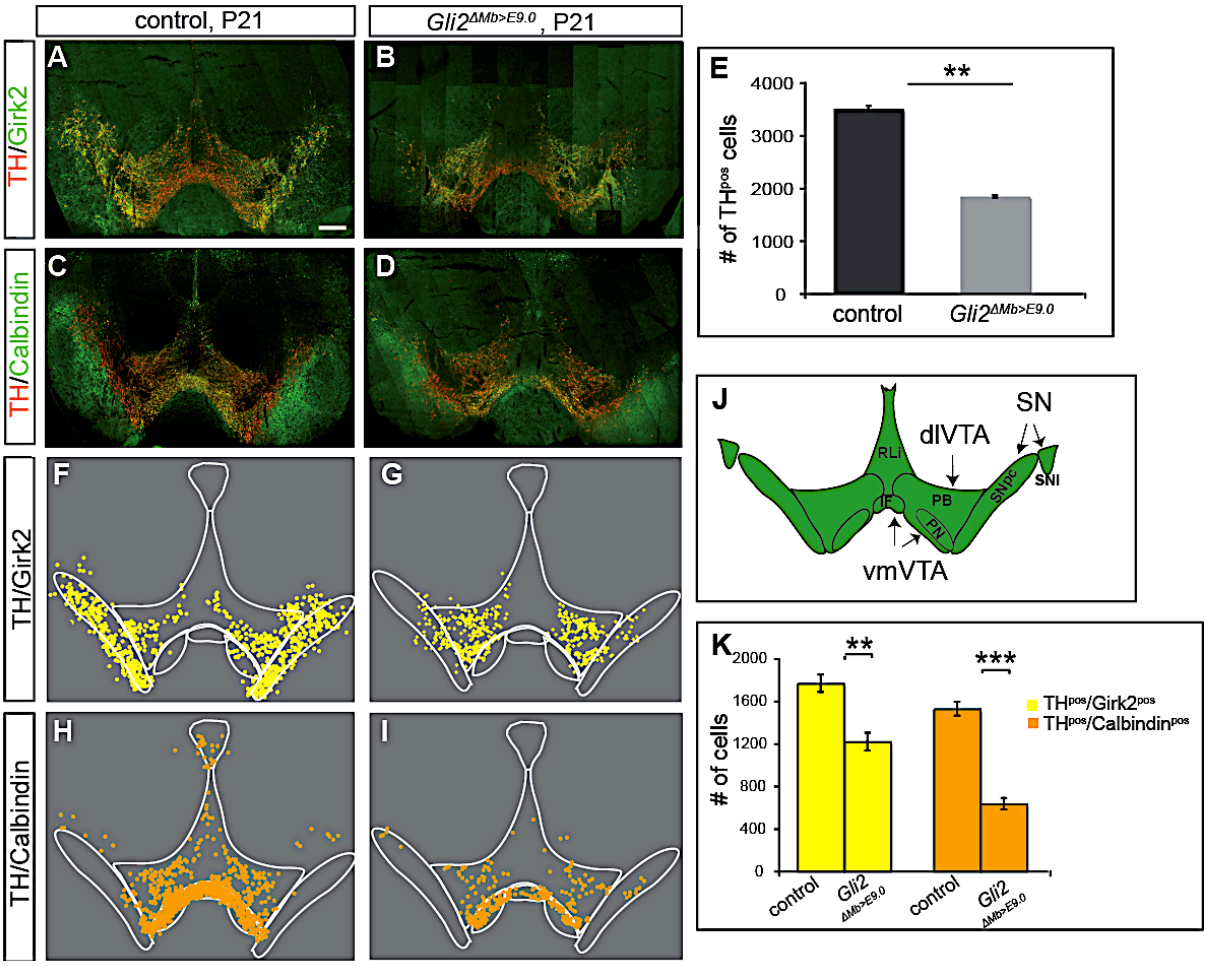

Figure 16 Severe loss of Calbindin positive cells in $Gli2^{\Delta Mb>E9.0}$ mice. (A-D) Immunostaining for MbDNs in the SNpc ($Girk2^{pos}$) and VTA ($Calbindin^{pos}$) on P21 coronal sections. Scale bar 500 µm. **(E)** Quantitative analysis of the number of TH^{pos} cells in sections A-D. **(F-I)** Schematic showing the distribution of $Girk2^{pos}$ (yellow dots) and $Calbindin^{pos}$ (orange dots) MbDNs in the vMb (sections in A-D). **(J)** Plane of section shown in A-D represents distinct subpopulations of MbDNs in the vMb. **(K)** Quantitative analysis of the number of $Girk2^{pos}$ and $Calbindin^{pos}$ cells at section levels shown in A-D. Error bars indicate SEM. Significance (p**<0.01; p***<0.001) was determined by Student's t-test.

Interestingly, along the rostrocaudal axis of the vMb the MbDN reduction was more prominent rostrally (Bregma -2.92 and -3.28 mm: 48.2% ± 2.09% of MbDNs in control brains) than caudally (Bregma -3.64 and -3.88 mm: 61.4% ± 4.3% of the MbDNs in control

brains). The distribution of MbDNs in the *Gli2*$^{\Delta Mb>E9.0}$ mutants was comparable to E18.5 (Figure 15B). Immunohistochemical and morphological analysis revealed that both, SNpc and VTA appeared to be affected, but the areas corresponding to the vmVTA (PN and IF) and RLi were most severely reduced (Figure 16A-D).

To investigate whether the reduction in VTA MbDNs was indeed more severe than the reduction in SNpc MbDNs in *Gli2*$^{\Delta Mb>E9.0}$ mice, the expression of Girk2 and Calbindin in P21 brains was analyzed. Girk2 and Calbindin are preferentially expressed in the SNpc and VTA, respectively (Section 1.4) (Figure 16A, C). Girk2^{pos}/TH^{pos} and Calbindin^{pos}/TH^{pos} MbDNs were counted bilaterally in sections from four rostrocaudal levels (approximately from Bregma in mm: -2.92, -3.28, -3.64 and -3.88; Franklin and Paxinos, 2007) of at least three *Gli2*$^{\Delta Mb>E9.0}$ and three control mice. In *Gli2*$^{\Delta Mb>E9.0}$ mice, the number of Calbindin^{pos}/TH^{pos} MbDNs (41.8% ± 4.6% of wildtype) was significantly more reduced than the number of Girk2^{pos}/TH^{pos} MbDNs (69.5% ± 7.4% of wildtype) (Figure 16F). Similar to the graded reduction of TH^{pos} MbDNs along the rostrocaudal axis in *Gli2*$^{\Delta Mb>E9.0}$ brains, the number of Calbindin^{pos}/TH^{pos} (40.7% ± 5.5% of the MbDNs in control) and Girk2^{pos}/TH^{pos} (63.4% ± 2.9% of the MbDNs in control) MbDNs was more prominently reduced rostrally than caudally (Calbindin^{pos}/TH^{pos}: 47.7% ± 5.8% and Girk2^{pos}/TH^{pos}: 77.06% ± 7.04% of the cells in control). These results demonstrate that inactivation of Shh signaling after E9.0 affects the generation of Calbindin^{pos} MbDNs in the VTA more severely than the generation of Girk2^{pos} MbDNs in the SNpc.

4.6 Shh signaling is required for the proper distribution of the MbDNs

Both the SNpc and the VTA appeared to be severely reduced in *Gli2*$^{\Delta Mb>E9.0}$ mutants, however MbDNs in the VTA are more affected then MbDNs in the SNpc. To exclude the possible change in the cell fates from one population to another, distribution of Calbindin^{pos} and Girk2^{pos} MbDNs on four rostrocaudal levels (approximately from Bregma in mm: -2.92, -3.28, -3.64 and -3.88; Franklin and Paxinos, 2007) in control and *Gli2*$^{\Delta Mb>E9.0}$ animals was analyzed. Interestingly, MbDNs located more anteriorly (Bregma -2.92 mm) are distributed properly in the mutant mice (data not shown). However, more posterior Calbindin^{pos}/TH^{pos} MbDNs were mainly located in the area that would correspond to the PN and PBP in the wildtype vMb, with only few cells found in the IF (Figure 16D, I). Notably, the RLi nucleus appeared to be devoid of MbDNs in the *Gli2*$^{\Delta Mb>E9.0}$ vMb. Interestingly, Girk2^{pos}/TH^{pos} MbDNs, which can be found in the SNpc in wildtype, were shifted to a more medial position in *Gli2*$^{\Delta Mb>E9.0}$ mice that corresponds to the dorsal VTA in the wildtype (Figure 16B, G).

MbDNs of the RRF appeared to be localized correctly. These data indicate that in addition to a decrease in the MbDN number in *Gli2*$^{\Delta Mb>E9.0}$ mice, remaining MbDNs are disorganized.

4.7 MbDNs co-expressing vGlut2 are reduced in *Gli2*$^{\Delta Mb>E9.0}$ mice

In the vmVTA, including the RLi nucleus, MbDNs are intermixed with glutamatergic neurons (vGlut2-only) and a subset of MbDNs in the vmVTA even co-expresses vGlut2 (MbDN-vGlut2), a marker for glutamatergic neurons (Yamaguchi, 2011) (Section 1.5).

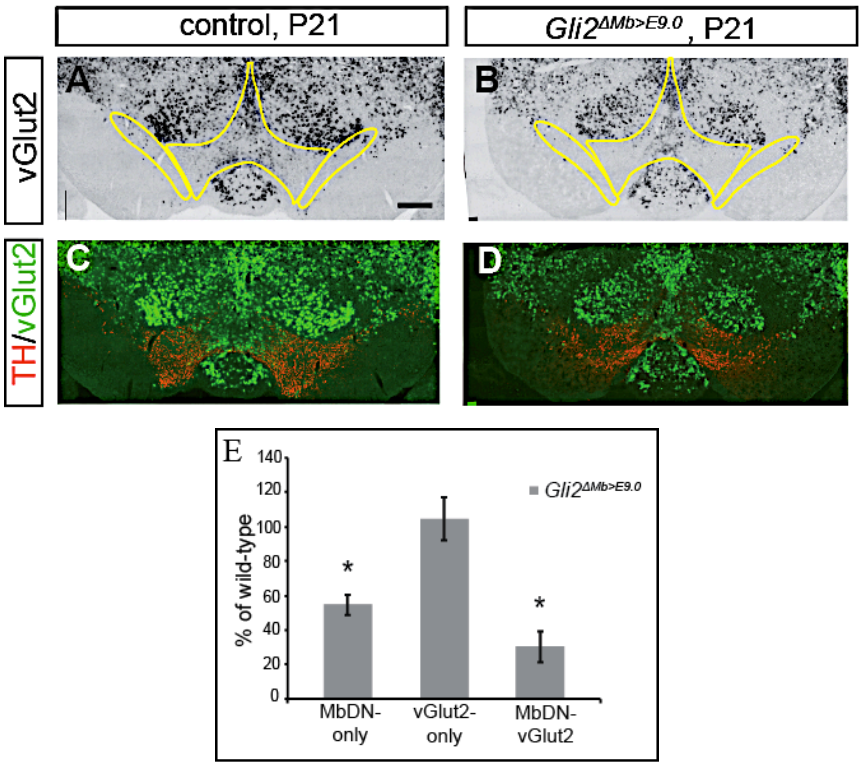

Figure 17 MbDN-vGlut2 are reduced in *Gli2*$^{\Delta Mb>E9.0}$ mice. (A-B) RNA *In Situ* hybridization for vGlut2, a marker for glutamatergic neurons. Yellow outlines indicate area used for quantitative analysis in E. **(C-D)** RNA *In Situ* hybridization for vGlut2 (image color was inverted and false colored in green) combined with immunostaining for TH. Scale bar 500 µm. **(E)** Quantitative analysis of the number of MbDN, vGlut2-only and MbDN-vGlut2 cells at the section level shown in A-D. Error bars indicate SEM. Significance (p*<0.05) was determined by Student's t-test.

The developmental origin of these glutamatergic neurons has not been determined, but their precursors might also depend on Shh signaling for their induction. Since MbDNs in the vmVTA are severely affected in *Gli2*$^{\Delta Mb>E9.0}$ mice, MbDN-vGlut2 could be particularly affected in the mutants as well. To this end, RNA *In Situ* hybridization for vGlut2, followed by immunostaining for TH to mark the MbDNs containing areas was performed (Figure 17A-D). The number of MbDNs (TH^{pos}/vGlut2^{neg}) was reduced by 46% in *Gli2*$^{\Delta Mb>E9.0}$ mice

(Figure 17E). Interestingly, there were only 30% of MbDN-vGlu2 neurons left in the mutant brains (Figure 17E).

Analysis of the number of vGlut2-only neurons in these areas showed no significant difference between *Gli2*$^{\Delta Mb>E9.0}$ and control brains (Figure 17E). These results demonstrate that the inactivation of Shh signaling does not affect the generation of glutamatergic neurons in the vMb, but leads to a severe reduction of MbDN-vGlut2.

4.8 Shh signaling is required to establish mesocortical MbDNs

MbDN, MbDN-vGlut2 and vGlut2-only neurons project to the NAc and the PFC, while SNpc MbDNs target primarily the dorsal striatum (Figure 18A) (Section 1.5, 1.6). Since MbDN and MbDN-vGlut2 in the vmVTA were severely reduced in *Gli2*$^{\Delta Mb>E9.0}$ mice, it raises a question how the preferential reduction of these neurons impacts on the formation of the dopaminergic circuitry. First, the projections of MbDNs in control and *Gli2*$^{\Delta Mb>E9.0}$ brains at P48 using immunostaining for TH were examined (Pickel et al., 1975). Since *En1* drives Cre expression and subsequent recombination only in the vMb and aHb, the forebrain targets of MbDNs should not be directly affected by the conditional inactivation of *Gli2* and any defects in the MbDN projections in *Gli2*$^{\Delta Mb>E9.0}$ mutant should be due to changes in the number and/or the fate of MbDNs. To quantify the density of the projections, the intensity of TH and glyco-DAT fluorescence in the striatum or the number of pixels in the amygdala and PFC were measured in wildtype and *Gli2*$^{\Delta Mb>E9.0}$ mutant brains (Figure 18B-K). Glyco-DAT is expressed at high levels in MbDN projections to the striatum, but only weakly in projections to the PFC or amygdala (Afonso-Oramas et al., 2009). Surprisingly, despite the significant reduction in the number of SNpc and VTA MbDNs in *Gli2*$^{\Delta Mb>E9.0}$ brains (Figure 16E), there was no significant difference in the fluorescent intensity of TH or glyco-DAT staining in the CPu complex of the mutants compared to control brains (Figure 18B-E). Moreover, no difference in the number of TH fluorescent pixels in the amygdala between *Gli2*$^{\Delta Mb>E9.0}$ and control animals was detected (Figure 18F-H).

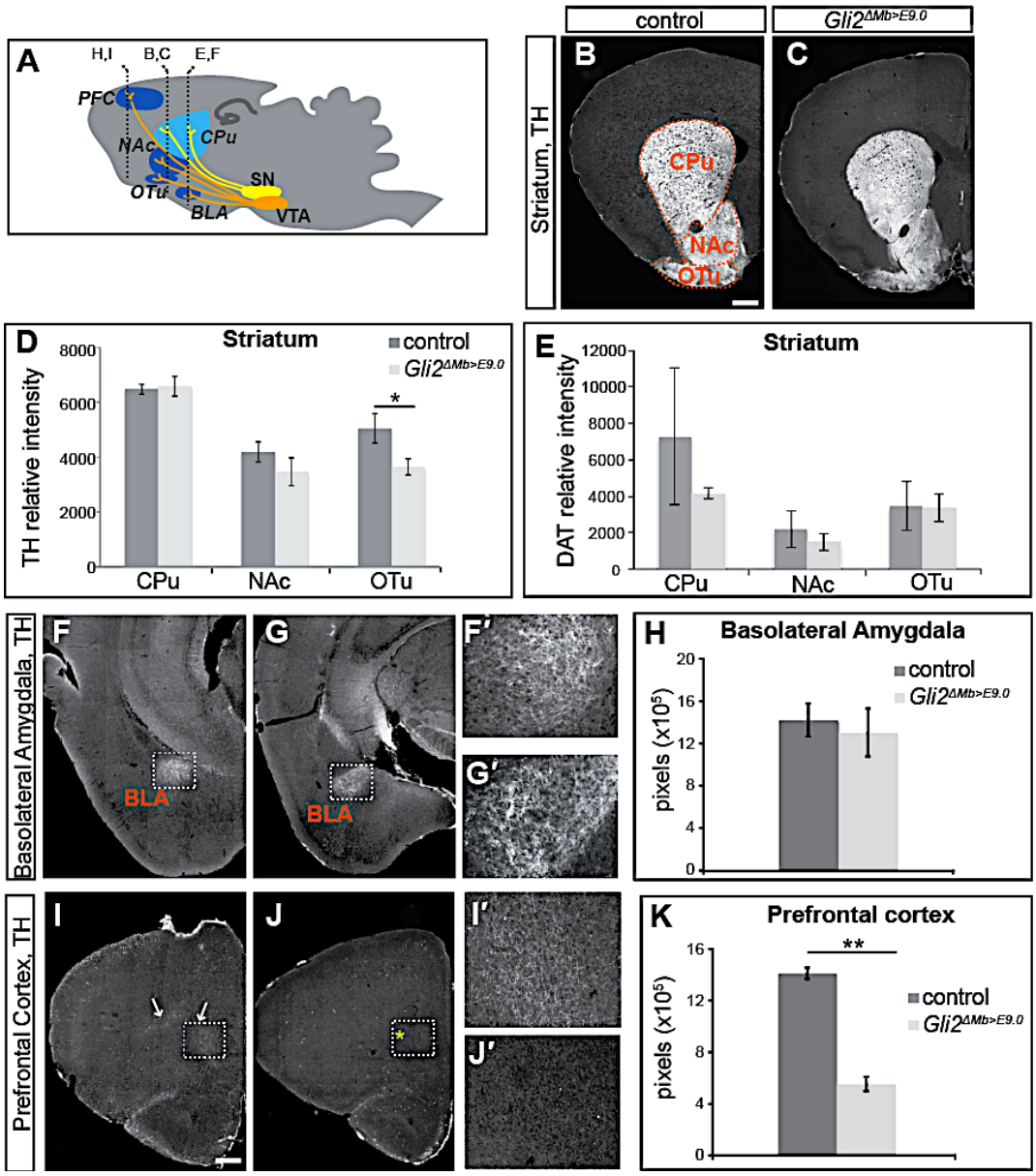

Figure 18 Mesocortical projections are severely reduced in *Gli2*$^{\Delta Mb>E9.0}$ mice. (A) Projections of MbDNs to the forebrain. Levels of sections in B-J are indicated. **(B-J)** Immunostaining for TH to visualize MbDN projections to the striatum (B-C), BLA (F-G) and PFC (I-J). (F'-J') Higher magnification of the boxed area in F-J. White arrows indicate TH^{pos} fibers in the PFC; yellow asterisks their absence. **(D, G, J)** Quantitative analysis of relative fluorescence (TH) intensity in the striatum (D) and number of fluorescent (TH) pixels above background in BLA (H) and PFC (K). **(E)** Quantitative analysis of relative fluorescence (glyco-DAT) intensity in the striatum. The relative fluorescent intensity in the striatum is normalized to the area. Error bars indicate SEM. Significance (p**<0.01) was determined by Student's t-test.

MbDN projections to the OTu were only slightly reduced in *Gli2*$^{\Delta Mb>E9.0}$ brains (Figure 18D, E). However, quantification of the number of TH fluorescent pixels in the PFC showed that the projections to the PFC were severely reduced in the *Gli2*$^{\Delta Mb>E9.0}$ mutants (Figure 18I-K). These data demonstrate that despite the significant reduction in the number of MbDNs in

SNpc and VTA, MbDN projections to the CPu, NAc and amygdala are not affected in the mutants, whereas MbDN projecting to the PFC are severely reduced in *Gli2*$^{\Delta Mb>E9.0}$ mice.

4.9 Tracing of MbDN axons originating in the ventromedial VTA confirms severe reduction in mesocortical projections*

Since the apparent loss of TH^{pos} projections to the PFC could potentially be due to a specific downregulation of TH in mesocortical MbDN axons in *Gli2*$^{\Delta Mb>E9.0}$ brains, MbDN axons were labeled with a fluorescent protein (EYFP). Strong EYFP expression in MbDN axons was achieved through stereotactic injection of rAAV harboring a ChR2-EYFP fusion gene into the vmVTA of postnatal brains of *Gli2*$^{\Delta Mb>E9.0}$ and control (*En1*$^{Cre/+}$) mice (Figure 19A). The rAAV harbors an expression cassette that results in ChR2 and EYFP expression only after Cre-mediated recombination (Kravitz et al., 2012). Since *En1* drives Cre expression primarily in MbDNs in the postnatal vMb (Simon et al, 2001), MbDN cell bodies and axons are labeled with EYFP. Immunohistochemical analysis showed that 60% of all EYFP^{pos} cells co-expressed TH in both, control and *Gli2*$^{\Delta Mb>E9.0}$ brains (Figure 19B-D). The absolute number of EYFP-expressing MbDNs and cells positive for EYFP and TH, was however severely reduced in the mutant mice (EYFP^{pos} cells: 34 ± 12; EYFP^{pos}/TH^{pos} cells: 22 ± 13) compared to control mice (EYFP^{pos} cells: 100 ± 4; EYFP^{pos}/TH^{pos} cells: 65 ± 21.9).

The pixel analysis of EYFP^{pos} fibers in the PFC confirmed that the mesocortical MbDN projections are severely reduced in the *Gli2*$^{\Delta Mb>E9.0}$ brains (4.1 ± 0.6 pixels x 10^5) compared to control (14,7 ± 2.2 pixels x 10^5) (Figure 19G-H, I). As expected VTA MbDN projections in control mice innervate only the ventral part of the striatum (NAc and OTu). Interestingly, in *Gli2*$^{\Delta Mb>E9.0}$ brains, MbDNs projected into the ventral, as well as the dorsal part of the striatum (CPu) (Figure 19E). Since only SNpc MbDNs normally project to the CPu complex, these results are consistent with the observation that SNpc MbDN are located in a more medial position in the *Gli2*$^{\Delta Mb>E9.0}$ brains. Alternatively, these results could be an indication for aberrant projections of the remaining VTA MbDNs in the *Gli2*$^{\Delta Mb>E9.0}$ mice. In conclusion, these data show that the population of MbDNs that normally projects to the PFC (mesocortical MbDNs) essentially is not formed when Shh signaling is inactivated after E9.0.

* Stereotactic injections of rAAV harboring a ChR2-EYFP fusion gene were performed by Milan Pabst, laboratory of Prof. Heinz Beck, Department of Epileptology, University of Bonn, Medical Center

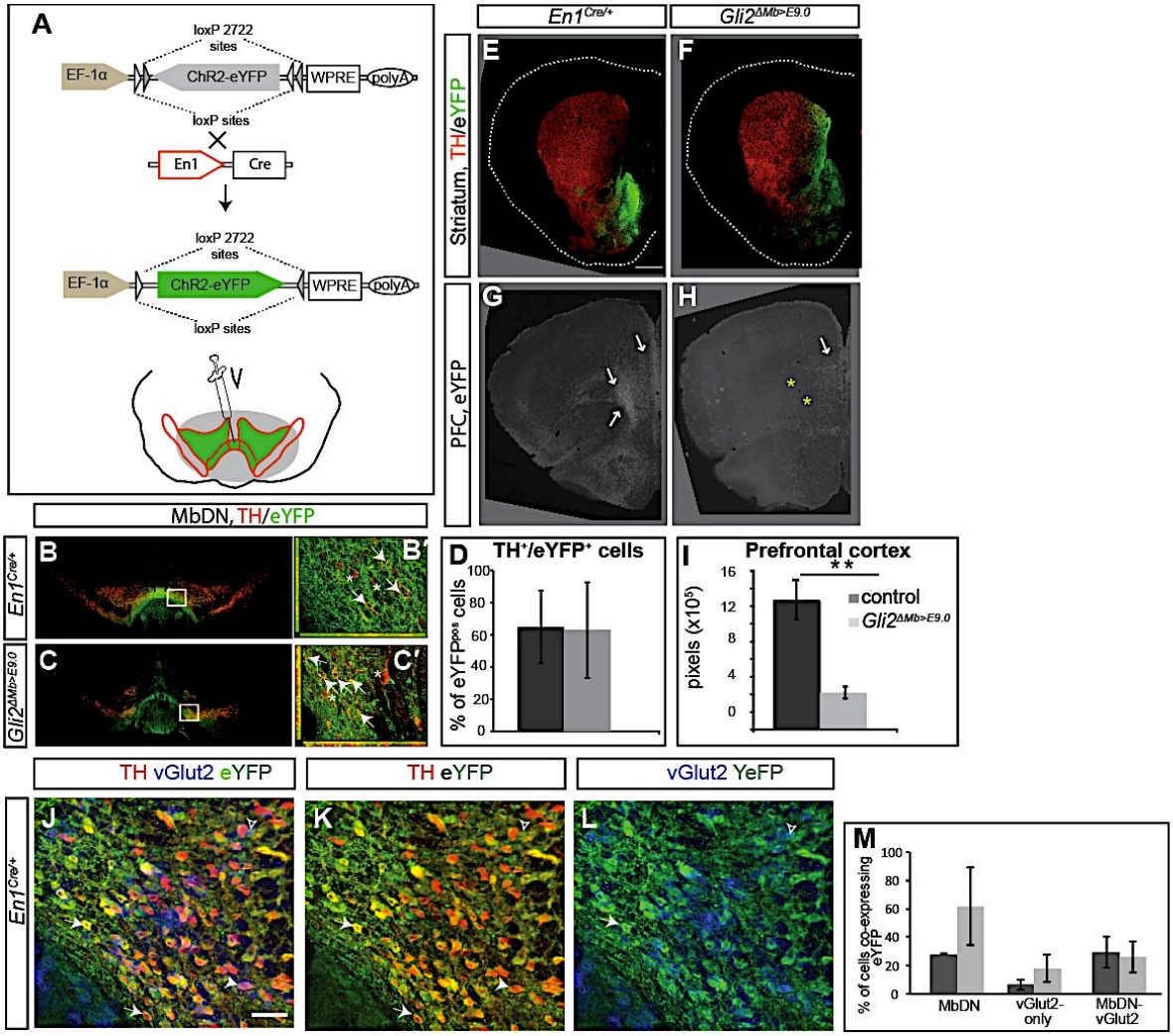

Figure 19 Tracing of MbDN axons shows severe reduction in mesocortical projections in *Gli2*$^{\Delta Mb>E9.0}$ mice. (A) Schematic showing double-floxed rAAV:ChR2-EYFP. Medial injection of the virus into the VTA (green area) results in EYFP expression in Cre-expressing neurons (red outline) in the VTA. **(B-C)** Immunostaining for MbDNs (TH, red) injected with the rAAV (EYFP, green). **(B'-C')** Higher magnification of the boxed area in B-C. Arrows indicate cells co-expressing TH and EYFP, asterisks represent cells expressing only TH. **(D)** Quantitative analysis of TH^{pos}/EYFP^{pos} cells expressed in percent of all EYFP^{pos} cells. **(E-H)** Immunostaining for projections stained with EYFP (green) and TH (red) into the striatum (E-F) and PFC (G-H). Arrows indicate presence of MbDN fibers in the PFC, while yellow asterisks indicate their absence. Scale bar 500 µm. **(I)** Quantitative analysis of the number of fluorescent (EYFP) pixels in the PFC. **(J-L)** RNA *In Situ* hybridization for vGlut2 (image color was inverted and false colored in blue) combined with immunostaining for TH (red) and EYFP (green) in control. Arrows indicate MbDN positive for TH and EYFP, filled arrowheads indicate MbDN positive for TH, vGlut2 and EYFP, arrowheads indicate cells positive for vGlut2 and EYFP. Scale bar 30 µm. **(M)** Quantitative analysis of MbDN (TH^{pos}), vGlut2-only (TH^{neg}/vGlut2^{pos}) and MbDN-vGlut2 (TH^{pos}/vGlut2^{pos}) cells co-expressing EYFP at this level (J-L). Error bars indicate SEM. Significance (p*<0.05; p**<0.01) was determined by Student's t-test.

4.10 Decreased dopamine content in the prefrontal cortex*

To determine whether reduction in MbDN projections in the PFC might result in decreased DA content in this area, DA level and its metabolites DOPAC were measured using HPLC (Section 3.16). Indeed, the levels of DA and DOPAC were reduced to 52.5% and 67.1% of control in the PFC of *Gli2*$^{\Delta Mb>E9.0}$ brains, respectively (Figure 20A). Striatal levels of DA (81.9% of control) and DOPAC (77.5% of control) were also decreased in *Gli2*$^{\Delta Mb>E9.0}$ mice compared to control, but the reduction was less severe than in the PFC (Figure 20B).

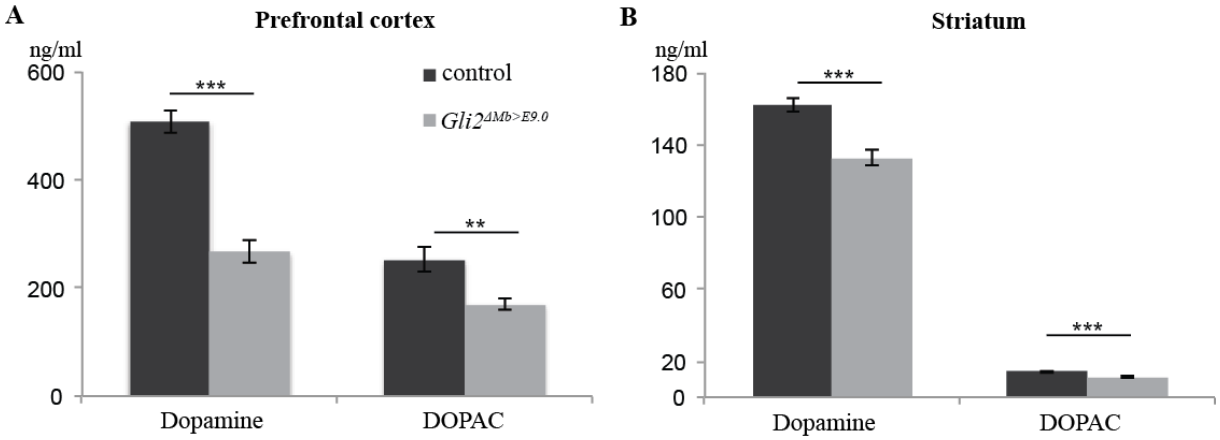

Figure 20 Dopamine content in the PFC and striatum as measured by HPLC. (A-B) The levels of DA and its metabolite DOPAC in the PFC (A) and the striatum (B). Data are expressed in ng/mL protein (A-B). Error bars indicate SEM. Significance (p**<0.01; p***<0.001) was determined by Student's t-test.

These data are consistent with the severe reduction observed in mesocortical projections in the *Gli2*$^{\Delta Mb>E9.0}$ mice. The mild reduction in DA and DOPAC levels in the striatum indicates, that the despite the apparent normal innervation of this region, the remaining MbDNs cannot fully compensate for the loss of MbDNs.

4.11 Functional assessment of mesocortical MbDN in *Gli2*$^{\Delta Mb>E9.0}$ and control mice using optogenetic approaches†

The mesocortical DA system is essential for cognitive and emotional function. However, while the neuroanatomical connectivity of mesocortical system has been extensively studied, little is known about its functional properties. To examine this, an optogenetic approach was used. To stimulate dopaminergic axons, MbDNs in the VTA were injected with rAAV

* HPLC analysis was performed by Dr. Ruth Musgrove, laboratory of Prof. Donato A. Di Monte, DZNE, Bonn

† Optogenetic and electrophysiological analysis was performed by Milan Pabst, laboratory of Prof. Heinz Beck, Department of Epileptology, University of Bonn, Medical Center

harboring a ChR2-EYFP fusion gene, flanked by two loxP sites and driven by EF1α promoter. Therefore, the presence of Cre recombinase in control (*En1*$^{Cre/+}$) and *Gli2*$^{\Delta Mb>E9.0}$ mice results in an irreversible expression of ChR2-EYFP. First, to analyze whether both, MbDN (TH^{pos}/vGlut2^{neg}) and MbDN-vGlut2 (TH^{pos}/vGlut2^{pos}) cells expressed ChR2-EYFP, RNA *In Situ* hybridization for vGlut2 followed by immunostaining for TH and EYFP was performed. Both MbDN subpopulations in the VTA area expressed EYFP in control and *Gli2*$^{\Delta Mb>E9.0}$ mice: 28% ± 0.5% (control) and 62% ± 27% (*Gli2*$^{\Delta Mb>E9.0}$) of all TH^{pos} MbDNs co-expressed EYFP and 29.6% ± 11% (control) and 26.2% ± 11.1% (*Gli2*$^{\Delta Mb>E9.0}$) of MbDN-vGlut2 co-expressed EYFP (Figure 19I-M). Only a low percentage of vGlut2-only cells co-expressed EYFP in the VTA area in both animals (control: 6.6% ± 3.7% and *Gli2*$^{\Delta Mb>E9.0}$: 17.8% ± 9.7%). These data demonstrate that despite severe reduction in MbDNs in the *Gli2*$^{\Delta Mb>E9.0}$ mutants, the percentage of the cells infected with the rAAV was not different from control mice.

Recording from ChR2-EYFP^{pos} VTA neurons, using the patch-clamp method revealed that blue light illumination (473 nm) caused large inward currents in VTA neurons (248 ± 43 pA for stimulation durations of 12 ms) (Figure 21B, C, firing behavioral and morphological reconstruction in Figure 21A). The expression levels of ChR2 were sufficient to induce precisely timed action potentials (AP) in VTA neurons at frequencies up to 33 Hz (Figure 21D). Next, the effects of light-based stimulation of ChR2-EYFP^{pos} axons originating from the VTA on neurons within the mPFC using multicell Ca^{2+} imaging were examined. Light-based stimulation elicited Ca^{2+} transients in a subset of mPFC neurons (Figure 21E, F). To analyze whether Ca^{2+} transients were caused by DA or glutamate release, dopaminergic and/or glutamatergic blockers were applied. While Ca^{2+} transients were unaffected by dopaminergic antagonists, the AMPA/kainate receptor blocker CNQX completely blocked these transients (Figure 21F, G). These results suggest that mesocortical MbDN projections exert their predominant effects via release of glutamate.

To pinpoint the effects of synaptic release of glutamate by MbDN projections, patch-clamp recordings from layer IV/V mPFC pyramidal neurons were obtained (Figure 21H). Light-based stimulation of ChR2-EYFP expressing axons originating from the VTA always caused inhibitory postsynaptic potentials (IPSP) in the mPFC pyramidal neurons (Figure 21J, blue bar indicates time of light stimulation, average latency from onset of light stimulation to the IPSP onset 28.3 ± 13.8 ms, average magnitude of the light-evoked IPSP 5.1 ± 0.7 mV). Moreover, application of GABA-receptor blocker gabazine (10 μm) fully blocked the IPSP. These results indicate that the light-evoked response is GABAergic (Figure 21J, K). To

examine if recruitment of local interneurons might underlie the inhibitory effects of light-based stimulation of VTA axons, GABAergic interneurons in the mPFC were analyzed. In GABAergic interneurons, light stimulation invariably elicited short-latency evoked postsynaptic potentials (EPSP) (average latency from onset of light stimulation to the EPSP onset 20.7 ± 3.79 ms, average magnitude of the light-evoked EPSP 6.4 ± 0.82 mV) (Figure 21I). Moreover, some of the EPSP were large enough to trigger AP (Figure 21L). Interestingly, the light-evoked excitation of interneurons was completely blocked by the glutamate antagonist CNQX (10 µM, Figure 21L, M). These results indicate that mesocortical MbDN projections cause glutamatergic excitation of interneurons, as well as inhibition of pyramidal neurons. Next, to examine whether IPSPs in the mPFC are caused by a direct release of GABA from VTA neurons, light-evoked IPSP were recorded from mPFC pyramidal neurons. Application of CNQX, completely blocked light-evoked IPSP (Figure 21N, O), indicating that IPSP in the mPFC are most likely not due to a direct release of GABA from VTA neurons. These results show that VTA MbDN axons are capable of generating fast inhibition in mPFC pyramidal neurons via glutamatergic excitation of inhibitory interneurons.

The amount of MbDN fibers in the PFC of *Gli2*$^{\Delta Mb>E9.0}$ mice was severely reduced, suggesting that the inhibition of the mPFC neurons might be impaired. Indeed, expression of ChR2-EYFP in VTA neurons in *Gli2*$^{\Delta Mb>E9.0}$ mice revealed that the excitation of the mPFC interneurons was strongly impaired in these mice (Figure 21Q). Furthermore, the inhibition observed in mPFC pyramidal neurons upon light-based stimulation of VTA afferents was also strongly reduced in magnitude (Figure 21P).

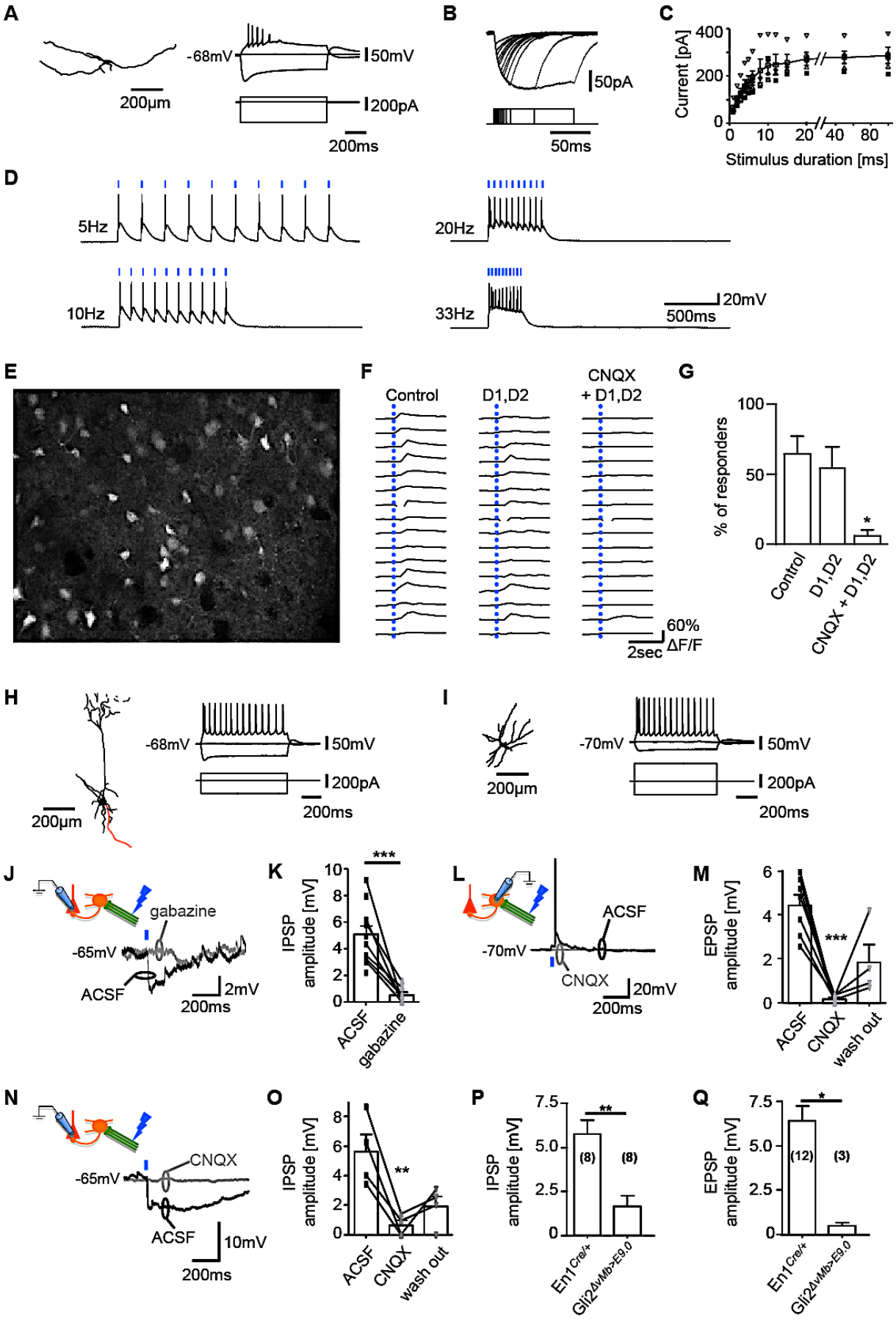

Figure legend (next page)

Figure 21 Functional assessment of mesocortical MbDNs in *Gli2*$^{\Delta Mb>E9.0}$ and control (*En1*$^{Cre+/-}$) mice using optogenetic approach. (A-C) Morphology and intrinsic firing properties of a ChR2-expressing VTA neuron (left panels). Blue light stimulation (473 nm) of EYFP^{pos} VTA neurons resulted in large inward currents in VTA neurons (rightmost panels). **(D)** Precise stimulation of ChR2-expressing VTA neurons with brief (20 ms) blue light illumination, which reliably triggered AP up to stimulation frequencies of 33 Hz. **(E)** Image of an OGB-1-AM pressure-loaded slice showing OGB-1-positive cells in the mPFC. **(F)** Traces of light stimulated Ca^{2+} transients in a representative subset of mPFC neurons. The dashed blue line indicates the light-based stimulation of ChR2-EYFP^{pos} axons originating from the VTA. The transients were not significantly affected by DA antagonists, but were completely blocked by additional application of the AMPA/kainite receptor blocker CNQX (10 μM). **(G)** Percentage of neurons that respond to optogenetic stimulation before and after application of D1 and D2 receptor blockers and subsequent glutamatergic antagonist CNQX. Significance (p***<0.001) was determined by Friedman test with Dunn's multiple comparison test. **(H-I)** Intrinsic properties and neuronal morphology of a representative PFC pyramidal neuron (H) and an interneuron (I). **(J)** Optogenetic stimulation of the axons projecting from the VTA caused IPSPs in layer IV/V mPFC pyramidal neurons (blue bar indicates time of light stimulation). **(K)** Light-evoked IPSP were blocked by the GABA-receptor blocker gabazine (10 μM). **(L)** Light-based stimulation of EYFP^{pos} axons originating from the VTA on PFC interneurons invariably elicited short-latency EPSPs that intermittently triggered AP. **(M)** The excitation of mPFC interneurons is blocked by the glutamate antagonists CNQX (10 μM). Significance (p***<0.001) was determined by Kruskal-Wallis test with Dunn's multiple comparison test. **(N-O)** The inhibition of mPFC pyramidal neurons is also blocked by CNQX. Significance (p*<0.1) was determined by ANOVA with Newman-Keuls post test. **(P-Q)** Light-evoked IPSPs in mPFC pyramidal neurons (P), as well as EPSP in inhibitory interneurons (Q) are significantly reduced in *Gli2*$^{\Delta Mb>E9.0}$ mice. Significance (p*<0.1; p**<0.01) was determined by Mann-Whitney test.

Thus, severe reduction of MbDNs capable of glutamatergic transmission in *Gli2*$^{\Delta Mb>E9.0}$ mice causes virtually complete loss of an inhibitory motif that normally inhibits mPFC pyramidal neurons.

4.12 Inactivation of Shh signaling at E9.0 affects the generation of other ventral neuronal cell types

Previously it has been shown that after E9.0 Shh signaling is required for the generation of more laterally located precursors such as precursors for the OM complex and RN (Blaess et al., 2006; Perez-Balaguer et al., 2009) (Section 1.18). OM and RN neurons are derived from the Shh^{pos}/Foxa2^{pos}/Nkx6-1^{pos} progenitor domain located laterally to MbDN Lmx1a^{pos} domain, whereas motoneurons (GABA^{pos}) originate from an even more lateral domain, which is positive for Nkx2-2 (Figure 7A). Conditional inactivation of Shh signaling at E9.0 results in complete loss of OM neurons (Blaess et al., 2006). To analyze whether development of RN neurons is dependent on Shh signaling after E9.0, *Nkx6-1* expressing progenitors that give rise to RN neurons were examined. The wildtype expression pattern of Nkx6-1 at E10.5, and later

at E12.5, consists of two positive domains, a medial Shh^{pos}/Foxa2^{pos}/Nkx6-1^{pos} and a lateral Shh^{neg}/Foxa^{neg}/Nkx6-1^{pos} domain (Figure 7, 22A). In E10.5 *Gli2*$^{\Delta Mb>E9.0}$ mice, the expression of Nkx6-1 was shifted medially (Figure 22B). Both domains are still present in the *Gli2*$^{\Delta Mb>E9.0}$ mice, however, the medial Shh^{pos}/Foxa2^{pos}/Nkx6-1^{pos} domain was dramatically reduced in size (Figure 22B). Interestingly, at E11.5 the Foxa2^{pos}/Nkx6-1^{pos} domain was absent in *Gli2*$^{\Delta Mb>E9.0}$ mice (Figure 22C-D). Another putative marker for precursors of the RN and motoneurons is Sim1. Whereas Sim1 overlaps with Foxa2 and Nkx6-1 in the progenitor area (VZ) and forms two vertical stripes in E11.5 wildtype mice, it is expressed outside of the VZ in *Gli2*$^{\Delta Mb>E9.0}$ mutants (Figure 22E-F). Thus, these data show that Shh signaling after E9.0 is required for the further expansion of Foxa2 and therefore for specification of RN and OM precursor domains.

To examine whether RN neurons are reduced in *Gli2*$^{\Delta Mb>E9.0}$ embryos, immunohistochemical analysis of the Pou4f1 (POU domain class 4 transcription factor 1) was carried out on coronal sections of E18.5 control and *Gli2*$^{\Delta Mb>E9.0}$ brains. The RN is organized in a parvocellular and a magnocellular part, which are located in the anterior and posterior midbrain, respectively (Massion, 1967) (Section 1.18). Surprisingly, the most anterior parvocellular part was maintained in *Gli2*$^{\Delta Mb>E9.0}$ brains. Interestingly, posteriorly located Pou4f1^{pos} neurons in *Gli2*$^{\Delta Mb>E9.0}$ mutants were detected medially, while laterally located cells were completely missing (Figure 22G-H). In addition the usual compacted round shape of the nucleus was less obvious in *Gli2*$^{\Delta Mb>E9.0}$ brains.

It has previously been demonstrated that the RN contains neurons secreting different neurotransmitters, which participate in corticorubral and/or cerebellorubral transmission. One of the neurotransmitter playing a role in cerebellorubral transmission is glutamate. To investigate whether the apparent reduction in the RN neurons affects a particular population of the neurotransmitter the expression of glutamate transporter was examined. RNA *In Situ* hybridization analysis showed that RN neurons positive for vGlut2 were reduced in P21 *Gli2*$^{\Delta Mb>E9.0}$ mutants compared to control (Figure 22I-J). Moreover, remaining vGlut2^{pos} RN neurons were located medially. These data suggest that there might be a temporal requirement of Shh signaling for generating laterally located RN neurons, which require Shh signaling for their induction after E9.0. It seems that more anteriorly located RN neurons might require Shh signaling for their induction before E9.0, since they were less affected in *Gli2*$^{\Delta Mb>E9.0}$ brains. Alternatively, generation of the parvocellular part of RN is controlled by different factors than Shh signaling or the RN progenitors might be generated in the diencephalon.

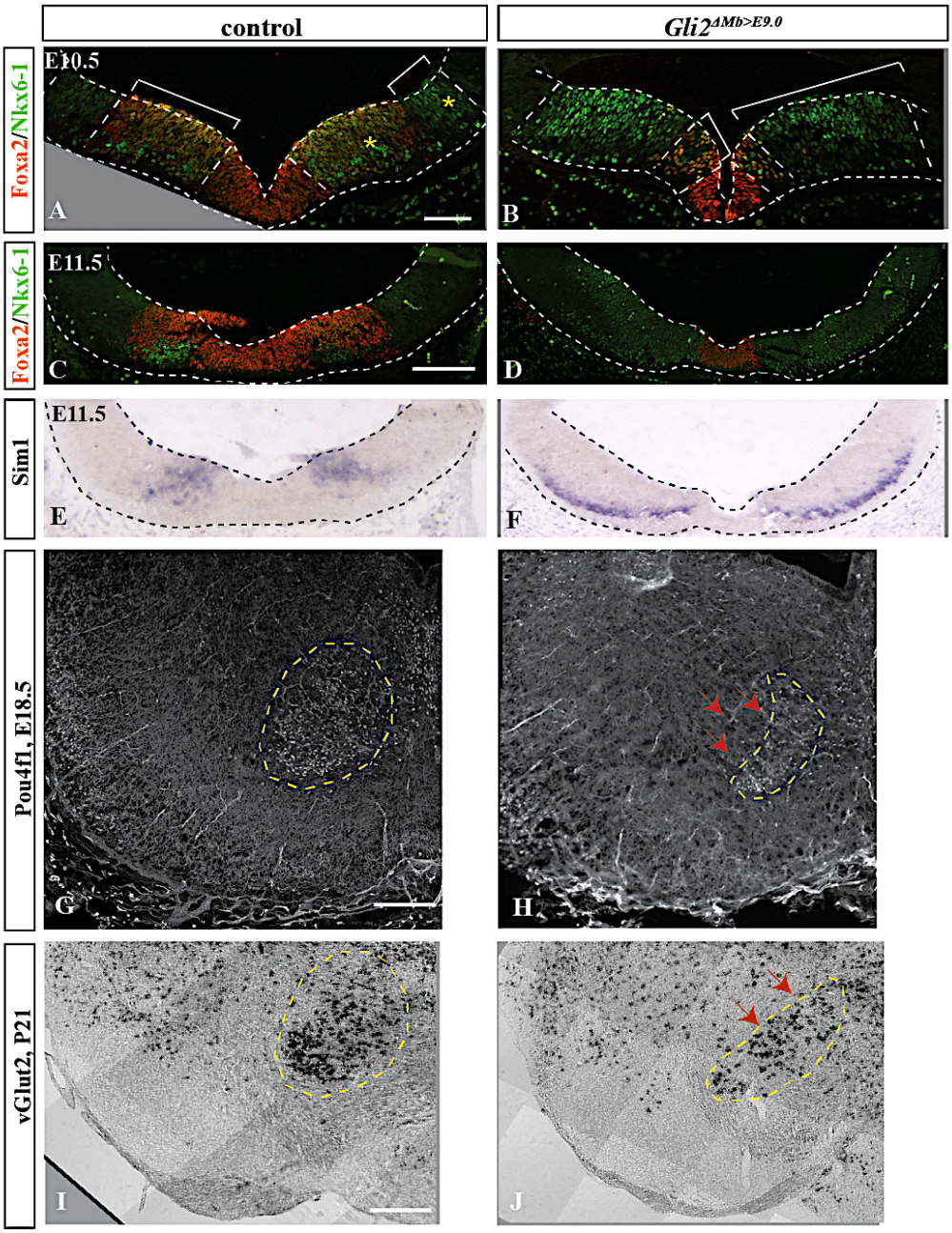

Figure 22 Requirement of Shh signaling after E9.0 for proper generation of red nucleus neurons. (A-D) Immunostaining for Foxa2 and Nkx6-1 in E10.5 (A-B) and E11.5 (C-D) control and *Gli2*$^{\Delta Mb>E9.0}$ embryos. Dashed lines and yellow asterisks (control) indicate medial Foxa2^{pos}/Shh^{pos}/Nkx6-1^{pos} and lateral Foxa2^{neg}/Shh^{neg}/Nkx6-1^{pos} domains. White bars indicate the size of these domains. **(E-F)** RNA *In Situ* hybridization for Sim1 in E11.5 control and *Gli2*$^{\Delta Mb>E9.0}$ embryos. **(G-H)** Immunostaining for RN neurons (Pou4f1) on coronal section in E18.5 control and *Gli2*$^{\Delta Mb>E9.0}$ brains. **(I-J)** RNA *In Situ* hybridization for vGlut2 in P21 control and *Gli2*$^{\Delta Mb>E9.0}$ brains. Yellow dashed lines outline the area of RN. Arrows indicate the missing neurons in the *Gli2*$^{\Delta Mb>E9.0}$ mutants. Scale bars 50 µm (A-B), 100 µm (C-F), 500 µm (G-J).

4.13 Constitutive activation of Shh signaling after E9.0 results in dramatic ectopic expansion of MbDN precursor domain

To further examine the role of Shh signaling in specification of MbDN subpopulations, mice that expressed a constitutively active form of the Shh receptor Smo (SmoM2) were generated (Section 3.11.6) (Jeong et al., 2004) (Figure 23A). To induce recombination and thereby the expression of *SmoM2* specifically in the midbrain and aHb after E9.0 (*SmoM2*$^{\uparrow Mb>E9.0}$) the *En1*$^{Cre/+}$ mouse line was used. Inactivation of high level Shh signaling led to a severe reduction in the lateral MbDNp domain and almost complete loss of mesocortical MbDNs in *Gli2*$^{\Delta Mb>E9.0}$ mutant mice. To investigate if constitutive activation of Shh signaling after E9.0 might have an opposite effect, the Lmx1a^{pos} domain, which gives rise to all MbDNs was examined (Section 1.14). The size of the Lmx1a^{pos} area was increased in the vMb of the *SmoM2*$^{\uparrow Mb>E9.0}$ embryos at E10.5, however, the increase in the size of this domain was more prominent caudally (146.2% ± 10.8% of control) than rostrally (125.9% ± 17.3% of control) (Figure 23C, I and data not shown for rostral vMb). Furthermore, the Arx^{pos} domain was also significantly increased in size in *SmoM2*$^{\uparrow Mb>E9.0}$ mutants compared to control embryos (131.6% ± 3.3% of control) (Figure 23E). To examine whether the lateral MbDNp can be induced in presence of fully activated Shh signaling, expression of Corin in E10.5 *SmoM2*$^{\uparrow Mb>E9.0}$ embryos was analyzed. The quantification of the Corin^{pos} and Lmx1a^{pos} areas on adjacent sections of the posterior vMb showed that the lateral Lmx1a^{pos}/Corin^{neg} domain was not significantly increased in size compared to control embryos (Figure 23D, H). Interestingly, in contrast to control animals, the medial Lmx1a^{pos}/Corin^{pos} domain was increased in size by 58.6% ± 5.8% in *SmoM2*$^{\uparrow Mb>E9.0}$ mice compared to control littermates (Figure 23C, H).

To assess whether constitutive activation of Shh signaling after E9.0 leads to an increase of Shh and Foxa2 domains, the expression of these markers was analyzed in E10.5 control and *SmoM2*$^{\uparrow Mb>E9.0}$ embryos. The Shh and Foxa2 domains were expanded into the dorsal midbrain (Figure 23F,G), resulting in ventralization of the dorsal midbrain. Moreover, the midbrain of *SmoM2*$^{\uparrow Mb>E9.0}$ was dramatically increased in size compared to control.

Taken together, after E9.0, only a very restricted population of midbrain precursors close to the Lmx1a^{pos} domain respond to increased Shh signaling by changing their fate to medial MbDNp, while a much larger population of precursors can respond by adopting a ventrolateral fate.

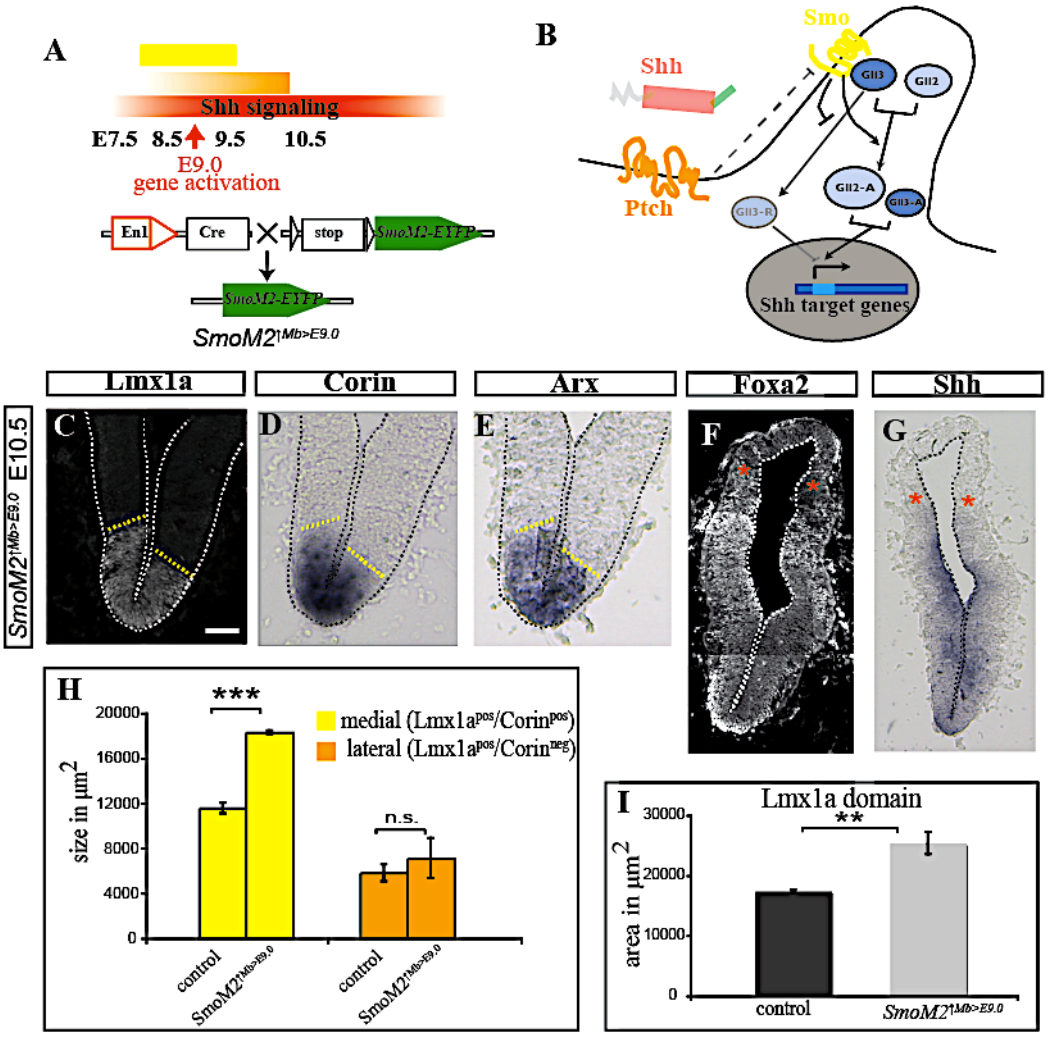

Figure 23 Constitutive activation of Shh signaling at E9.0 leads to dramatic ectopic expansion of MbDNp domain. (A) Schematic of the conditional activation of Shh signaling in *SmoM2*$^{\uparrow Mb>E9.0}$ mice. **(B)** Schematic of constitutive activation of Shh signaling. SmoM2 is active in absence of Shh. **(C-G)** Immunofluorescent staining (C, F) and RNA *In Situ* hybridization (D-E, G) on E10.5 coronal sections for markers of MbDNp domain (Lmx1a, Arx, Corin, Shh and Foxa2). The Lmx1a domain is outlined in sections C-E (dashed line). Red asterisks indicate the dorsal expansion of Foxa2 and Shh. Scale bar 100 µm. **(H)** Quantitative analysis of the size of the medial (Lmx1a^{pos}/Corin^{pos}) and lateral (Lmx1a^{pos}/Corin^{neg}) MbDNp domain in the vMb. **(I)** Quantitative analysis of the Lmx1a^{pos} domain in E10.5 control and *SmoM2*$^{\uparrow Mb>E9.0}$ embryos. Error bars indicate SEM. Significance (p**<0.01; p***<0.001) was determined by Student's t-test.

4.14 Expansion of MbDN precursor domain is not caused by increase in cell proliferation

To examine whether the expansion of MbDNp domain is a result of increased proliferation, proliferating cells were labeled with an one hour BrdU pulse in E10.5 *SmoM2*$^{\uparrow Mb>E9.0}$ and control embryos. Quantification of BrdU^{pos} cells within the Lmx1a^{pos} domain showed that the proliferation in the MbDNp domain in *SmoM2*$^{\uparrow Mb>E9.0}$ mutants (56 ± 3.6 cells) was not

significantly different from control littermates (62 ± 5 cells), indicating that proliferation of MbDNp is not affected in *SmoM2*$^{\uparrow Mb>E9.0}$ mutants (Figure 24A-C).

To analyze whether neurogenesis occurs normally in the mutant mice, the expression of the proneural marker Ngn2 was examined. Quantification of the number of Ngn2^{pos} cells within the Lmx1a^{pos} domain in *SmoM2*$^{\uparrow Mb>E9.0}$ and control embryos at E10.5 showed that the number of Ngn2^{pos} cells was significantly increased in *SmoM2*$^{\uparrow Mb>E9.0}$ mutants (46 ± 10 cells) compared to control (20 ± 3.4 cells) embryos when normalized for the size of the MbDNp domain (Figure 24D-F). These data suggest that prolongated Shh signaling did not affect the proliferation of MbDNp, however leads to the upregulated neurogenesis, meaning that constitutively active Shh signaling prompts the cell cycle exit of proliferating cells. However, the proliferation was not analyzed at later stages, meaning that increase in the neurogenesis might be transient.

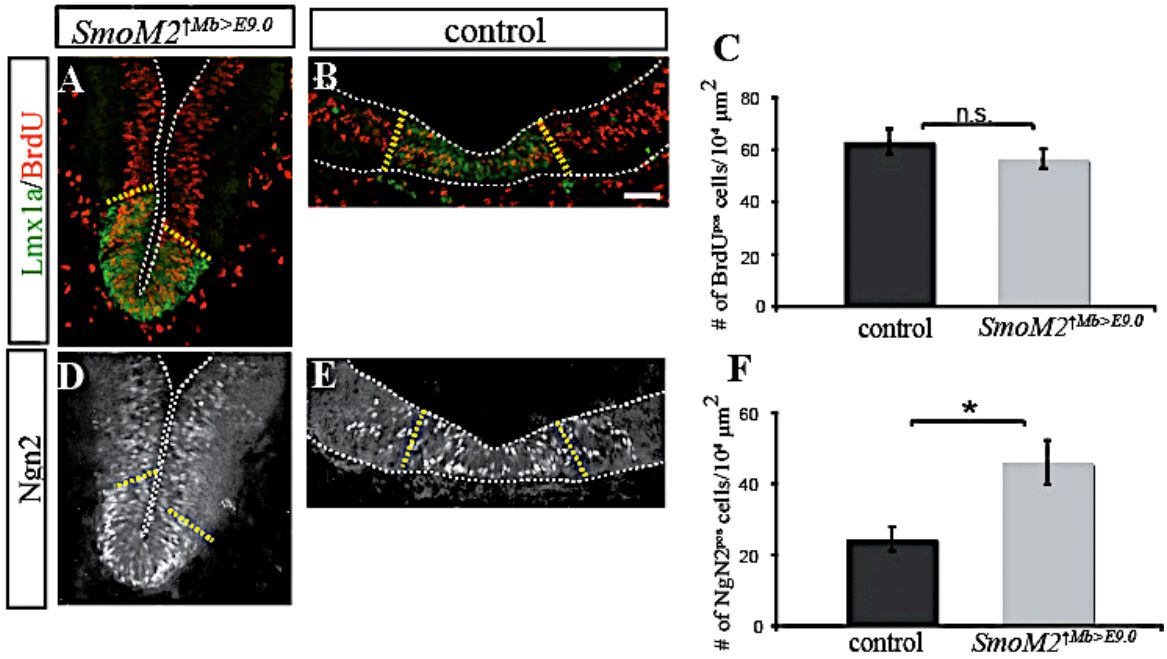

Figure 24 Proliferation in the MbDNp domain is not affected in E10.5 *SmoM2*$^{\uparrow Mb>E9.0}$ mice, whereas neurogenesis is increased. (A-B) One hour BrdU pulse to label proliferating precursors in the vMb at E10.5. **(C)** Quantitative analysis of the number of BrdU^{pos} cells normalized to the size of the Lmx1a^{pos} domain. **(D-E)** Immunostaining for Ngn2 on E10.5 coronal sections. Dashed lines indicate the Lmx1a^{pos} domain. Scale bars 100 µm. (F) Quantitative analysis of the number of Ngn2^{pos} cells normalized to the size of the Lmx1a^{pos} domain. Error bars indicate SEM. Significance (p*<0.05) was determined by Student's t-test.

4.15 Constitutive activation of Shh signaling after E9.0 results in ectopic MbDNs in the dorsal midbrain

To test whether the expansion of the Lmx1a^{pos} domain and the increased neurogenesis at E10.5 results in an increased number of MbDNs, immunohistochemistry for TH was carried out on coronal sections through the rostrocaudal extent of the developing vMb in E10.5, E12.5 and E18.5 control and *SmoM2*$^{\uparrow Mb>E9.0}$ embryos (Figure 25A-D, Figure 14C, Figure 15A).

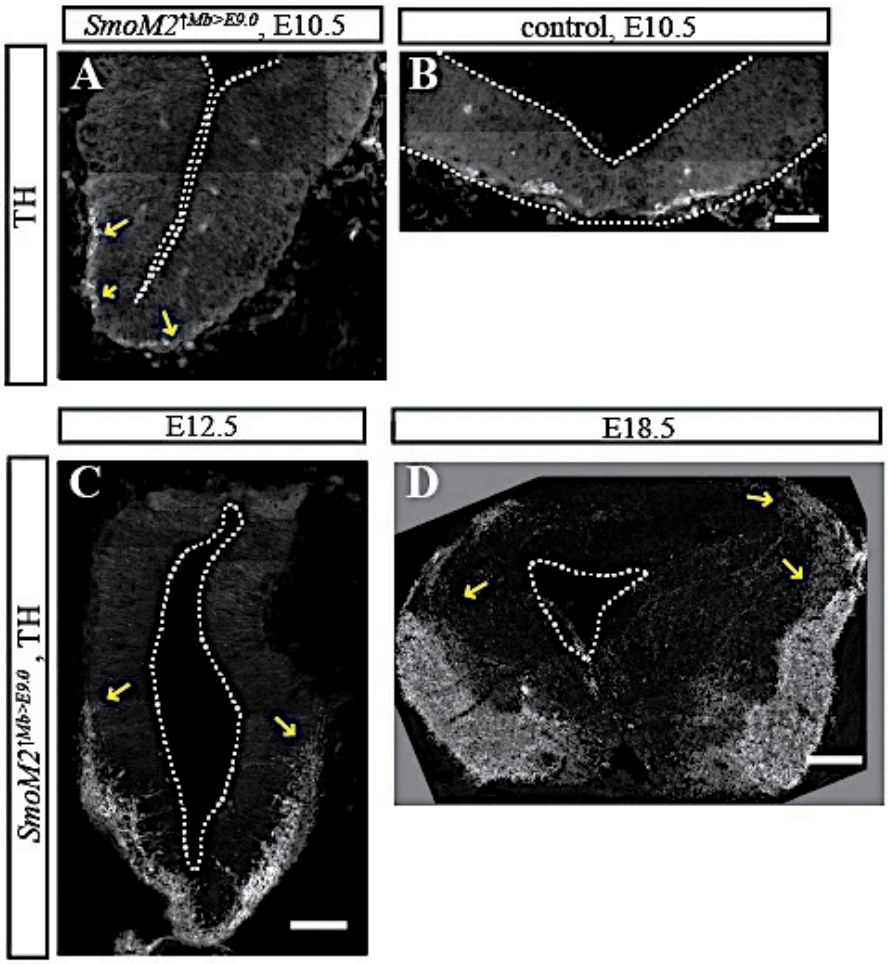

Figure 25 Activation of Shh signaling after E9.0 results in ectopic MbDNs in the dorsal midbrain. (A-F) Immunostaining for differentiated MbDNs (TH) in E10.5 (A-B), E12.5 (C) and E18.5 (D) wildtype and *SmoM2*$^{\uparrow Mb>E9.0}$ embryos. Yellow arrows indicate TH^{pos} MbDNs. Scale bars 100 µm (A-C), 500 µm (D).

The first differentiated TH^{pos} MbDNs in control and *SmoM2*$^{\uparrow Mb>E9.0}$ mice were detected at E10.5. MbDNs in *SmoM2*$^{\uparrow Mb>E9.0}$ embryos seem not to be increased at this time point. However, at E12.5 MbDNs were severely increased and expanded towards the dorsal midbrain (Figure 25C, Figure 14C). These results correlate with the increased neurogenesis at E10.5. In contrast to the controls, in which the newly generated TH^{pos} MbDNs are located at the ventral midline, the TH^{pos} cells in the mutant were expanded laterally. Notably, the

increase in MbDNs was more obvious caudally, while there was no change in the rostral MbDN population. This phenotype persisted at E18.5. At this stage, the strong increase in the MbDNs became even more evident. The TH^{pos} cells were almost completely excluded from the midline, areas corresponding to the RLi and vmVTA (Figure 25D, Figure 15A). These findings demonstrate that constitutive activation of Shh signaling results in a severe increase of MbDN and their expansion towards the dorsal midbrain.

5. Discussion

MbDNs in the adult brain are diverse on a functional and anatomical level, but it is largely unexplored how this diversity is established during development. To address this question, Shh signaling was inactivated in the midbrain immediately after lateral MbDNp start to respond to Shh signaling. The conditional gene inactivation was achieved by the removal of *Gli2*, the main transcriptional activator downstream of Shh signaling. In the mutant mice ($Gli2^{\Delta Mb>E9.0}$) with inactivated Shh signaling, the lateral MbDNp domain was severely reduced in size and MbDNs were disorganized and decreased in number in the developing and adult brain. Analysis of MbDN subset markers showed that the majority of the remaining MbDNs adopted the fate of SNpc MbDNs in mutant mice. Characterization of MbDN connections in control and $Gli2^{\Delta Mb>E9.0}$ mutant mice using immunofluorescence and axonal tracing, showed that the severe reduction of lateral MbDNp in $Gli2^{\Delta Mb>E9.0}$ mutant mice is associated with the loss of mesocortical projections from the VTA. Optogenetics and electrophysiological analysis showed that mesocortical MbDNs modulate a cortical microcircuit by inhibiting cortical pyramidal neurons via release of glutamate.

Furthermore, constitutive activation of Shh signaling after E9.0 results in a massive increase in the number of MbDNs. Analysis of MbDNp domain showed that the medial MbDNp domain was significantly increased in size, whereas the lateral domain was only slightly affected. Due to the perinatal lethality of the mutant mice, investigation of MbDNp specification in the adult brains was not possible. This study shows a causal link between early developmental induction mechanisms and the connective and functional properties of MbDNs in the mature brain.

5.1 Establishing of specific circuits in the mesocorticolimbic system

MbDN cell bodies and their projections to the forebrain display a mediolateral topographic arrangement. The most laterally located cells (SNpc and lVTA) project to the dorsal striatum, mediolateral MbDNs of the lVTA innervate the lateral part of the striatum and medially located MbDNs of the vmVTA send their axons to the medial striatum, the PFC and the amygdala (Ikemoto, 2007 and 2010). However, significant intermixing of MbDN populations with different projection targets, particularly in the VTA, makes it difficult to assess the circuitry that determines the function of particular subsets of VTA MbDNs. Recent studies, using optogenetic approach revealed that distinct circuits indeed encode different MbDN functions (Lammel et al., 2008 and 2012), but how these circuits are established during development is still unclear.

After MbDN neuronal identity is specified in the VZ of the ventral midline, MbDNs differentiate and migrate to their final position while extending projections to their forebrain targets. It has been proposed that the target and functional specificity of MbDNs is established at late embryonic stages, through interaction with their target areas or by receiving specific inputs (Hu et al., 2004). However, fate-mapping studies suggest that MbDN populations are already pre-specified during their precursor phase. Medial MbDNp co-express *Corin* and *Msx1/2* along with *Lmx1a* and give rise to MbDNs of the SNpc and dlVTA, whereas lateral MbDNp domain expresses only *Lmx1a* and preferentially give rise to MbDNs in the vmVTA (Blaess et al., 2011; Hayes et. al., 2011). This study demonstrates that inactivation of high level Shh signaling at E9.0 results in reduction of the medial ($Lmx1a^{pos}$/$Corin^{pos}$) MbDNp domain and almost complete loss of the lateral ($Lmx1a^{pos}$/$Corin^{neg}$) MbDNp domain in $Gli2^{\Delta Mb>E9.0}$ mice. Analysis of postnatal $Gli2^{\Delta Mb>E9.0}$ brains shows that axonal projections to the PFC are severely reduced, whereas projections to the ventral striatum and amygdala are not significantly altered. These data indicate that the MbDNp population that gives rise to mesocortical MbDNs is not induced in $Gli2^{\Delta Mb>E9.0}$ mutant mice. Thus, mesocortical MbDNs have a different profile in their differentiation phase that results in the distinct physiology of these MbDNs and determines the formation of the specialized circuitry in the adult brain (Lammel et al., 2008 and 2012).

The developmental specification of neuronal subtypes has been described in other areas of the nervous system. Thus, the different subtypes of cortical interneurons are specified before cells become postmitotic (Corbit et al., 2011). The fate of spinal cord neurons and cortical interneurons is determined by their location and the timing of origin. Moreover, the identity of neural progenitors is defined by combinatorial function of specific sets of transcription factors during their precursor or differentiation phase. These sets of transcription factors play a role by forming proper connectivities as well as functional integration of these neurons (Livesey et al., 2001; Polleux and Ghosh, 2002; Berghuis et al., 2004; Molyneaux et al., 2007).

5.2 Temporal requirement of Shh signaling in the specification of lateral MbDN precursors

The induction of all MbDNp is dependent on Shh signaling. Analysis of the Lmx1a expression domain, which is thought to give rise to all MbDNs, revealed that Shh signaling is crucial for the induction of Lmx1a domain before E9.0 but not required for its maintenance after E9.0 (Andersson et al., 2006; Nakatani et al., 2010). Furthermore, Shh signaling is necessary for the further expansion of the Lmx1a domain, since Lmx1a expression domain is

severely decreased in *Gli2*$^{\Delta Mb>E9.0}$ mice. These results are consistent with the gain-of-function data (*SmoM2*$^{\uparrow Mb>E9.0}$ mutant mice), which show an expansion of the Lmx1a^{pos} MbDNp domain and further confirm that Shh signaling is crucial for the induction of Lmx1a domain. However, inactivation of Shh signaling after E9.0 affects the generation of the lateral MbDNp in *Gli2*$^{\Delta Mb>E9.0}$ mutant embryos. This raises the question how Shh signaling regulates the induction of different MbDNp domains.

In the spinal cord, Shh is secreted from a fixed population of cells located in the notochord and FP (Dessaud et al., 2007; Ribes et al., 2010). It forms a stable morphogen gradient, i.e. Shh acts at a distance from the point source in a concentration-dependent manner. Different concentrations of Shh induce distinct transcriptional factor expression domains, which define different neuronal precursors. In addition to different concentrations of Shh, changes in the duration of active Shh signaling and in the sensitivity of the receiving cells to ongoing Shh signaling determine ventral neuronal cell type in the spinal cord (Dessaud et al., 2007; Ribes et al., 2010). In contrast, expression of Shh in the vMb is dynamic. A changing competence model for the response to Shh would makes more sense in the vMb, since the dynamic Shh expression does not lead to a stable morphogen gradient and with different mediolateral cell populations being exposed to high levels of Shh signaling, the expansion of the most medial cell fate could go ad infinitum until the entire midbrain is ventralized. How the changes in competence are regulated is not clear, it could be due to the memory of low levels of Shh signaling and/or could be controlled extrinsically through the interaction with other signaling pathways in the vMb, such as Wnts (Joksimovic et al., 2009).

Based on this study's data the following model on how Shh induces different precursor domains in the vMb can be proposed. Initially, the most medial progenitors are exposed to high levels of Shh from the notochord starting around E8.0. Their response to Shh signaling is rapidly downregulated once they start to express Shh between E8.5 and E9.0. Simultaneously they cease to express Gli transcriptional factors, which are necessary for Shh signal transduction. In this short time window ventral midline precursors are specified into medial MbDNp fate (Shh^{pos}/Foxa^{pos}/Lmx1a^{pos}/Corin^{pos}/Msx1/2^{pos}). Induction of the medial MbDNp fate is only possible with early exposure (starting at E8.0) to high levels of Shh signaling, since the medial MbDNp domain is induced in *Gli2*$^{\Delta Mb>E9.0}$ mice. However, reduction in the medial MbDNp domain in *Gli2*$^{\Delta Mb>E9.0}$ mice indicates that the inactivation of *Gli2* occurs within the time window in which Shh is still required for the medial MbDNp domain induction.

Precursor cells in a slightly more lateral domain initially receive either no or low levels of Shh signaling. Once Shh is expressed in the ventral midline (E8.5-E9.0), lateral domain receives high levels of Shh signaling that induces the lateral MbDNp fate (Shh^{pos}/$Foxa^{pos}$/$Lmx1a^{pos}$/$Corin^{neg}$/$Msx1/2^{neg}$). Thus, delayed exposure to Shh signaling is necessary to induce lateral MbDNp. This population is severely reduced in $Gli2^{\Delta Mb>E9.0}$ mutant mice. However, constitutive exposure to high levels of Shh signaling in $SmoM2^{\uparrow Mb>E9.0}$ mutant mice does not lead to the expansion of lateral MbDNp, meaning that there might be another mechanism controlling cell fate specification. Thus, initial prolongated exposure to low levels of Shh signaling could result in desensitization of lateral precursors in their response to Shh. Thereby, following exposure to high levels of Shh would not lead to full activation of the pathway. Taken together, these findings suggest that the time point of exposure to high levels of Shh or level of Shh expression can determine the induction of a specific MbDN fate.

Taken together, the data show that the timing of Shh expression plays a role in defining different MbDNp fates. However, it is still unclear which transcriptional factors determine the distinct fates of medial versus lateral MbDNs downstream of Shh. Msx1/2 is a transcription factor, which is exclusively expressed in medial MbDNp and excluded from the lateral MbDNp domain (Blaess et al., 2011), could be involved in determining the fate of medial MbDNp. Moreover, it has been demonstrated, that mice lacking *Msx1/2* show a 40% reduction of MbDNs at E11.5 (Houzelstein et al., 1997; Andersson et al., 2006). However, it has not been investigated whether inactivation of *Msx1/2* affects specific MbDN subpopulation. In addition, Lmx1a and Lmx1b are possible candidates for the determination of different precursor domains in the vMb. Thus, *Lmx1a* and *Lmx1b* mouse mutants showed that Lmx1a is required to establish the medial MbDNp domain, while Lmx1b determines the lateral MbDNp (Deng et al., 2011).

5.3 Proliferation and neurogenesis in the MbDN progenitor domain are not affected in $Gli2^{\Delta Mb>E9.0}$ mutants

It has been demonstrated that Shh is involved in regulating the survival of the basal, young neuroblasts as well as in enhancing their proliferation (Dahmane et al., 2001; Ingham and Placzeck, 2006). A previous study showed that inactivation of Shh receptor Smo in *Shh*-expressing cells affects the proliferation of MbDNp (Hayes et al., 2013). Loss of Shh signaling at E9.0 resulted in an increase of cells remaining in a proliferative state and a reduction in postmitotic MbDNp, showing the role of Shh signaling in regulating cell cycle

exit in the vMb (Hayes et al., 2013). In contrast to these results, no changes in the proliferation rates in MbDNp in *Gli2*$^{\Delta Mb>E9.0}$ mice were detected in this study, suggesting that the observed effects of *Smo* inactivation could potentially be mediated by non-canonical Shh signaling. In contrast to control mice, no postmitotic MbDNp were found in E10.5 *Gli2*$^{\Delta Mb>E9.0}$ mice, meaning that there might be a delay in the generation of newly differentiated MbDNs. However, the number of Ngn2^{pos} cells in E11.5 *Gli2*$^{\Delta Mb>E9.0}$ mice was not different from the wildtype. There might be other mechanism or extrinsic factors controlling cell proliferation and neurogenesis in the vMb. It has been shown that canonical Wnt/β-catenin signaling pathway regulates cell cycle exit and midbrain FP neurogenesis (Tang et al., 2009; Joksimovic et al., 2009; Tang et al., 2010; Yang et al., 2013). Depletion of β-catenin in MbDNp led to a perturbation of cell polarity and reduced MbDN neurogenesis (Tang et al., 2009). It has been suggested that β-catenin mediated Wnt1 signaling suppresses Shh levels at the ventral midline around E10.5, creating an appropriate milieu for normal rates of proliferation. However, despite the significant reduction of *Wnt1* expression and a lack of downregulation of Shh in the ventral midline in *Gli2*$^{\Delta Mb>E9.0}$ mice, proliferation and neurogenesis are unaffected. These data suggest that in *Gli2*$^{\Delta Mb>E9.0}$ mice reduced *Wnt1* expression still can activate proliferation and neurogenesis in the vMb. In addition, *Msx1/2* has been suggested to control the timing of MbDN neurogenesis. Premature activation of *Msx1/2* resulted in upregulation of *Ngn2* expression, a loss of FP characteristics, and premature induction of MbDNs (Houzelstein et al., 1997; Andersson et al., 2006).

Depletion of canonical Wnt/β-catenin signaling pathway and/or Smo-mediated Shh signaling resulted in an increased cell apoptosis (Blaess et al., 2006; Tang et al., 2009), which contributes to the reduction of MbDNs. In contrast, no detectable changes in the cell death were observed in this study, meaning that the remaining MbDNs proliferate and differentiate properly.

5.4 Normal innervation of non-cortical forebrain targets, but loss of mesocortical projections in *Gli2*$^{\Delta Mb>E9.0}$ mice

Inactivation of high levels of Shh signaling results in a preferential loss of the lateral MbDNp domain, which gives rise to the vmVTA (Blaess et al., 2011; Hayes et al., 2011). However, both SNpc and VTA MbDNs were reduced in *Gli2*$^{\Delta Mb>E9.0}$ mice by 30% and 60%, respectively compared to control. Anatomical and morphological analysis showed that the reduction of VTA MbDNs was mainly restricted to the medially located neurons. Moreover, cells of the RLi and IF were almost entirely missing in the *Gli2*$^{\Delta Mb>E9.0}$ mice. Furthermore, the

PBP MbDNs were severely reduced and intermixed with the SNpc neurons. Moreover, SNpc neurons were found in the lateral region of the VTA, practically replacing the neurons of the PBP.

To examine how the reduction of MbDNs in the vmVTA and the SNpc affects the formation of dopaminergic circuitry in *Gli2*$^{\Delta Mb>E9.0}$ mice, their target areas were examined. Thus, mesocortical projections were severely reduced in *Gli2*$^{\Delta Mb>E9.0}$ mice. However, no significant changes in the density of projections to the dorsal striatum, NAc or amygdala were detected. MbDNs have huge terminal axonal arborizations in the striatum (Matsuda, 2009). Each MbDN might give rise to approximately 150000 presynaptic terminals in the striatum (Oorschot, 1996). 6-OHDA lesion of the SNpc MbDNs during postnatal development leads to sprouting and extensive arborization of the remaining MbDN axons in the dorsal striatum (Finkelstein, 2000), indicating that there could be compensatory axonal arborization when the absolute number of MbDN cell bodies and axons is reduced. In *Gli2*$^{\Delta Mb>E9.0}$ mice MbDNs are reduced already during embryonic development. Therefore remaining MbDN axons could sprout in the dorsal striatum and amygdala to compensate for reduced innervation. Measuring DA levels using HPLC, however, shows that DA content was decreased by almost 20% in the striatum in the *Gli2*$^{\Delta Mb>E9.0}$ mice, meaning that the remaining MbDNs cannot fully compensate for the loss of MbDNs.

5.5 Mesocortical MbDNs co-releasing glutamate

The PFC is the major cortical recipient of DA inputs and DA is believed to play a critical modulatory role in several cognitive processes conducted by the PFC network, including working memory, attention and decision making. To examine the consequences of the loss of mesocortical projections in *Gli2*$^{\Delta Mb>E9.0}$ mice on microcircuits in the PFC, ChR2-EYFP expressing VTA neurons were activated in slice preparations of mutant (*Gli2*$^{\Delta Mb>E9.0}$) and control (*En1*$^{Cre/+}$) brains using an optogenetic approach and recorded the activity in the PFC. The optical activation of ChR2-EYFP expressing VTA neurons in the control mice resulted in glutamate-mediated EPSPs in local interneurons and GABA-dependent IPSPs in pyramidal neurons in the PFC. In contrast, upon optical stimulation of VTA neurons no activity in the *Gli2*$^{\Delta Mb>E9.0}$ brains mice was detected. These results suggest that VTA MbDN modulate the excitability of PFC neurons via interneurons by release of glutamate.

The mesocorticolimbic pathway originating in the VTA is classically viewed as dopaminergic. However, it has been shown that only 30-40% of mesocortical projection neurons are dopaminergic (Swanson, 1982), while the rest of neurons express mRNA for

vGlut2 (Kawano et al, 2006; Yamaguchi et al, 2011; Gorelova et al., 2012; Hnasko et al., 2012). Detailed analysis of *vGlut2*-expressing neurons in the vMb identified three cell populations: MbDN, MbDN-vGlut2 and vGlut2-only neurons (Kawano et al., 2006; Yamaguchi et al., 2007; Yamaguchi et al., 2011). These cells are located in the vmVTA, in particular in the IF and RLi and project to the NAc and the PFC. Interestingly, the loss of MbDN and MbDN-vGlut2 in the $Gli2^{\Delta Mb>E9.0}$ mice is mostly apparent in the vmVTA. However, vGlut2-only neurons were not affected in $Gli2^{\Delta Mb>E9.0}$ mutant mice. In the adult brain of $En1^{Cre/+}$ mice, Cre-mediated recombination occurs primarily in MbDNs, including MbDN-vGlut2, but also in a small percentage of vGLut2-only neurons. Therefore, the glutamate- evoked activation of local PFC interneurons upon optogenetic stimulation of ChR2-EYFP expressing neurons could be mediated by vGLut2-only neurons and/or MbDN-vGlut2. However, in $Gli2^{\Delta Mb>E9.0}$ mice in which MbDN-vGlut2, but not vGlut2-only neurons, are severely reduced, glutamate-mediated EPSPs in PFC-interneurons were eliminated upon light stimulation of VTA neurons. Taken together, these results provide evidence that the glutamate-dependent activation of interneurons in the PFC is predominantly mediated by glutamate co-release from MbDN-vGlut2 and not vGlut2-only neurons.

Optogenetic and conditional gene inactivation studies confirmed the ability of DA neurons to release glutamate in the NAc (Stuber et al., 2010; Tecualetla et al., 2010; Tritsch et al., 2012). Optical stimulation of dopaminergic terminals in the NAc shell resulted in glutamate-mediated EPSP (Stuber et al., 2010). Glutamatergic responses were eliminated by glutamate but not DA antagonists (Lavin et al., 2005; Stuber et al., 2010). Even more direct support for glutamate release from the VTA MbDNs was provided by conditional gene inactivation studies, showing that selective removing of *vGlut2* expression in MbDNs eliminated the EPSP in the NAc spiny neurons (Hnasko et al., 2010; Stuber et al., 2010).

Considerable efforts have been invested in elucidating the cellular mechanisms by which DA modulates PFC function. Electrophysiological stimulation of VTA axons can rapidly depolarize PFC neurons or evoke EPSP-IPSP sequences (Lavin et al., 2005). It was suggested that the IPSP is mediated by VTA-induced feedforward activation of local PFC interneurons. The stimulation of the 6-OHDA-lesioned VTA failed to evoke EPSP in the PFC, confirming the idea that VTA MbDNs modulate PFC function by release of glutamate (Levin et al., 2005; Gorelova et al., 2012). However, this conclusion is somewhat premature given that vGlut2-only neurons also die as a secondary consequence of the destruction of MbDNs by 6-OHDA. Thus, it still not clear whether the evoked responses in the PFC were due to release of glutamate from MbDN-vGlut2 or vGlut2-only cells.

5.6 Functional implication of glutamate co-release in the PFC

Tracing and immunohistochemical studies demonstrated that between 12% and 30% of dopaminergic axons in the PFC contain vGlut2^{pos} varicosities, indicating that only a subset of dopaminergic synapses are able to co-release glutamate (Gorelova et al., 2012). However, it is still unclear how glutamate acts on cortical interneurons. Sequela et al. (1988) reported that between 16% and 22% of MbDN terminals in the PFC made asymmetric synapses, which are classically viewed as excitatory or glutamatergic. Forming both symmetric and asymmetric synaptic contacts, DA as a neuromodulator modulates acts through DA receptors. It has been shown that majority of dopaminergic axons form thin, symmetric synapses on distal dendrites of interneurons, but a small number of asymmetric synapses were observed as well (Sesack et. al., 1995). These data suggest that the EPSPs elicited in PFC interneurons upon stimulation of neurons in the VTA might originate from a subset specialized synaptic contacts.

However, it is still questionable why VTA MbDNs release glutamate to modulate the PFC function. MbDN respond by firing a 200 ms burst of spikes to primary rewards, conditioned or secondary rewards, rewards that are not predicted and novel or unexpected stimuli (Hollerman and Schultz, 1998; Schultz 1998; Hyland et al., 2002). They generate a prediction error about reward by emitting brief bursts in response to events that are better than predicted or a brief cessation of firing to events that are worse than predicted (Lavin et al., 2005). However, DA may not be ideal to transmit this type of fast signal to the PFC. VTA MbDNs encode prediction error by changing their firing on the order of 500 ms or less (Schultz et al., 1997). This leads to an increased PFC DA levels (Watanabe et al., 1997; Ahn and Phillips, 1999), due to low levels of DAT and, consequently, slow uptake of DA (Garris et al., 1993; Lavin at al., 2005). Furthermore, a negative event such stress, which is presumably worse than expected, increases PFC DA levels for prolongated periods (Finlay et al., 1995). Thus, within the PFC the DA signal is not temporally precise and slow in its response to events of positive and negative valence (Gorelova et al., 2012). In contrast, glutamate is tightly coupled to neuronal firing and could provide temporally precise prediction error signal in the PFC, whereas the slower DA signal might modulate the state of the PFC (Lavin et al., 2005; Lapish et al., 2007; Gorelova et al., 2012).

5.7 Determining of MbDN identity of embryonic stem cell-derived MbDNs

The pathological hallmark of PD is the preferential loss of the SNpc MbDNs (Barzilai and Melamed, 2003). The transplantation studies demonstrated that only MbDNs that form synaptic connections with the host striatum exhibit characteristics of the SNpc, are

therapeutically useful in cell replacement therapy in animal models of PD (Hudson et al., 1994; Thompson et al., 2005). In order to provide a scalable pool of MbDNs for transplantation purposes in PD patients continued efforts have been made to direct stem cell reprogramming and differentiation towards the dopaminergic phenotype. In recent years, a number of protocols have been developed to derive dopaminergic neuron-like cells from human embryonic or induced pluripotent stem cells (iPSC) (Elkabetz et al, 2008; Koch et al., 2009; Soldner et al., 2009; Swistowski et al., 2010; Chung et al., 2011; Kriks et al., 2011; Jaeger et al., 2011). A more recent breakthrough has been the direct conversion of fibroblasts into DA neuron-like cells (Pfisterer et al., 2011; Caiazzo et al., 2011). However, iPSC-derived DA neuron-like cells are heterogeneous and do not all exhibit midbrain identity (Marchetto et al., 2010). In addition, the final characterization and validation of MbDNs is mostly based on the expression of TH and not on the expression of specific markers to distinguish two MbDN subpopulations. In order to improve MbDN induction protocols, it is essential to identify signaling pathways and transcriptional factors crucial for MbDNs specification. This study provides an additional regulatory means to control the specification of MbDN subpopulations by changing the cell competence in response to dynamic changes in Shh signaling to produce more specific types of MbDNs. The detailed knowledge about the mechanisms underlying the specification of MbDN subpopulations will help to improve the successful differentiation of stem/iPSC into transplantable MbDNs that can functionally replace neurons generated in PD.

5.8 Prolongated Shh signaling is crucial for proper generation of red nucleus neurons

Besides MbDNs, the vMb contains other neuronal populations such as OM and RN neurons. Due to the clinical relevance of MbDNs, the SNpc and the VTA are the best characterized structures in the vMb, whereas little is known about the cues and mechanisms controlling the development of RN neurons. Anatomical studies have demonstrated that RN neurons are divided into two populations: the parvocellular and the magnocellular part. While the magnocellular part projects to interneurons in the brain stem and spinal cord and forms the rubrospinal tract, the parvocellular part gives rise to the central tegmental tract, relaying information from the motor cortex to the cerebellum through the inferior olivary complex (ten Donkelaar, 1988). Developmental studies showed that Foxa2 and Nkx6-1 play essential roles in establishing RN neurons (Prakash et al., 2009; Moreno-Bravo et al., 2010). Surprisingly, despite the almost complete loss of Foxa2 and Nkx6-1 domain in $Gli2^{\Delta Mb>E9.0}$ mutant mice, RN neurons are still generated. Interestingly, the rostrally located RN neurons were

unaffected, whereas the caudal part of the RN was severely reduced. These data suggest that there might be a spatiotemporal requirement of Shh signaling for the induction of RN neurons. However, it remains unclear how these two populations are generated.

Classically both parts of RN are thought to be located in the midbrain. However, expression patterns of early RN markers, in particular Nkx6-1, Nkx6-2 and Pou4f1 showed their extension into the posterior diencephalon (Massion, 1967; Moreno-Bravo et al., 2010), meaning that neurons of the parvocellular RN might arise from diencephalic precursors. This idea is supported by the fact that in order to inactivate Shh signaling, *En1* was used as a promoter, which is specifically expressed in the vMb and aHb. Thus, removal of Shh signaling at E9.0 does not affect the forebrain regions and thereby generation of the parvocellular RN neurons.

Another conditional gene inactivation study, in which Shh was inactivated in the vMb and aHb at E9.0, shows no defects in the development of RN neurons (Perez-Balaguer et al., 2008). Expression of Nkx6.1 and Foxa2 in these mutants was almost unaltered, meaning that RN neurons still can be specified in the absence of Shh. It was suggested that the induction of the RN neurons is independent of Shh function. However, present loss-of-function study demonstrated that inactivation of Shh signaling after E9.0 in the $Gli2^{\Delta Mb>E9.0}$ mice results in severe loss of RN neurons. The differences in the results might be due to not complete removal of functional *Shh* RNA in *Shh* conditional knockout mice.

6. Summary

Midbrain dopaminergic neurons (MbDNs) in the ventral tegmental area (VTA) and substantia nigra pars compacta (SNpc) modulate cognition, reward behavior and voluntary movement, respectively. Recent findings indicate that VTA and SNpc MbDNs form subpopulations that are divergent in their electrophysiological features, functions and vulnerability to neurodegeneration in Parkinson's disease. This diversity can be correlated with the anatomical organization of these two populations and their afferent and efferent connections. However, it is largely unexplored how MbDN diversity is established during development. Previous studies have demonstrated that the identity of MbDN subtypes can be directly linked to their temporal and spatial origin in the embryonic midbrain (Blaess et al., 2011; Hayes et al., 2011). Different subsets of MbDNs are derived from a ventral progenitor pool in the developing midbrain that is subdivided into a medial and a lateral domain. The relationship between developmental origin and the identity of MbDNs in the adult brain is likely reflected by the regulated activity of genes inducing cell fate during embryogenesis. Thus, the timing of Sonic hedgehog (Shh) signaling might play a role in the determination of the fate of MbDN subpopulations, since MbDN precursors respond differently to Shh.

To address whether Shh signaling regulates the specification of MbDN subtypes, conditional gene inactivation approach was used in this study. Removal of Shh signaling at particular time point during MbDN induction results in the selective loss of a specific subset of MbDN precursors in the embryo. Using viral tracing and immunohistochemical analysis, this study demonstrates that this population of MbDN precursors gives rise to mesocortical projection neurons in the VTA. Furthermore, optogenetics and physiological analysis reveals that mesocortical MbDNs inhibit prefrontal cortical pyramidal neurons via an inhibitory cortical microcircuit. Other MbDN-derived projections are largely unaffected. Thus, temporally precise Shh signaling in the midbrain is required for establishing a specific mesocortical microcircuit. This is the first study establishing a causal link between early developmental induction mechanisms and the functional properties of MbDNs in the adult brain.

Furthermore, constitutive activation of Shh signaling results in a massive increase in the number of MbDNs and the ventralization of the dorsal midbrain. Interestingly, analysis of MbDNp domain shows that only medial MbDN precursor domain was significantly increased. Due to the perinatal lethality of the mutant mice, investigation of MbDN specification in the adult brains was not possible.

In addition, this study demonstrates that the development of the red nucleus (RN) neuron subpopulations is determined by the duration of Shh signaling as well. While inactivation of

Shh signaling does not affect the generation of the parvocellular RN neurons, the neurons of magnocellular RN are severely reduced and disorganized.

7. Acknowledgement

I am grateful to Prof. Dr. Oliver Brüstle for giving me the opportunity to work in the Institute of Reconstructive Neurobiology.

My special thanks go to Dr. Sandra Blaess for letting me join her Neurodevelopmental Genetics group allowing me to pursue research in one of the most interesting subjects of developmental biology. I also want to thank her for introducing me to the fascinating project of Sonic hedgehog, to many laboratory techniques and to the wonderful world of neuroscience research. Her profound knowledge, professionalism and kindness have been present in every single step of this work. I would like to thank her for her trust placed in me concerning the strategic alignment and the realization of this thesis.

I am deeply appreciative to Prof. Michael Hoch who agreed to act as a second assessor of this thesis.

It is a pleasure to thank to all my colleagues for the nice working atmosphere and especially those who helped in specific parts of this thesis:

- Prof. Dr. Heinz Beck for great collaboration and interest in this project
- Milan Pabst for performing viral injections into the prefrontal cortex, optogenetic and electrophysiological experiments
- Oliver Braganza for performing Ca^{2+} imaging analysis
- Dr. Ruth Musgrove for performing HPLC analysis
- Martin Jansen and Viktoria Bosch for the excellent technical assistance
- Gabriela O. Bodea for introducing me to the biochemical techniques and for the great working atmosphere during last four years
- Dr. Anne Bohlen for proof-read this thesis and for her endless emotional support

Lastly, I would like to wholeheartedly thank my family and my husband for their encouragement and advice whenever it was needed. Without your love and tremendous support, I could have never achieved my goals. You have helped to make me who I am and for that I am forever grateful.

8. Appendix

8.1 Abbreviations

AC	adenylyl cyclase
ACSF	artificial cerebrospinal fluid
ADHD	attention-deficit/hyperactivity disorder
aHb	anterior Hindbrain
Ahd2	aldehyde dehydrogenase family 1, subfamily A1
AP	action potential
Arx	aristaless related homeobox gene (Drosophila)
bHLH	basic-helix-loop-helix
BLA	basolateral amygdala
BMP	bone morphogenetic protein
BrdU	bromodeoxyuridine
CA	catecholamine
cDNA	complementary DNA
ChR2	channelrhodopsin-2
CLi	caudal linear nucleus
CNS	central nervous system
CPu	caudatoputamen complex
Cre	Cre recombinase
DA	dopamine
DAT	dopamine transporter
DNA	deoxyribonucleic acid
dNTP	deoxy-A/C/G/T-trisphosphate
dlVTA	dorsolateral VTA
DOPAC	3,4-Dihydroxyphenylacetic acid
E	embryonic day
EDTA	ethylenediaminetetraacetic acid
En1	engrailed 1
EPSP	excitatory postsynaptic potential
EtBr	ethidium bromide
EtOH	ethanol
EYFP	enhanced yellow fluorescent protein
Foxa2	forkhead box A2

Fgf8	fibroblast growth factor 8
FP	floor plate
g	gram
GABA	gamma-aminobutyric acid
Gbx2	gastrulation brain homeobox 2
GFP	green fluorescent protein
GIFM	genetic inducible fate mapping
Girk2	potassium inwardly rectifying channel, subfamily J, member 6
Gli1-3	Gli zinc finger transcription factor 1-3
GliA	Gli protein activator form
Gli R	Gli protein repressor form
hrs	hours
HCl	hydrochloric acid
HCN	hyperpolarization-activated cyclic nucleotide-gated channel
Hes5	hairy and enhancer of split 5 (Drosophila)
HPLC	high-performance liquid chromatography
Hz	Hertz
IF	nucleus intrafasciculus
iPSC	induced pluripotent stem cell
IPSP	inhibitory postsynaptic potential
Isl1	LIM homeodomain transcriptional factor islet1
kb	kilobase
L	liter
LB	Luria Bertani Medium
L-DOPA	L-3,4-dihydroxyphenylalanine
Lmx1a	LIM homeobox transcriptional factor 1 alpha
M	Mol per liter/molar
MbDNs	midbrain dopaminergic neurons
MbDNp	midbrain dopaminergic precursor
mfb	medial forebrain bundle
mg	milligram
MHB	mid-hindbrain boundary
min	minute
mL	milliliter

mM	millimolar
µm	micrometer
Mnx1	motor neuron and pancreas homeobox 1
mPFC	medial prefrontal cortex
MPTP	1-methyl-4-phenyl-1,2,3,6-tetrahydropyridine
mRNA	messenger RNA
ms	millisecond
Msx1	homeobox, msh-like 1
NAc	nucleus accumbens
NDS	normal donkey serum
ng	nanogram
Ngn2	neurogenin 2
NGS	normal goat serum
Nkx2-2	NK2 transcriptional factor related, locus 2 (Drosophila)
Nkx6-1	NK6 transcription factor related, locus 1 (Drosophila)
n.s.	not significant
nt	nucleotide
Nurr1	nuclear receptor subfamily 4, group A, member 2
OB	olfactory bulb
6-OHDA	6-hydroxydopamine
OM	oculomotor nucleus
OTu	olfactory tubercle
Otx2	orthodenticle homolog 2 (Drosophila)
P	postnatal stage
PBP	parabrachial nucleus
PBS	phosphate buffered saline
PCR	polymerase chain reaction
PD	Parkinson’s disease
PFA	paraformaldehyde
PFC	prefrontal cortex
Pitx3	paired-like homeodomain transcriptional factor 3
PN	paranigral nucleus
Pou4f1	POU domain, class 4, transcription factor 1
Ptch	Patched

rAAV	recombinant adeno-associated virus
RA	retinoic acid
RLi	rostral linear nucleus
RNA	ribonucleic acid
RN	red nucleus
rpm	rounds per minute
s	second
SEM	standard error of the mean
Sim1	single-minded homolog 1 (Drosophila)
SK	apamin-sensitive small-conductance calcium-activated potassium channel
Shh	Sonic hedgehog
Smo	Smoothened
SNl	substantia nigra lateralis
SNpc	substantia nigra pars compacta
SNr	substantia nigra reticulata
TAE	triethanolamine
TH	tyrosine hydroxylase
vGAT	vesicular GABA transporter
vGlut2	vesicular glutamate transporter
vMAT2	vesicular monoamine transporter
vMb	ventral midbrain
vmVTA	ventromedial VTA
VTA	ventral tegmental area
VZ	ventricular zone
Wnt1	wingless-type MMTV integration site family, member 1

9. Bibliography

1. Abeliovich, A., Hammond, R. (2007). Midbrain dopamine neuron differentiation: factors and fates. *Developmental Biology*, 304 (2): 447-54
2. Abou-Sleiman, P.M., Muqit, M.M., Wood, N.W. (2006). Expanding insights of mitochondrial dysfunction in Parkinson's disease. *Nature Reviews Neuroscie*nce, 7: 207-219
3. Acampora, D., Avantaggiato, V., Tuorto, F., Simeone, A. (1997). Genetic control of brain morphogenesis through Otx gene dosage requirement. *Development*, 124 (18): 3639-3650
4. Afonso-Oramas, D., Cruz-Muros, I., Alvarez de la Rosa, D., Abreu, P., Giraldez, T., Castro-Hernandez, J., Salas-Hernandez, J., Lanciego, J.L., Rodriguez, M., Gonzales-Hernandez, T. (2009). Dopamine transporter glycosylation correlates with the vulnerability of midbrain dopaminergic cells in Parkinson's disease. *Neurobiology of disease*, 36: 494-508
5. Agarwala, S., Ragsdale, C.W. (2002). A role of midbrain arcs in nucleogenesis. *Development*, 129: 5779-5788
6. Ahn, S., Phillips, A.G. (1999). Dopaminergic correlates of sensory-specific satiety in the medial prefrontal cortex and nucleus accumbens of the rat. *Journal of Neuroscience*, 19: RC29 (1-6)
7. Alcedo, J., Ayzenzon, M., Von Ohlen, T., Noll, M., Hooper, J.E. (1996). The Drosophila smoothened gene encodes a seven-pass membrane protein, a putative receptor for the hedgehog signal. *Cell*, 86 (2): 221-32
8. Altman, J., Bayer, S.A. (1981). Development of the brain stem in the rat. V. Thymidine-radiographic study of the time of origin of neurons in the midbrain tegmentum. *Journal of Comparative Neurology*, 198 (4): 677-716
9. Andersson, E., Jensen, J. B., Parmar, M., Guillemont, F., Bjorklund, A. (2006). Development of the mesencephalic dopaminergic neuron system is compromised in the absence of neurogenin 2. *Development*, 133 (3): 507-516
10. Andersson, E., Tryggvason, U., Deng, Q., Frilling, S., Alekseenko, Z., Robert, B., Perlmann, T., Ericson, J. (2006). Identification of intrinsic determinants of midbrain dopamine neurons. *Cell*, 124: 393-405
11. Ang, S.L., Jin, O., Rhinn, M., Daigle, N., Stevenson, L., Rossant, J. (1996). A target mouse Otx2 mutation leads to severe defects in gastrulation and formation of axial mesoderm and to deletion of rostral brain. *Development*, 122: 243-252

12. Arts, M.P., Groenenwegen, H.J., Veening, J.G. and Cools, A.R. (1996). Efferent projections of the retrorubral nucleus to the substantia nigra and ventral tegmental area in cats as shown by anterograde tracing. *Brain Research Bulletin*, 40: 219-228
13. Bai, C.B., Auerbach, W., Lee, J.S., Stephen, D., Joyner, A.L. (2002). Gli2, but not Gli1, is required for initial Shh signaling and ectopic activation of the Shh pathway. *Development*, 129 (20): 4753-61
14. Bai, C.B., Stephen, D., Joyner, A.L. (2004). All mouse ventral spinal cord patterning by hedgehog is Gli dependent and involves an activator function of Gli3. *Developmental Cell*, 6 (1): 103-15
15. Balaskas, N., Ribeiro, A., Panovska, J., Dessaud, E., Sasai, N., Page, K.M., Briscoe, J., Ribes, V. (2012). Gene regulatory logic for reading the Sonic Hedgehog signaling gradient in the vertebrate neuronal tube. *Cell*, 148 (1-2): 273-84
16. Barraud, Q., Obeid, I., Aubert, I., Barriere, G., Contamin, H., McGuire, S., Ravenscroft, P., Porras, G., Tison, F., Bezard, E., Ghorayeb, I. (2010). Neuroanatomical study of the A11 diencephalospinal pathways in the non-human primate. *PLoS One*, 13: 5
17. Barzilai, A. and Melamed, E. (2003). Molecular mechanisms of selective dopaminergic neuronal death in Parkinson's disease. *Trends in Molecular Medicine*, 9: 126-132
18. Bayly, R.D., Ngo, M., Agyamova, G.V., Agarwala, S. (2007). Regulation of ventral midbrain patterning by Hedgehog signaling. *Development*, 134, 2115-2124
19. Berghuis, P., Dobszay, M.B., Sousa, K.M., Schlte, G., Mager, P.P., Hartig, W., Gorcs, T.J. (2004). Brain-derived neurotrophic factor controls functional differentiation and microcircuit formation of selectively isolated fast-spiking GABA-ergic interneurons. *European Journal of Neuroscience*, 20: 1290-1306
20. Berridge, K.C., Robinson, T.E. (1998). What is the role of dopamine in reward: hedonic impact, reward learning, or incentive salience? *Brain Research Brain Review*, 28 (3): 309-69
21. Berube-Carriere, N., Riad, M., Dal Bo, G., Levesque, D., Trudeau, L-E., Descarries, L. (2009). The dual dopamine-glutamate phenotype of growing mesencephalic neurons regress in mature rat brain. *Journal of Comparative Neurology*, 517: 873-891
22. Birtwistle, J., Baldwin, D. (1998). Role of dopamine in schizophrenia and Parkinson's disease. *British Journal of Nursing*, 7 (14): 832-4, 836, 838-41
23. Bjorklund, A. and Lindvall, O. (1984). Catecholaminergic brain stem regulatory

system. In Handbook of Physiology, Section 1: The nervous system, Vol.4. Intrinsic regulatory systems of the brain (eds Mountcastle V. B., Bloom, F. E. and Geiger, S. R.): 155-235

24. Bjorklund, A., Dunnett, S.B. (2007). Dopamine neuron systems in the brain: an update. *Trends in Neuroscience*, 30: 194–202
25. Blaess, S., Corrales, J.D., Joyner, A.L. (2006). Sonic hedgehog regulates Gli activator and repressor functions with spatial and temporal precision in the mid/hindbrain region. *Development*, 133 (9): 1799-1809
26. Blaess, S., Bodea, G.O., Kabanova, A., Chanet, S., Mugniery, E., Derouiche, A., Stephen, D., Joyner, A.L. (2011). Temporal-spatial changes in Sonic Hedgehog expression and signaling reveal different potentials of ventral mesencephalic progenitors to populate distinct ventral midbrain nuclei. *Neural Development*, 6: 29
27. Bonilla, S., Hall, A.C., Pinto, L., Attardo, A., Gotz, M., Huttner, W.B., Arenas, E. (2008). Identification of midbrain floor plate radial glia-like cells as dopaminergic progenitors. *Glia*, 56: 809-820
28. Briscoe, A., Pierani, T.M., Jessel, T.M., Ericson, J. (2000). A homeodomain protein code specifies progenitor identity and neuronal fate in the ventral neural tube. *Cell*, 101 (4): 434-445
29. Briscoe, J., Chen, Y., Jessell, T.M., Struhl, G. (2001). A hedgehog-intensive form of patched provides evidence for direct long-range morphogen activity of sonic hedgehog in the neural tube. *Molecular Cell*, 7: 1279-1291
30. Brocolli, V., Boncinelli, E., Wurst, W. (1999). The caudal limit of Otx2 expression positions the isthmic organizer. *Nature*, 401 (6749): 164-168
31. Brodski, C., Weisenhorn, D.M., Signore, M., Sillaber, I., Oesterheld, M., Brocolli, V., Acampora, D., Simeone, A., Wurst, W. (2003). Location and size of dopaminergic and serotoninergic cell populations are controlled by the position of the midbrain-hindbrain organizer. *Journal of Neuroscience*, 23 (10): 4199-4207
32. Caiazzo, M., Dell'Anno, M.T., Dvoretskova, E, Lazarevic, D., Taverna, S., Leo, D., Sotnikova, T.D., Menegon, A., Roncaglia, P., Colciago, G., Russo, G., Carninci, P., Pexxoli, G., Gainetdinov, R. R., Gustincich, S., Dityatev, A., Brocolli, V. (2011). Direct generation of functional dopaminergic neurons from mouse and human fibroblasts. *Nature*, 476 (7359): 224-7
33. Cardin, J.A, Carlen, M., Meletis, K., Knoblich, U., Zhang, F., Deisseroth, K., Tsai, L.H., Moore, C.I. (2009). Driving fast-spiking cells induces gamma rhythm and

controls sensory responses. *Nature*, 459 (7247): 663-7

34. Carlsson, A. (1959a). The occurrence, distribution and physiological role of catecholamines in the nervous system. *Pharmacological Reviews*, 2 (2): 490-3
35. Carlsson, A. (1959b). Detection and assay of dopamine. *Pharmacological Reviews*, 2 (2): 300-4
36. Chan, G.S., Guzman, J.N., Ilijic, E., Mercer, J.N., Rick, C., Tkatch, T., Meredith, G.E., Surmeier, D.J. (2007). "Rejuvenation" protects neurons in mouse models of Parkinson's disease. *Nature,* 447: 1081-1086
37. Cheer, J.F., Aragona, B.J., Heien, M.L., Seipel, A.T., Garelli, R.M., Wightman, R.M. (2007). Coordinated accumbal dopamine release and neural activity drive goal-directed behavior. *Neuron*, 54: 237-244
38. Chen Y., Struhl, G. (1996). Dual roles for patched in sequestering and transducing Hedgehog. *Cell*, 87 (3): 553-63
39. Chi, C.L., Martinez, S., Wurst, W., Martin, G.R. (2003). The isthmic organizer signal FGF8 is required for cell survival in the prospective midbrain and cerebellum. *Development*, 130 (12): 2633-44
40. Chilov, D., Sinjushina, N., Saarimaki-Vire, J., Taketo, M.M., Partanen, J. (2010). beta-Catenin regulates intercellular signaling networks and cell-type specific transcription in the developing mouse midbrain-rhombomere 1 region. *PLoS One*, 5 (6): e10881
41. Chung, S., Leung, A., Han, B-S., Chang, M-Y., Moon, J-I., Kim, C-H., Hong, S., Pruszak, J., Isacson, O., Kim, K-S. (2009). Wnt1-Lmx1a forms a novel autoregulatory loop and controls midbrain dopaminergic differentiation synergistically with the Shh-Foxa2 pathway. *Cell Stem Cell*, 5: 646-658
42. Chung, S., Moon, J.I., Aldrich, D., Lukianov, S., Kitayama, Y., Park, S., Li, Y., Bolshakov, V.Y., Lamonerie, T., Kim, K.S. (2011). ES cell-derived renewable and functional midbrain dopaminergic progenitors. *Proceedings of the National Academy of Science*, 108 (23): 9703-8
43. Corbit, K.C., Aanstad, P., Singla, V., Norman, A.R., Stainier, D.Y., Reiter, J.F. (2005). Vertebrate smoothened functions at the primary cilium. *Nature*, 437: 1018-1021
44. Corrales, J.D., Blaess, S., Mahoney, E.M., and Joyner, A.L. (2006). The level of sonic hedgehog signaling regulates the complexity of cerebellar foliation. *Development,* 133: 1811-1821

45. Dailly, E., Chenu, F., Renard, C.E. and Bourin, M. (2004). Dopamine, depression and antidepressants. *Fundamental Clinical Pharmacology*, 18: 601-607
46. Dahlstrom, A. and Fuxe, K. (1964). Evidence for the existence of monoamine containing neurons in the central nervous system. I. Demonstration of monoamines in the cell bodies of brain stem neurons. *Acta Physiol. Scand*., 62: 231-255
47. Dahmane, N., Sanchez, P., Gitton, Y., Palma, V., Sun, T., Beyna, M., Weiner, H., Ruiz I Altaba, A. (2001). The Sonic Hedgehog-Gli pathway regulates dorsal brain growth and tumorigenesis. *Development*, 128 (24): 5201-12
48. Dal Bo, G., St-Gelais, F., Danik, M., Williams, S., Cotton, M., Trudeau, L.E. (2004). Dopamine neurons in culture express VGLUT2 explaining their capacity to release glutamate at synapses in addition to dopamine. *Journal of Neurochemistry*, 88: 1398-1405
49. Damier, P., Hirsch, E.C., Agid, Y., Graybiel, A.M. (1999). The substantia nigra of the human brain: II. Patterns of loss of dopamine-containing neurons in Parkinson's disease. *Brain*, 122 (Pt. 8): 1437-1448
50. Del-Fava, F., Hasue, R.H., Ferreira, J.G., Shammah-Lagnado, S.J. (2007). Efferent connections of the rostral linear nucleus of the ventral tegmental area in the rat. *Neuroscience*, 175: 1059-1076
51. Deng, Q., Andersson, E., Hedlund, E., Alekseenko, Z., Coppola, E., Panman, L., Millonig, J.H., Brunet, J.F., Ericson, J., Perlmann, T. (2011). Specific and integrated roles of Lmx1a, Lmx1b and Phox2a in ventral midbrain development. *Development,* 138 (16): 3399-408
52. Dessaud, E., Yang, L.L., Hill, K., Cox, B., Ulloa, F., Ribeiro, A., Mynett, A., Novitch, B.G., Briscoe, J. (2007). Interpretation of the sonic hedgehog morphogen gradient by a temporal adaptation mechanism. *Nature*, 450: 717-720
53. Dessaud, E., McMahon, A.P., Briscoe, J. (2008). Pattern formation in the vertebrate neural tube: a sonic hedgehog morphogen-regulated transcriptional network. *Development*, 135: 2489-2503
54. Di Salvio, M., Di Giovannatonio, L. G., Omodei, D., Acampora, D., Simeone, A. (2010). Otx2 expression is restricted to dopaminergic neurons of the ventral tegmental area I the adult brain. *International Journal of Developmental Biology*, 54: 939-945
55. Eisenstat, D.D., Liu, J.K., Mione, M., Zhong, W., Yu, G., Anderson, S.A., Ghattas, I., Puelles, L., and Rubenstein, J.L. (1999). DLX-1, DLX-2, and DLX-5 expression define distinct stages of basal forebrain differentiation. *The Journal of comparative*

neurology, 414: 217-237

56. Elkabetz, Y., Panagiotakos, G., Al Shamy, G., Socci, N.D., Tabar, V., Studer, L. (2008). Human ES cell-derived neuronal rosettes reveal a functionally distinct early neural stem cell stage. *Genes & Development*, 22 (2): 152-65
57. Ericson, J., Thor, S., Edlund, T., Jessel, T.M., Yamada, T. (1992). Early stages of motor neuron differentiation revealed by expression of homeobox gene Islet-1. *Science*, 256: 1555-1560
58. Everitt, B.J., Parkinson, J.A., Olmsted, M.C., Arroyo, M., Robledo, P., Robbins, T.W. (1999). Associative processes in addiction and reward. The role of amygdala-ventral striatal subsystems. *Annals of the New York Academy of Sciences*, 877: 412-38
59. Evinger, C. (1988). Extraocular motor nuclei: location, morphology and afferents. *In Neuroanatomy of the oculomotor system*, Amsterdam: Elsevier: 81-117
60. Fan, X., Xu, M., Hess, E.J. (2010). D2 dopamine receptor subtype-mediated hyperactivity and amphetamine responses in a model of ADHD. *Neurobiology of Disease*, 37 (1): 228-236
61. Fearnley, J.M., Lees, A. (1991). Ageing and Parkinson's disease: substantia nigra regional selectivity. *Brain*, 114: 2283-2301
62. Fedtsova, N., Turner, E.E. (1995). Brn-3.0 expression identifies early post-mitotic CNS neurons and sensory neural precursors. *Mechanisms of Development*, 53 (3): 291-304
63. Fedtsova, N., Turner, E.E. (2001). Signals from the ventral midline and isthmus regulate the development of Brn3.0-expressing neurons in the midbrain. *Mechanisms of Development*, 105 (1-2): 129-44
64. Ferreira J.G., Del-Fava F, Hasue R.H., Shammah-Lagnado S.J. (2008). Organization of ventral tegmental area projections to the ventral tegmental area-nigral complex in the rat. *Neuroscience*, 153:196–213
65. Fields, H.L., Hjelmstad, G.O., Margolis, E.B., Nicola, S.M. (2007). Ventral tegmental area neurons in learned appetitive behavior and positive reinforcement. *Annual Review of Neuroscience*, 30: 289-316
66. Finkelstein, D.I., Stanic, D., Parish, C.L., Tomas, D., Dickson, K., Horne, M.K. (2000). Axonal sprouting following lesions of the rat substantia nigra. *Neuroscience*, 97 (1): 99-112
67. Finlay, J.M., Zigmond, M.J., Abercrombie, E.D. (1995). Increased dopamine and norepinephrine release in medial prefrontal cortex induced by acute and chronic stress:

effects of diazepam. *Neuroscience*, 6 (4): 619-628

68. Fogel, J.L., Chiang, C., Huang, X., Agarwala, S. (2008). Ventral specification and perturbed boundary formation in the mouse midbrain in the absence of Hedgehog signaling. *Developmental Dynamics*, 237: 1359-1372
69. Fuccillo, M., Joyner, A.L., Fishel, G. (2006). Morphogen to mitogen: the multiple roles of hedgehog signaling in vertebrate neural development. *Nature Reviews. Neuroscience*, 7 (10): 772-83
70. Gale, E., Li, M. (2008). Midbrain dopaminergic neuron fate specification: Of mice and embryonic stem cells. *Molecular Brain*, 1: 8
71. Garaschuk, O., Milos, R.I., Konnerth, A. (2006). Targeted bulk-loading of fluorescent indicators for two-photon brain imaging in vivo. *Nature Protocols*, 1 (1): 380-6
72. Garlezon, W.A., Devine, D.P., Wise, R.A. (1995). Habit-forming actions of nomifensine in nucleus accumbens. *Psychopharmacology*, 122 (2): 194-7
73. Garris, P.A., Collins, L.B., Jones, S.R., Wightman, R.M. (1993). Evoked extracellular dopamine in vivo in the medial prefrontal cortex. *Journal of Neurochemistry*, 61: 637-647
74. Gasbarri, A., Packard, M.G., Campana, E., Pacitti, C. (1994). Anterograde and retrograde tracing of projections from the ventral tegmental area to the hippocampal formation in the rat. *Brain Research Bulletin*, 33 (4): 445-52
75. Gerfen, C.R., Herkenham, M., Thibault, J. (1987). The neostriatal mosaic. II. patch-directed and matrix-directed mesostriatal dopaminergic and non-dopaminergic systems. *Journal of Neuroscience*, 7: 3915–3934
76. German, D.C., Manaye, K., Smith, W.K., Woodward, D.J., Saper, C.B. (1989). Midbrain dopaminergic cell loss in Parkinson's disease: computer visualization. *Annals of Neurology*, 26: 507-514
77. Giros, B., Jaber, M., Jones, S.R., Wightman, R.M., Caron, M.G. (1996). Hyperlocomotion and indifference to cocaine and amphetamine in mice lacking the dopamine transporter. *Nature*, 379: 606-612
78. Goldman-Rakic, P.S. (1998). The cortical dopamine system: role in memory and cognition. *Advances in Pharmacology*, 42: 707-11
79. Gonzalez-Hernandez, T., Barroso-Chinea, P., De la Cruz-Muros, I., Perez-Delgado, M. M., Rodriguez, M. (2004). Expression of dopamine and vesicular monoamine transporters and differential vulnerability of mesostriatal dopaminergic neurons. *Journal of Comparative Neurology*, 479: 198-215

80. Goodrich, L.V., Milenkovic, L., Higgis, K.M., Scott, M.P. (1997). Altered neural cell fares and medulloblastoma in mouse patched mutants. *Science*, 277: 1109-1113
81. Gorelova, N., Mullholland, P.J., Chandler, L.J., Seamans, J.K. (2012). The glutamatergic component of the mesocortical pathway emanating from different subregions of the ventral midbrain. *Cerebral Cortex*, 22: 327-336
82. Grace, A.A., Bunney, B.S. (1984). The control of firing pattern in nigral dopamine neurons: burst firing. *Journal of Neuroscience*, 4 (11): 2877-90
83. Grace, A. A., Floresco, S. B., Goto, Y., and Lodge, D. J. (2007). Regulation of firing of dopaminergic neurons and control of goal-directed behaviors. *Trends in Neuroscience*, 30: 220-227
84. Guo, C., Qui, H.Y., Huang, Y., Chen, H., Yang, R.Q., Chen, S.D., Johnson, R.L., Chen, Z. F., Ding, Y.Q. (2007). Lmx1b is essential for Fgf8 and Wnt1 expression in the isthmic organizer during tectum and cerebellum development in mice. *Development*, 134: 317-325
85. Guzman J.N., Sanchez-Padilla, J., Wokosin, D., Kondapalli, J., Ilijic, E., Schumacker, P.T., Surmeier, D.J. (2010). Oxidant stress evoked by pacemaking in dopaminergic neurons is attenuated by DJ-1. *Nature*, 468: 696-700
86. Hasue, R.H., Shammah-Lagnado, S. J. (2002). Origin of the dopaminergic innervation of the central extended amygdala and accumbens shell: a combined retrograde tracing and immunohistochemical study in the rat. *Journal of Comparative Neurology*, 454: 15-33
87. Haycraft, C.J., Banizs, B., Aydin-Son, Y., Zhang, Q., Michaud, E.J., Yoder, B.K. (2005). Gli2 and Gli3 localize to cilia and require the intraflagelar transport protein Polaris for processing and function. *PLoS Genetics*, 1: e53
88. Hayes, L., Zhang, Z., Albert, P., Zervas, M., Ahn, S. (2011). Timing of Sonic hedgehog and Gli1 expression segregates midbrain dopamine neurons. *Journal of Comparative Neurology*, 519 (15): 3001-18
89. Hayes, L., Ralls, S., Wang, H., Ahn, S. (2013). Duration of Shh signaling contributes to mDA neuron diversity. *Developmental Biolo*gy, 374 (1): 115-26
90. Henny, P., Brown, M., Northrop, A., Faunes, M., Ungless, M. A., Magill, P.J., Bolam, J.P. (2012). Structural correlates of heterogeneous *in vivo* activity of midbrain dopaminergic neurons. *Nature Neuroscience*, 15 (4): 613-9
91. Hirsch, E., Graybiel, A.M., Agid, Y.A. (1988). Melanized dopaminergic neurons are differentially susceptibility to degeneration in Parkinson's disease. *Nature*, 334

(6180): 345-8

92. Hnasko, T.S., Chuhma, N., Zhang, H., Goh, G.Y., Sulzer, D., Palmiter, R.D., Rayport, S., Edwards, R.H. (2010). Vesicular glutamate transport promotes dopamine storage and glutamate corelease *in vivo. Neuron*, 65: 643-656
93. Hnasko, T.S., Hjelmstad, G.O., Fields, H.L., Edwards, R.H. (2012). Ventral tegmental area glutamate neurons: electrophysiological properties and projections. *Journal of Neuroscience*, 32 (43): 15076-15085
94. Hollerman, J.R., Schultz, W. (1998). Dopamine neurons report an error in the temporal prediction of reward during learning. *Nature Neuroscience*, 1: 304-309
95. Houzelstein, D., Cohen, A., Buckingham, M.E., and Robert, B. (1997). Insertional mutation of the mouse Msx1 homeobox gene by an nlacZ reporter gene. *Mechanisms of development* 65: 123-133
96. Hu, Z., Cooper, M., Crockett, D.P., Zhou, R. (2004). Differentiation of the midbrain dopaminergic pathways during mouse development. *Journal of Comparative Neurology*, 476 (3): 301-11
97. Hudson, J.L., Bickford, P., Johansson, M., Hoffer, B.J., Stromberg, I. (1994). Target and neurotransmitter specificity of fetal central nervous system transplants: importance for functional reinnervation. *Journal of Neuroscience*, 14 (1): 283-290
98. Hui, C.C., Slusarski, D, Platt, K.A., Holmgren, R., Joyner, A.L. (1993). Expression of three homologs of the Drosophila segment polarity gene cubitus interuptus, Gli, Gli-2, Gli-2, in ectoderm and mesoderm-derived tissue suggest multiple roles during postimplantation development. *Developmental Biology*, 162 (12): 402-413
99. Hyland, B.I., Reynolds, J.N., Hay, J., Perk, C.G., Miller, R. (2002). Firing modes of midbrain dopamine cells in the freely moving rat. *Neuroscience*, 114: 475-492
100. Hynes, M., Porter, J.A., Chiang, C., Chang, D., Tessier-Lavigne, M., Beachy, P.A., Rosenthal, A. (1995). Induction of midbrain dopaminergic neurons by Sonic hedgehog. *Neuron*, 1: 35-44
101. Hynes, M., Poulsen, K., Tessier-Lavigne, M., Rosenthal, A. (1995). Control of neuronal diversity by the floor plate: contact-mediated induction of midbrain dopaminergic neurons. *Cell*, 80 (1): 95-101
102. Ikemoto, S., Glazier, B.S., Murphy, J.M., McBride, W.J. (1997). Role of D1 and D2 receptors in the nucleus accumbens in mediating reward. *Journal of Neuroscience*, 17: 8580-8587
103. Ikemoto, S. (2003). Involvement of the olfactory tubercle in cocaine reward:

intracranial self-administration studies. *Journal of Neuroscience*, 23: 9305-9311

104. Ikemoto, S., Qin, M., Liu, Z.H. (2005). The functional divide for primary reinforcement of d-amphetamine lies between the medial and lateral ventral striatum: is the division of the accumbens core, shell and olfactory tubercle valid? *Journal of Neuroscience*, 25: 5061-5065
105. Ikemoto S. (2007). Dopamine reward circuitry: two projection systems from the ventral midbrain to the nucleus accumbens–olfactory tubercle complex. *Brain Research Review*: 56:27–78
106. Ikemoto, S. (2010). Brain reward circuitry beyond the mesolimbic dopamine system: a neurobiological theory. *Neuroscience & Biobehavioral Reviews*, 35 (2): 129-50
107. Ingham, P.W., McMahon, A.P. (2001). Hedgehog signaling in animal development: paradigms and principles. *Genes & Development*, 15: 3059-3087
108. Ingham, P.W., Plaszek, M. (2006). Orchestrating ontogenesis: variations on a theme by sonic hedgehog. *Nature Reviews Genetics*, 7 (11): 841-50
109. Ishibashi, M., McMahon, A.P. (2002). A sonic hedgehog-dependent signaling relay regulates growth of diencephalic and mesencephalic primordial in the early mouse embryo. *Development*, 129 (20): 4807-19
110. Jacobs, F.M., Smits, S.M., Noorlander, C.W., Oerthel, L., van der Linden, A., Burbach, P.H., Smidt, M.P. (2007). Retinoic acid counteracts developmental defects in the substantia nigra caused by Pitx3 deficiency. *Development*, 134: 2673-2684
111. Jaeger, I., Arber, C., Risner-Janiszek, J. R., Kuechler, J., Pritzische, D., Chen, I. C., Naveenan, T., Ungless, M. A., Li, M. (2011). Temporally controlled modulation of FGF/ERK signaling directs midbrain dopaminergic neural progenitor fate in mouse and human pluripotent stem cells. *Development*, 138 (20): 4363-74
112. Jeong, Y., Epstein, D.J. (2003). Distinct regulators of Shh transcription in the floor plate and notochord indicate separate origins for these tissues in the mouse node. *Development*, 130: 3891-3902
113. Jeong, J., Mao, J., Tenzen, T., Kottmann, A.H., McMahon, A.P. (2004). Hedgehog signaling in the neural crest cells regulates the patterning and growth of facial primordial. *Genes & Development*, 18 (8): 937-51
114. Jessel, T.M. (2000). Neuronal specification in the spinal cord: inductive signals and transcriptional codes. *Nature Reviews Genetics*, 1: 20-29
115. Joksimovic M., Yun, B.A., Kittappa, R., Anderegg, A.M., Chang, W.W., Taketo, M.M., McKey, R.D., Awatramani, R.B. (2009). Wnt antagonism of Shh facilitates

midbrain floor plate neurogenesis. *Nature Neuroscience*, 12: 125-131

116. Joksimovic M., Anderegg, A., Roy, A., Campochiaro, L., Yun, B., Kittappa, R., McKey, R.D., Awatramani, R.B. (2009). Spatiotemporally separable Shh domains in the midbrain define distinct dopaminergic progenitor pools. *Proceedings of the National Academy of Science*, 106: 19185-19190
117. Joyes, M. P., Rayport, S. (2000). Mesoaccumbens dopamine neuron synapses reconstructed in vitro are glutamatergic. *Neuroscience*, 99: 445-456
118. Kala, K., Haugas, M., Lillevalli, K., Guimera, J., Wurst, W., Salminen, M., Partanen, J. (2009). Gata2 is a tissue-specific post-mitotic selector gene for midbrain GABAergic neurons. *Development*, 136 (2): 253-62
119. Kaplan, H.I., Sadock, B.J. (1995). Comprehensive Textbook of Psychiatry. Baltimore, MD: Williams & Wilkins
120. Kawano, M., Kawasaki, A., Sakata-Haga, H., Fukui, Y., Kawano, H., Nogami, H., Hisano, S. (2006). Particular subpopulations of midbrain and hypothalamic dopamine neurons express vesicular glutamatergic transporter 2 in the rat brain. *Journal of Comparative Neurology,* 498: 581-592
121. Keifer, J., Houk, K.C. (1994). Motor function of the cerebellorubrospinal system. *Physiological Reviews*, 74: 509-542
122. Kele, J., Simplicio, N., Ferri, A. L., Mira, H., Guillemont, F., Arenas, E., Ang, S.L. (2006). Neurogenin 2 is required for the development of ventral midbrain dopaminergic neurons. *Development*, 133 (3): 495-505
123. Kelley, A.E. and Berridge, K.C. (2002) The neuroscience of natural rewards: relevance to addictive drugs. *Journal of Neuroscience*, 22: 3306-3311
124. Kennedy, P.R. (1990). Corticospinal, rubrospinal and rubro-olivary projections: a unifying hypothesis. *Trends in Neuroscience*, 13: 474-479
125. Khaliq, Z.M., Bean, B.P. (2010). Pacemaking in dopaminergic ventral tegmental area neurons: depolarizing drive from background and voltage-dependent sodium conductances. *Journal of Neuroscience*, 30: 7401-7413
126. Kilpatrick, I.C., Jones, M.W., Phillipson, O.T. (1986). A semiautomated analysis method for catecholamines, and some prominent metabolites in microdissected regions of the nervous system: an isocratic HPLC technique employing coulometric detection and minimal sample preparation. *Journal of Neurochemistry*, 46 (6): 1865-76
127. Kimmel, R. A., Turnbull, D.H., Blanquert, V., Wurst, W., Loomis, C.A., Joyner, A.L.

(2000). Two lineage boundaries coordinate vertebrate apical ectodermal ridge formation. *Genes & Development*, 14: 1377-1389

128. Kittappa, R., Chang, W.W., Awatramani, R.B., McKay, R.D. (2007). The foxa2 gene controls the births and spontaneous degeneration of dopamine neurons in old age. *PLoS Biology*, 5: e325
129. Klein, C., Schlossmacher, M.G. (2006). The genetics of Parkinson disease: implications for neurological care. *Nature Clinical Practice Neurology*, 2: 136-146
130. Koch, P., Opitz, T., Steinbeck, J. A., Ladewig, J., Brüstle, O. (2009). A rosette-type, self-renewing human ES cell-derived neural stem cell with potential for in vitro instruction and synaptic integration. *Proceedings of the National Academy of Science*, 106 (9): 3225-30
131. Koob, G.F. (1999). The role of the striatopallidal and extended amygdala systems in drug addiction. *Annals of the New York Academy of Science,* 877: 445-60
132. Krause, J. (2008). SPECT and PET of dopamine transporter in attention-deficit/hyperactivity disorder. *Expert Review of Neurotherapeutics*, 8 (4): 611-25
133. Krause, K.H., Dresel, S.H., Krause, J., la Fougere, C., Ackenheil, M. (2003). The dopamine transporter and neuroimaging in attention deficit hyperactivity disorder. *Neuroscience & Biobehavioral Reviews*, 27 (7): 605-13
134. Kravitz, A.V., Owen, S.F., Kreitzer, A.C. (2012). Optogenetic identification of striatal projection neuron subtypes during in vivo recording. *Brain Research*, 12
135. Kriks, S., Shim, J. W., Piao, J., Ganat, Y.M., Wakeman, D.R., Xie, Z., Carrillio-Reid, L., Auyeung, G., Antonacci, C., Buch, A., Yang, L., Beal, M. F., Surmeier, D.J., Kordower, J.H., Tabar, V., Studer, L. (2011). Dopamine neurons derived from human ES cells efficiently engraft in animal models of Parkinson's disease. *Nature*, 480 (7378): 547-51
136. Krosigk, M., Smith, A.D. (1991). Descending Projections from the Substantia Nigra and Retrorubral Field to the Medullary and Pontomedullary Reticular Formation. *European Journal of Neuroscience*, 3(3): 260-273
137. Lammel, S., Hetzel, A., Haeckel, O., Jones, I., Liss, B. and Roeper, J. (2008). Unique properties of mesoprefrontal neurons within a dual mesocorticolimbic dopamine. *Neuron*, 57: 760-773
138. Lammel, S., Ion, D.I., Roeper, J., Malenka, R.C. (2011). Protein-specific modulation of dopamine neuron synapses by aversive and rewarding stimuli. *Neuron*, 70: 855-862

139. Lammel, S., Lim, B.K., Ran, C., Huang, K.W., Betley, M.J., Tye, K.M., Deisseroth, K., Malenka, R.C. (2012). Input-specific control of reward and aversion in the ventral tegmental area. *Nature*, 491 (8): 212-217

140. Lapish, C.C., Kroener, S., Durstewitz, D., Lavin, A., Seamans, J.K. (2007). The ability of the mesocortical dopamine system to operate in distinct temporal modes. *Psychopharmacology*, 191: 609-625

141. Lavin A., Noqueira, L., Lapish, C.C., Wightman, R.M., Phillips, P.E., Seamans, J.K. (2005). Mesocortical dopamine neurons operate in distinct temporal domains using multimodal signaling. *Journal of Neuroscience,* 25: 5013-5023

142. Lee, K.J., Jessell, T.M. (1999). The specification of dorsal cell fates in the vertebrate central nervous system. *Annual Review of Neuroscience*, 22: 261-94

143. Li, J.Y., Lao, Z., Joyner, A.L. (2002). Changing requirements for Gbx2 in development of the cerebellum and maintenance of the mid/hindbrain organizer. *Neuron*, 36: 31-43

144. Li, L. B., Chen, N., Ramamoorthy, S., Chi, L., Cui, X.N., Wang, L.C., Reith, M.E. (2004). The role of N-glycosylation in function and surface trafficking of the human dopamine transporter. *The Journal of Biological Chemistry*, 279: 21012-21020

145. Liss, B., Roeper, J. (2007). Individual dopamine midbrain neurons: functional diversity and flexibility in health and disease. *Brain Research Reviews*, 58 (2): 314-21

146. Livesey, F.J., and Cepko, C.L. (2001). Vertebrate neural cell-fate determination: lessons from the retina. *Nature reviews Neuroscience,* 2: 109-118

147. Liu, A., Joyner, A.L. (2001). Early anterior/posterior pattering of the midbrain and cerebellum. *Annual Review of Neuroscience*, 24: 869-96

148. Liu, A., Wang, B., Niswander, L.A. (2005). Mouse intraflagellar transport proteins regulate both the activator and repressor functions of Gli transcription factors. *Development*, 132: 3103-3111

149. Lupo, G., Harris, W.A., Lewis, K.E. (2006). Mechanisms of ventral patterning in the vertebrate nervous system. *Nature Review Neuroscience*, 7: 103-114

150. Marchetto, M.C., Winner, B., Gage, F.H. (2010). Pluripotent stem cells in neurodegenerative and neurodevelopmental diseases. *Human Molecular Genetics*, 19 (R1): R71-6

151. Maren, S., Fanselow, M.S. (1996). The amygdala and fear conditioning: has the nut been cracked? *Neuron*, 16 (2): 237-40

152. Marigo, V., Davey, R.A., Zuo, Y., Cunningham, J.M., Tabin, C.J. (1996). Biochemical evidence that patched is the Hedgehog receptor. *Nature*, 384: 176-179

153. Marsden, C.D. (1994). Parkinson's disease. *Journal of Neurology, Neurosurgery & Psychiatry*, 57 (6): 672-81

154. Massion, J. (1967). The mammalian red nucleus. *Physiology Review*, 47: 383-436

155. Matise, M.P., Epstein, D.J., Park, H.L., Platt, K.A., Joyner, A.L. (1998). Gli2 is required for induction of floor plate and adjacent cells, but not most ventral neurons in the mouse central nervous system. *Development*, 125 (15): 2759-2770

156. Matsunaga, E., Katahira, T., Nakamura, H. (2002). Lmx1b and Wnt1 in mesencephalon and metecephalon development. *Development*, 129: 5269-5277

157. Mavromatakis, Y.E., Lin, W., Metzakopian, E., Ferri, A.L., Yan, C.H., Sasaki, H., Whisett, J., Ang, S.L. (2011). Foxa1 and Foxa2 positively and negatively regulate Shh signaling to specify ventral midbrain progenitor identity. *Mechanisms of Development*, 128 (1-2): 90-103

158. Maxwell, S., Ho, H.Y., Kuehner, E., Zhao, S., Li, M. (2005). Pitx3 regulates tyrosine hydroxylase expression in the substantia nigra and identifies a subgroup of mesencephalic dopaminergic progenitor neurons during mouse development. *Developmental Biology*, 282: 467-497

159. May, S.R., Ashique, A.M., Karien, M., Wang, B., Shen, Y., Zarbalis, K., Reiter, J., Ericson, J., Peterson, A.S. (2005). Loss of the retrograde motor for IFT disrupts localization of Smo to cilia and prevents the expression of progenitor pool. *Developmental Biology*, 287: 378-389

160. McCaffery, P.J., Adams, J., Maden, M., Rosa-Molinar, E. (2003). Too much of a good thing: retinoic acid as an endogenous regulator of neural differentiation and exogenous teratogen. *European Journal of Neuroscience*, 18: 457-472

161. McEvilly, R.J., Erkman, L., Luo, L., Sawchenko, P.E., Ryan, A.F., Rosenfeld, M.G. (1996). Requirement for Brn3 in differentiation and survival of sensory and motor neurons. *Natur*e, 384: 574-577

162. McMahon, A.P., Bradley, A. (1990). The Wnt-1 (int-1) proto-oncogene is required for development of a large region of the mouse brain. *Cell,* 62: 1073-1085

163. McRitchie, D.A., Hardman, C.D., Haliday, G.M. (1996). Cytoarchitectual distribution of calcium binding proteins in midbrain dopaminergic regions of rats and humans. *Journal of Comparative Neurology*, 364: 121-150

164. Mendez, J.A., Bourque, M.J., Dal Bo, G., Bourdeau, M.L., Danik, M., Williams, S.,

Lacaille, J.C., Trudeau, L.E. (2008). Developmental and target-dependent regulation of vesicular glutamate transporter expression by dopamine neurons. *Journal of Neuroscience*, 28: 6309-6318

165. Mezey, E., Dehejia, A.M., Harta, G., Tresser, N., Suchy, S.F., Nussbaum, R.L., Brownstein, M.J., Polymeropolus, M.H. (1998). Alpha synuclein is present in Lewy bodies in sporadic Parkinson's disease. *Molecular Psychiatry*, 3: 493-499
166. Missale, C., Nash, S.R., Robinson, S.W., Jaber, M., Caron, M.G. (1998). Dopamine receptors: from structure to function. *Physiological Reviews*, 78 (1): 189-225
167. Mo, R., Freer, A.M., Zinyk, D.L., Crackower, M.A., Michaud, J., Heng, H.H., Chik, K.W., Shi, X.M., Tsui, L.C., Cheng, S.H., Joyner, A.L., Hui, C. (1997). Specific and redundant functions of Gli2 and Gli3 zinc finger genes in skeletal patterning and development. *Development*, 124 (1): 113-123
168. Molyneaux, B.J., Arlotta, P., Macklis, J.D. (2007). Molecular development of corticospinal motor neuron circuitry. *Novatis Found Symp*. 288: 3-15
169. Moore, D.J., West, A.B., Dawson, V.L., Dawson, T.M. (2005). Molecular pathophysiology of Parkinson's disease. *Annual Review of Neuroscience,* 28: 57-87
170. Moreno-Bravo, J.A., Perez-Balaguer, A., Martinez, S., Puelles, E. (2010). Dynamic expression patterns of Nkx6.1 and Nkx6.2 in the developing mes-diencephalic basal plate. *Developmental Dynamics*, 239 (7): 2094-101
171. Nakatani, T., Kumai, M., Mizuhara, E., Minaki, Y., Ono, Y. (2010). Lmx1a and Lmx1b cooperate with Foxa2 to coordinate the specification of dopaminergic neurons and control of floor plate cell differentiation in the developing mesencephalon. *Developmental Biology*, 339 (1): 101-13
172. Neuhoff, H., Neu, A., Liss, B., Roeper, J. (2002). I(h) channels contribute to the different functional properties of identified dopaminergic subpopulations in the midbrain. *Journal of Neuroscience*, 22: 1290-1302
173. Ohtsuka, T., Ishibashi, M., Gradwohl, G., Nakatashi, S., Guillemot, F., Kageyama, R. (1999). Hes1 and Hes5 as notch effectors in mammalian neuronal differentiation. *EMBO Journal*, 18 (8): 2196-207
174. Ono, Y., Nakatani, T., Sakamoto, Y., Mizuhara, E., Minaki, Y., Kumai, M., Hamaguchi, A., Nishimura, M., Inoue, Y., Hayashi, H., Takahashi, J., Imai, T. (2007). Differences in neurogenic potential in floor plate cells along an anteroposterior location: midbrain dopaminergic neurons originate from mesencephalic floor plate cells. *Development*, 134: 3213-3225

175. Oorschot, D.E. (1996). Total number of neurons in the neostriatal, pallidal, subthalamic, and substantia nigral nuclei of the rat basal ganglia: a stereological study using the cavalieri and optical dissector methods. *Journal of Comparative Neurobiology*, 366 (4): 580-99

176. Pan, Y., Bai, C.B., Joyner, A.L., Wang, B. (2006). Sonic hedgehog signaling regulates Gli2 transcriptional activity by suppressing its processing and degradation. *Molecular Cell Biology*, 26 (9): 3365-77

177. Pavletich, N.P., Pabo, C.O. (1993). Crystal structure of a five-finger Gli-DNA complex: new perspectives on zinc fingers. *Science*, 216 (5129): 1701-1707

178. Paxinos, G. and Franklin, K. B. J. (2007). The Mouse Brain in Stereotaxic Coordinates. *Academic Press*, San Diego

179. Perez-Balaguer, A., Puelles, E., Wurst, W., Martinez, S. (2009). Shh dependent and independent maintenance of basal midbrain. *Mechanisms of Development*, 126: 301-313

180. Persson, M., Stamataki, D., te Welscher, P., Andersson, E., Bose, J., Ruther, U., Ericson, J., Briscoe, J. (2002). Dorsal-ventral patterning of the spinal cord requires Gli3 transcriptional repressor activity. *Genes & Development*, 16 (22): 2865-78

181. Pfaff, S.L., Mendelsohn, M., Stewart, C.L., Edlund, T., Jessel, T.M. (1996). Requirement for LIM homeobox gene Isl1 in motor neuron generation reveals a motor neuron-dependent step in interneuron differentiation. *Cell*, 84: 309-320

182. Pfisterer, U., Kirkeby, A., Torper, O., Wood, J., Nalander, J., Dufour, A., Bjorklund, A., Lindvall, o., Jakobson, J., Parmar, M. (2011). Direct conversion of human fibroblasts to dopaminergic neurons. *Proceedings of the National Academy of Science*, 108 (25): 10343-8

183. Phillipson, O.T. (1979). Afferent projections to the ventral tegmental area of Tsai and intrafascicular nucleus: a horseradish peroxidase study in the rat. *Journal of Comparative Neurology*, 187 (1): 117-43

184. Pickel, V.M., Joh, T.H., Field, P.M., Becker, C.G., Reis, D.J. (1975). Cellular localization of tyrosine hydroxylase by immunohistochemistry. *Journal of Histochemistry & Cytochemistry*, 23 (1): 1-12

185. Polleus, F., Ghosh, A. (2002). The slice overlay assay: a versatile tool to study the influence of extracellular signals on neuronal development. *Science STKE*, 2002 (136): 19

186. Polleux, F., Ghosh, A. (2002). The slice overlay assay: A versatile tool to study the

influence of extracellular signals on neuronal development. *Science* STKE: PL9

187. Prakash, N., Brodski, C., Naserke, T., Puelles, E., Gogoi, R., Hall, A., Panhuysen, M., Echevarria, D., Sussel, L., Weisenhorn, D.M. (2006). A Wnt1-regulated genetic network controls the identity and fate of midbrain dopaminergic progenitors in vivo. *Developmen*t, 133: 89-98
188. Prakash, N., Wurst, W. (2004). Specification of midbrain territory. *Cell Tissue Research*, 318 (1): 5-14
189. Prakash, N., Wurst, W. (2006). Development of dopaminergic neurons in the mammalian brain. *Cellular and Molecular Life Science*, 63 (2): 187-206
190. Prakash, N., Puelles, E., Freude, K., Trumbach, D., Omodei, D., Di Salvio, M., Sussel, L., Ericson, J., Sander, M., Simeone, A., Wurst, W. (2009). Nkx6-1 controls the identity and fate of red nucleus and oculomotor nucleus in the mouse midbrain. *Development*, 136: 2545-2555
191. Puelles, E., Annino, A., Tuorto, F., Usiello, A., Acampora, D., Czerny, T., Brodski, C., Ang, S.L., Wurst, W., Simeone, A. (2004). Otx2 regulates the extent, identity and fate of neuronal progenitor domains in the ventral midbrain. *Development*, 131: 2037-2048
192. Puopolo, M., Raviola, E., Bean, B.P. (2007). Roles of subthreshold calcium current and sodium current in spontaneous firing of mouse midbrain dopamine neurons. *Journal of Neuroscience*, 27: 645-656
193. Ramirez, A., Heimbach, A., Grundemann, J., Stiller, B., Hampshire, D., Cid, L.P., Goebel, I., Mubaidin, A.F., Wriekat, A.L., Roeper, J. (2006). Hereditary Parkinsonism with dementia is caused by mutations in ATP13A2, encoding a lysosomal type 5 P-type ATPase. *Nature Genetics*, 38: 1184-1191
194. Ribes, V., Balaskas, N., Sasai, N., Cruz, C., Dessaud, E., Cayuso, J., Tozer, S., Yang, L. L., Novitch, B., Marti, E., Briscoe, J. (2010). Distinct Sonic Hedgehog signaling dynamics specify floor plate and ventral neuronal progenitors in the vertebrate neural tube. *Genes & Development*, 24 (11): 1186-200
195. Robinson, S., Smith, D.M., Mizumori, S.J., Palmiter, R.D. (2004). Firing properties of dopamine neurons in freely moving dopamine-deficient mice: effects of dopamine receptor activation and anesthesia. *Proceedings of the National Academy of Sciences*, 101 (36): 13329-34
196. Rocha, B.A., Fumagalli, F., Gainetdinov, R.R., Jones, S.R., Ator, R., Giros, B., Miller, G.W., Caron, M.G. (1998). Cocaine self-administration in dopamine-

transporter knockout mice. *Nature Neuroscience*, 1: 132-137

197. Rodd-Henricks, Z.A., McKinzie, D.L., Murphy, J.M., McBride, W.J. (2002). Cocaine is self-administered into the shell but not the core of the nucleus accumbens of Wistar rats. *Journal of Pharmacology*, 303: 1216-1226
198. Salamone J. D., Correa M. (2002). Motivational views of reinforcement: implications for understanding the behavioral functions of nucleus accumbens dopamine. *Behavioral Brain Research*, 137 (1-2): 3-25
199. Sasaki, H., Hui, C., Nakafuku, M., Kondoh, H. (1997). A binding site for Gli proteins is essential for HNF-3beta floor plate enhancer activity in transgenics and can respond to Shh in vitro. *Development*, 124: 1313-1322
200. Saucedo-Cardenas, O., Quintana-Hau, J., Le, W., Smidt, M., Cox, J., Mayo, F.D., Burbach, J., Conneely, O. (1998). Nurr1 is essential for the induction of the dopaminergic phenotype and the survival of ventral mesencephalic late dopaminergic precursor neurons. *Proceedings of the National Academy of Science*, 95: 4013-4018
201. Schapira, A.H. (2006). Etiology of Parkinson's disease. *Neurology*, 66: S10-S23
202. Schultz, W., Dayan, P., Montague, P.R. (1997). A neural substrate of prediction and reward. *Science*, 275 (5306): 1593-9
203. Schultz, W. (1998). Predictive reward signal of dopamine neurons. *Journal of Neurophysiology*, 80 (1): 1-27
204. Schultz, W. (2002). Getting formal with dopamine and reward. *Neuron*, 36: 241–263
205. Sedvall, G. and Farde, L. (1995). Chemical brain anatomy in schizophrenia. *The Lancet*, 346: 743-749
206. Sesack, S.R., Snyder, C.L., Lewis, D.A. (1995). Axon terminals immunolabeled for dopamine or tyrosine hydroxylase synapse on GABA-immunoreactive dendrites in rat and monkey cortex. *Journal of Comparative Neurology*, 363 (2): 264-80
207. Sesack, S.R. and Carr, D. B. (2002). Selective prefrontal cortex inputs to dopamine cells: implications for schizophrenia. *Physiology &. Behavior*, 77: 513-517
208. Seutin, V., Massotte, L., Renette, M. F., Dresse, A. (2001). Evidence for a modulatory role of I(h) on the firing of a subgroup of midbrain dopamine neurons. *NeuroRepor*t, 12: 255-258
209. Simeone, A., Puelles, E., Omodei, D., Acampora, D., Di Giovannantonio, L.G., Di Salvio, M., Mancuso, P., Tomasetti, C. (2011). Otx genes in neurogenesis of mesencephalic dopaminergic neurons. *Developmental Neurobiology*, 71 (8): 665-79
210. Simon, H.H., Saueressig, H., Wurst, W., Goulding, M.D., O'Leary, D.D. (2001). Fate

of midbrain dopaminergic neurons controlled by the engrailed genes. *Journal of Neuroscience*, 21 (9): 3126-34

211. Smidt, M.P., van Schaick, H.S., Lanctot, C., Tremblay, J.J., Cox, J.J., van der Kleij, A.A., Wolterink, G., Drouin, J., Burbach, J.P. (1997). A homeodomain gene Pitx3 has highly restricted brain expression in mesencephalic dopaminergic neurons. *Proceedings of the National Academy of Sciences*, 94 (24): 13305-10
212. Smidt, M.P., Asbreuk, C.H., Cox, J.J., Chen, H., Johnson, R.L., Burbach, J.P.A (2000). Second independent pathway for development of mesencephalic dopaminergic neurons requires Lmx1b. *Nature Neuroscience*, 3 (4): 337-41
213. Smidt, M.P., Smits, S.M., Bouwmeester, H., Harmes, F.P., van der Linden, A.J., Hellemons, A.J., Graw, J., Burbach, J. P. (2004). Early developmental failure of substantia nigra dopamine neurons in mice lacking the homeodomain gene Pitx3. *Development*, 131 (5): 1145-55
214. Smits, S.M., Burbach, J.P., Smidt, M.P. (2006). Developmental origin and fate of meso-diencephalic dopamine neurons. *Progress in Neurobiology*, 78: 1-16
215. Sohal, V.S., Zhang, F., Yizhar, O., Deisseroth, K. (2009). Parvalbumin neurons and gamma rhythms enhance cortical circuit performance. *Nature*, 459 (7247): 698-702
216. Soldner, F., Hockmeyer, D., Beard, C., Gao, Q., Bell, G.W., Cook, E.G., Hargus, G., Blak, A., Cooper, O., Mitalipova, M., Isacson, O., Jaenisch, R. (2009). Parkinson's disease patient-derived induced pluripotent stem cells free of viral reprogramming factors. *Cell*, 136 (5): 964-77
217. Sonnier, L., Le Pen, G., Hartmann, A., Bizot, J. C., Trovero, F., Krebs, M.O., Prochiantz, A. (2007). Progressive loss of dopaminergic neurons in the ventral midbrain of adult mice heterozygote for Engrailed1. *Journal of Neuroscience*, 27: 1063-1071
218. Spencer, T.J., Biederman, J., Madras, B.K., Faraone, S.V., Dougherty, D.D., Bonab, A.A., Fischman, A.J. (2005). In vivo neuroreceptor imaging in attention-deficit/hyperactivity disorder: a focus on the dopamine transporter. *Biological Psychiatry*, 57 (11): 1293-300
219. Spillantini, M.G., Schmidt, M.L., Lee, V.M., Trojanowski, J.Q., Jakes, R., Goedert, M. (1997). Alpha-synuclein in Lewy bodies. *Nature*, 388: 839-840
220. Stamataki, D., Ulloa, F., Tsoni, S. V., Mynett, A., Briscoe, J. (2005). A gradient of Gli activity mediates graded Sonic Hedgehog signaling in the neural tube. *Genes & Development*, 19 (5): 626-41

221. Stone, D.M., Hynes, M., Armanini, M., Swanson, T.A., Gu, Q., Johnson, R.L., Scott, M.P., Pennica, D., Goddard, A., Phillips, H., Noll, M., Hooper, J.E., de Sauvage, F., Rosenthal, A. (1996). The tumor-supressor gene patched encodes a candidate receptor for Sonic hedgehog. *Nature*, 384: 129-134

222. Stuber, G.D., Hnasko, T.S., Britt, J.P., Edwards, R.H., Bonci, A. (2010). Dopaminergic terminals in the nucleus accumbens but not the dorsal striatum corelease glutamate. *Journal of Neuroscience*, 30 (24): 8229-33

223. Swanson, L.W. (1982). The projections of the ventral tegmental area and adjacent regions: a combined fluorescent retrograde tracer and immunofluorescence study in the rat. *Brain Research Bulletin*, 9: 321-353

224. Swistowski, A., Peng, J., Liu, Q., Mali, P., Rao, M.S., Cheng, L., Zeng, X. (2010). Efficient generation of functional dopaminergic neurons from human induced pluripotent stem cells under defined conditions. *Stem Cells*, 28 (10): 1893-904

225. Taipale J., Chen, J.K., Cooper, M.K., Wang, B., Mann, R.K., Milenkovic, L., Scott, M.P., Beachy, P.A. (2000). Effects of oncogenetic mutations in Smoothened and Patched can be reversed by cyclopamine. *Nature*, 406 (6799): 1005-9

226. Tang, M., Miyamoto, Y., Huang, E. (2009). Multiple roles of beta-catenin in controlling the neurogenic niche for midbrain dopamine neurons. *Development*, 136: 2027-2038

227. Tang, M., Villaescusa, J.C., Luo, S.X., Guitarte, C., Lei, S., Miyamoto, Y., Taketo, M.M., Arenas, E., Huang, E.J. (2010). Interaction of Wnt/ beta-catenin signaling and sonic hedgehog regulate the neurogenesis of ventral midbrain dopamine neurons. *Journal of Neuroscience*, 30 (27): 9280-91

228. Tecuapetla, F., Patel, J.C., Xenias, H., English, D., Tadros, I., Shah, F., Berlin, J., Deisseroth, K., Rice, M.E., Tepper, J.M., Koos, T. (2010). Glutamatergic signaling by mesolimbic dopamine neurons in the nucleus accumbens. *Journal of Neuroscience*, 30 (20): 7105-10

229. Ten Donkelaar, H.J. (1988). Evolution of the red nucleus and rubrospinal tract. *Behavioral Brain Research*, 28 (1-2): 9-20

230. Thompson, L., Barraud, P., Andersson, E., Kirik, D. and Bjorklund, A. (2005). Identification of dopaminergic neurons of nigral and ventral tegmental area subtypes in grafts of fetal ventral mesencephalon based on cell morphology, protein expression, and efferent projections. *Journal of Neuroscience*, 25: 6467-647

231. Tork, I., Halliday, G., Scheibner, T. and Turner, S. (1984). The organization of the

mesencephalic ventromedial (VMT) in the cat. In R. Bandler (Ed.), Modulation of sensomotror activity during alteration in behavioral states. *Alan Liss*, New York: 39-73

232. Torres, G.E., Carneiro, A., Seamans, K., Fiorentini, C., Sweeney, A., Yao, W.D., Caron, M.G. (2003). Oligomerization and trafficking of the human dopamine transporter. Mutational analysis identifies critical domains important for the functional expression of the transporter. *Annals of Neurology*, 35: 494-498
233. Tritsch, N.X., Jung, B.D., Sabatini, B.L. (2012). Dopaminergic neurons inhibit striatal output through non-canonical release of GABA. *Nature*, 490 (7419): 262-6
234. Trokovic, R., Trokovic, N., Hernesniemi, S., Pirvola, U., Vogt Weisenhorn, D.M., Rossant, J., McMahon, A.P., Wurst, W., Partanen, J. (2003). FGFR1 is independently required in both developing mid- and hindbrain for sustained response to isthmic signals. *EMBO Journal*, 22: 1811-1823
235. Trokovic, R., Jukkola, T., Saarimaki, J., Peltopuro, P., Naserke, T., Weisenhorn, D.M., Trokovic, N., Wurst, W., Partanen, J. (2005). Fgfr1-dependent boundary cells between developing mid- and hindbrain. *Developmental Biology*, 278 (2): 428-39
236. Turner, E.E., Jenne, K.J., Rosenfeld, M.G. (1994). Brn3.2: A Brn-3-related transcription factor with distinctive central nervous system expression and regulation by retinoic acid. *Neuron*, 12: 205-218
237. Ungless, M.A., Magill, P.J., and Bolam, J.P. (2004). Uniform inhibition of dopamine neurons in the ventral tegmental area by aversive stimuli. *Science*, 303: 2040–2042
238. Veening, J.G., Cornelissen, F.M., Lieven, P.A. (1980). The topical organization of the afferents to the caudoputamen of the rat. A horseradish peroxidase study. *Neuroscience*, 5 (7): 1253-68
239. Volkow, N.D., Wang, G.J., Fowler, J.S., Tomasi, D., Telang, F. (2010). Addiction: Beyond dopamine reward circuitry. *Proceedings of the National Academy of Sciences,* 108 (37): 15037-42
240. Watabe-Uchida, M., Zhu, L., Ogawa, S. K., Vamanrao, A., Uchida N. Whole-brain mapping of direct inputs to midbrain dopamine neurons. (2012). *Neuron*, 74: 858-873
241. Watanabe, M., Kodama, T., Hikosaka, K. (1997). Increase of extracellular dopamine in primate prefrontal cortex during working memory task. *Journal of Neurophysiology*, 78: 2795-2798
242. Watanabe, Y., Nakamura, H. (2000). Control of chick tectum territory along dorsoventral axis by Sonic hedgehog. *Development*, 127 (5): 1131-40

243. Wightman, R.M. and Robinson, D.L. (2002). Transient changes in mesolimbic dopamine and their association with 'reward'. *Journal of Neurochemistry*, 82: 721-735

244. Wijgerde, M., McMahon, J.A., Rule, M., McMahon, A.P. (2002). A direct requirement for Hedgehog signaling for normal specification of all ventral progenitor domains in the presumptive mammalian spinal cord. *Genes & Development*, 16 (22): 2849-64

245. Williams, G.V., Goldman-Rakic, P.S. (1995). Modulation of memory fields by dopamine D1 receptors in prefrontal cortex. *Nature*, 376 (6541): 572-5

246. Winterer, G., and Weinberger, D.R. (2004). Genes, dopamine and cortical signal-to-noise ratio in schizophrenia. *Trends in Neuroscience*, 27: 683–690

247. Wise, R.A. (2002). Brain reward circuitry: insights from unsensed incentives. *Neuron*, 36 (2): 229-40

248. Wise, R.A. (2009). Roles for nigrostriatal—not just mesocorticolimbic—dopamine in reward and addiction. *Trends in Neuroscience*, 32: 517–524

249. Wolfart, J., Neuhoff, H., Franz, O., Roeper, J. (2001). Differential expression of the small-conductance, calcium-activated potassium channel SK3 is critical for pacemaker control in dopaminergic midbrain neurons. *Journal of Neuroscience*, 21: 3443-3456

250. Wong, D.F., Kuwabara, H., Schretlen, D.J., Bonson, K.R., Zhou, Y., Nandi, A., Brasic, J.R., Kimes, A.S., Maris, M.A., Kumar, A., London, E.D. (2006). Increased occupancy of dopamine receptors in human striatum cue-elicited cocaine craving. *Neuropsychopharmacology*, 31 (12): 2716-27

251. Xiang, M., Gan, L., Zhou, L., Klein, W.H., Nathans, J. (1996). Targeted deletion of the mouse POU domain gene Brn-3a causes a selective loss of neurons in the brainstem and trigeminal ganglion, uncoordinated limb movement, and impaired suckling. *Proceedings of the National Academy of Sciences,* 93: 11950-11955

252. Xie, J., Murone, M., Luoh, S.M., Ryan, A., Gu, Q., Zhang, C., Bonifas, J.M., Lam, C.W., Hynes, M., Goddard, A., Rosenthal, A., Epstein, E.H., de Sauvage, F.J. (1998). Activating Smoothened mutations in sporadic basal-cell carcinoma. *Nature*, 391 (6662): 90-2

253. Yamaguchi, T., Sheen, W., Morales, M. (2007). Glutamatergic neurons are present in the rat ventral tegmental area. *European Journal of Neuroscience*, 25: 106-118

254. Yamaguchi, T., Wang, H.L., Li, X., Ng, T.H., Morales, M. (2011).

Mesocorticolimbic glutamatergic pathway. *Journal of Neuroscience*, 31 (23): 8476-90

255. Yan, C., Levesque, M., Claxton, S., Johnson, R. L., Ang, S.L. (2011). Lmx1a and Lmx1b function cooperatively to regulate proliferation, specification, and differentiation of midbrain dopaminergic progenitors. *Journal of Neuroscience*, 31 (35): 12413-12425
256. Yang, J., Brown, A., Ellisor, D., Paul, E., Hagan, N., Zervas, M. (2013). Dynamic temporal requirement of Wnt1 in midbrain dopamine neuron development. *Development*, 140: 1342-1352
257. Yavich, L., Forsberg, M.M., Karayiorgou, M., Gogos, J.A., Mannisto, P.T. (2007). Site-specific role of catechol-O-methyltransferase in dopamine overflow within prefrontal cortex and dorsal striatum. *Journal of Neuroscience*, 27: 10196-10209
258. Ye, W., Shimamura, K., Rubenstein, J.L., Hynes, M.A., Rosenthal, A. (1998). FGF and Shh signals control dopaminergic and serotonergic cell fate in the anterior neural plate. *Cell*, 93: 755-766
259. Zetterstrom, R.H., Solomin, L., Jansson, L., Hoffer, B.J., Olson, L., Perlmann, T. (1997). Dopamine neuron agenesis in Nurr1-deficient mice. *Science*, 276 (5310): 248-50
260. Zhang, X.M., Ramalho-Santos, M., McMahon, A.P. (2001). Smoothened mutants reveal redundant roles for Shh and Ihh signaling including regulation of L/R symmetry by the mouse node. *Cell*, 106: 781-792
261. Zhao, S., Maxwell, S., Jimenez-Beristain, A., Vives, J., Kuehner, E., Zhao, J., O'Brien, C., de Felipe, C., Semina, E., Li, M. (2004). Generation of embryonic stem cells and transgenic mice expressing green fluorescence protein in midbrain dopaminergic neurons. *European Journal of Neuroscience*, 19 (5): 1133-40
262. Zolles, G., Klocker, N., Wenzel, D., Weisser-Thomas, J., Fleischmann, B.K., Roeper, J., Fakler, B. (2006). Pacemaking by HCN channels requires interaction with phosphoionositides. *Neuron*, 52: 1027-1036